

Cell Imprinted In Vitro Models for Normal and Cancer Cell Migration and Separation

Ph.D. Thesis
Chemistry Department

The Dissertation Submitted to the University of Hamburg by:

Hessam Hosseinkazemi

Matrikelnummer: 7491283

Supervised by:

Prof. Dr. Wolfgang J. Parak

Dr. Shahin Bonakdar

October 2024

Evaluators

Written Evaluators:

- 1- Professor Dr. Wolfgang J. Parak
- 2- Dr. Florian Schulz

Oral Evaluators:

- 1- Professor Dr. Wolfgang J. Parak
- 2- Professor Dr. Dirk Dorfs
- 3- Dr. Birgit Hankiewicz

Disputation Date: 20.12.2024

Table of Contents

Abstract	I
Zusammenfassung	II
Table of Figures	III
List of Tables	IV
List of Acronyms	V
<i>Chapter 1: Introduction</i>	1
1.1. Cell-Surface Interactions	4
1.1.1. Effects of Surface Topography on Cells	6
1.2. Cell Migration and Separation	10
1.2.1. Single-Cell Migration	13
1.2.2. Collective Cell Migration.....	13
1.2.3. Cell Migration in 3D.....	14
1.2.4. Cell Migration and Surface Properties	15
1.3. MCF7, MDA-MB-231 and 3T3 Cell Lines	16
1.4. Cell Imprinting	18
1.5. Quantum Dots	21
1.5.1. Core/Shell Cadmium Selenide/Cadmium Sulfide QDs.....	22
1.6. Fluorophores	24
1.6.1. Cell Staining with Fluorophores	24
<i>Chapter 2: Experimental Part</i>	27
2.1. Materials	28
2.2. Methods	29
2.2.1. Cell Culture	29
2.2.2. PDMS Preparation	30
2.2.3. Template Preparation	31
2.2.4. Substrates Development.....	33
2.2.5. PMA Coating of CdSe/CdS QDs	34
2.2.6. Substrate Characterization	35
2.2.7. CdSe/CdS QDs Characterization	39
2.2.8. Migration Assay.....	43
<i>Chapter 3: Results and Discussion</i>	49
3.1. Substrates Characterization	50
3.1.1. Light Microscopy Images	50
3.1.2. Contact Angle Measurement.....	51

3.1.3. Fourier-Transform Infrared Spectroscopy	57
3.2. Characterization of CdSe/CdS QDs	59
3.2.1. Dynamic Light Scattering	59
3.2.2. Fluorescence Spectroscopy	61
3.2.3. Endocytosis Assay	62
3.2.4. Presto Blue Cytotoxicity Assay	64
3.2.5. Transmission Electron Microscopy.....	65
3.3. Migration Assay	67
3.3.1. Crystal Violet Assay	67
3.3.2. Scanning Electron Microscopy (SEM)	76
3.3.3. Red/Blue Ratio Assay	78
<i>Chapter 4: Conclusion and Future Outlook</i>	93
4.1. Conclusion	94
4.2. Future Outlook.....	94
<i>Chapter 5: Bibliography</i>	96
Acknowledgment	VI
Appendix.....	VII
A1.Declaration Upon Oath.....	VII
A2. List of the Hazardous Substances.....	VIII

Abstract

Cancer cell migration signifies an intricate dimension of neoplastic invasion backed by various cellular and molecular interactions. The dynamics of cancer cells concerning their microenvironment, including the extracellular matrix and stromal cells, can govern this process. Furthermore, the cytoskeleton's architecture and the nucleus's deformation can significantly impact the cellular properties, thereby influencing this phenomenon. Cell imprinting is a highly advanced technique that entails the fabrication of a physical replica of a cell's membrane to modulate cell behavior and functionality. This technique mimics the endogenous milieu of cells, thus steering their interactions and reactions in vitro. The procedure incorporates the utilization of polydimethylsiloxane to capture the architectural features of cellular membranes, which can subsequently be leveraged to manipulate cellular activities such as adhesion, differentiation, and proliferation. In the initial phase of this study, an array of cell-imprinted substrates incorporating cancerous (MCF7) and non-cancerous (3T3) cell morphology were employed as cellular culture substrates. This was done to assess the impact of cell imprinting on cellular migration utilizing the crystal violet assay methodology. The results show that MCF7 and 3T3 cells prefer patterned substrates to migrate rather than plain (Unpatterned) polydimethylsiloxane or polystyrene tissue culture plates. Also, it is noteworthy that the cellular entities exhibit a pronounced affinity for a specific configuration when encountering double-patterned substrates. In other words, cells discern and favor their respective pattern over an alternate cellular pattern for migration. In the section of this research, we executed co-cultivation of MCF7/3T3 alongside MCF7/MDA-MB-231 cell lines on monolayer and bilayer surfaces to examine the significance of cellular imprinting in cellular differentiation. To distinguish the cells, one tagged with CdSe/CdS quantum dots coated with Poly (isobutylene-alt-maleic anhydride)-graft-dodecyl as red, and Hoechst-stained as blue cells. Then, the Red to Blue cells ratio was calculated to quantify the cell populations in different regions. All the cells showed higher proportions on similar patterns to their original morphology, rather than the imprints that differed from their shape on Double-Coating substrates. The results demonstrate that cells can smartly select and prefer their morphology on the cell-imprinted substrates over dissimilar patterns. Therefore, cell imprinted substrates can be utilized as in vitro models to study migrating and separating normal and cancer cells.

Keywords: Cell Imprinting, Migration, Separation, CdSe/CdS Quantum Dots, Hoechst Staining Polydimethylsiloxane, Poly (isobutylene-alt-maleic anhydride)-graft-dodecyl.

Zusammenfassung

Die Migration von Krebszellen stellt eine komplexe Dimension der neoplastischen Invasion dar, die durch verschiedene zelluläre und molekulare Interaktionen unterstützt wird. Die Dynamik der Krebszellen in Bezug auf ihre Mikroumgebung, einschließlich der extrazellulären Matrix und Stromazellen, kann diesen Prozess steuern. Darüber hinaus können die Architektur des Zytoskeletts und die Verformung des Zellkerns die zellulären Eigenschaften erheblich beeinflussen und somit dieses Phänomen beeinflussen. Das Zell-Imprinting ist eine hochentwickelte Technik, die die Herstellung einer physischen Nachbildung der Zellmembran zur Modulation des Zellverhaltens und der Funktionalität umfasst. Diese Technik imitiert die endogene Umgebung von Zellen und steuert somit deren Interaktionen und Reaktionen in vitro. Das Verfahren beinhaltet die Verwendung von Polydimethylsiloxan, um die architektonischen Merkmale von Zellmembranen einzufangen, die anschließend genutzt werden können, um zelluläre Aktivitäten wie Adhäsion, Differenzierung und Proliferation zu manipulieren. In der Anfangsphase dieser Studie wurde eine Reihe von Zell-geprägten Substraten, die krebsartige (MCF7) und nicht-krebsartige (3T3) Zellmorphologien beinhalteten, als Zellkultursubstrate verwendet. Dies geschah, um den Einfluss des Zell-Imprintings auf die Zellmigration mithilfe der Kristallviolett-Assay-Methodik zu bewerten. Die Ergebnisse zeigen, dass MCF7- und 3T3-Zellen bevorzugt auf gemusterten Substraten migrieren, anstatt auf einfachen (ungeprägten) Polydimethylsiloxan- oder Polystyrol-Gewebekulturplatten. Außerdem ist bemerkenswert, dass die zellulären Einheiten eine ausgeprägte Affinität zu einer bestimmten Konfiguration zeigen, wenn sie auf doppelt gemusterte Substrate treffen. Mit anderen Worten: Zellen erkennen und bevorzugen ihr entsprechendes Muster gegenüber einem alternativen Zellmuster für die Migration. Im weiteren Verlauf dieser Forschung führten wir eine Ko-Kultivierung von MCF7/3T3 sowie MCF7/MDA-MB-231-Zelllinien auf Monolayer- und Bilayer-Oberflächen durch, um die Bedeutung des Zell-Imprintings bei der Zelldifferenzierung zu untersuchen. Um die Zellen zu unterscheiden, wurde eine Gruppe mit CdSe/CdS-Quantenpunkten, beschichtet mit Poly(isobutylene-alt-maleinsäureanhydrid)-graft-dodecyl, als rot markiert und die andere mit Hoechst als blaue Zellen gefärbt. Anschließend wurde das Verhältnis von roten zu blauen Zellen berechnet, um die Zellpopulationen in verschiedenen Regionen zu quantifizieren. Alle Zellen zeigten auf ähnlichen Mustern zu ihrer ursprünglichen Morphologie höhere Anteile, anstatt auf den Abdrucken, die sich auf Doppelschicht-Substraten von ihrer Form unterschieden. Die Ergebnisse zeigen, dass Zellen intelligent ihre Morphologie auf den Zell-geprägten Substraten gegenüber unähnlichen Mustern auswählen und bevorzugen können. Daher können Zell-geprägte Substrate als in vitro-Modelle verwendet werden, um die Migration und Trennung normaler und krebsartiger Zellen zu untersuchen.

Schlüsselwörter: Zell-Imprinting, Migration, Trennung, CdSe/CdS-Quantenpunkte, Hoechst-Färbung, Polydimethylsiloxan, Poly(isobutylene-alt-maleinsäureanhydrid)-graft-dodecyl.

Table of Figures

Figure 1. Cellular Responses to Mechanical and Topographical Cues..	6
Figure 2. Effect of Matrix Stiffness and Topography.	7
Figure 3. Effect of Mechanotransduction on Biological Mechanisms.....	8
Figure 4. Effect of Mechanical Forces on Chromatin Transcription.	9
Figure 5. Cell Migration Steps.....	12
Figure 6. Single and Collective Cell Migration.....	14
Figure 7. Cell Imprinting Schematic.	19
Figure 8. Cell Imprinting Applications.....	20
Figure 9. PDMS-Curing Agent Mixture.....	30
Figure 10. Single-Coating Substrates. 5×10^4 MCF7 cells per well in 500 μ l DMEM in a 24-well plate.....	31
Figure 11. Semi-Circle Blockers Preparation..	32
Figure 12. Double-Coating Substrates	33
Figure 13. Sample Preparation..	34
Figure 14. Schematic Illustration of Contact Angle.....	37
Figure 15. Cell Seeding Schematic..	44
Figure 16. Cell Seeding.....	47
Figure 17. Light Microscopy Images of the Substrates..	51
Figure 18. Contact Angle Measurement.	53
Figure 19. FTIR Analysis.	58
Figure 20. Size Distribution by Intensity.....	60
Figure 21.PMA-QDs Emission Spectrum..	61
Figure 22. Endocytosis	62
Figure 23. Cytotoxicity by Presto Blue	65
Figure 24. TEM Micrographs of PMA-QDs. A-F) TEM images with various magnifications.	66
Figure 25. The Histogram and Distribution Curve of CdSe/CdS QD Particles' Size	66
Figure 26. MCF7 On Different Substrates..	69
Figure 27. 3T3 On Different Substrates.....	70
Figure 28- Diagram of Cell Density on Single-Coating Substrates.	72
Figure 29- Diagram of Cell Density on Double-Coating Substrates. A) MCF7 cells B) 3T3 Cells.....	75
Figure 30. SEM Micrographs. The SEM images show MCF7 cells on different substrates.....	77
Figure 31. Cross Section View.....	78
Figure 32. The Cells Distribution.	79
Figure 33. Diagram of Cell Distribution on Single-Coating Substrates. MCF7 Cells=Red, 3T3 Cells=Blue.	79
Figure 34. Diagram of Cell Distribution on Double-Coating Substrates. MCF7 Cells=Red, 3T3 Cells=Blue.	81
Figure 35. Diagram of Cell Distribution on Single-Coating Substrates. 3T3 Cells=Red, MCF7 Cells=Blue.	82
Figure 36. Diagram of Cell Distribution on Double-Coating Substrates. 3T3 Cells=Red, MCF7 Cells=Blue.	84
Figure 37. Diagram of Cell Distribution on Single-Coating Substrates. MDA-MB-231Cells=Red, MCF7 Cells=Blue.....	85
Figure 38. Diagram of Cell Distribution on Double-Coating Substrates. MDA-MB-231 Cells=Red, MCF7 Cells=Blue ...	87

List of Tables

<i>Table 1. Materials' Information Summary.....</i>	<i>29</i>
<i>Table 2. Contact Angle Values. The values for the contact angles of different substrates.....</i>	<i>55</i>
<i>Table 3. Cell Density on Single-Coating Substrates.....</i>	<i>71</i>
<i>Table 4. Cell Density on Double-Coating Substrates.</i>	<i>73</i>
<i>Table 5. Cell Distribution on Single-Coating Substrates. MCF7 Cells=Red, 3T3 Cells=Blue.</i>	<i>79</i>
<i>Table 6. Cell Distribution on Double-Coating Substrates. MCF7 Cells=Red, 3T3 Cells=Blue.</i>	<i>80</i>
<i>Table 7. Cell Distribution on Single-Coating Substrates. 3T3 Cells=Red, MCF7 Cells=Blue.</i>	<i>82</i>
<i>Table 8. Cell Distribution on Double-Coating Substrates. 3T3 Cells=Red, MCF7 Cells=Blue.</i>	<i>83</i>
<i>Table 9. Cell Distribution on Single-Coating Substrates. MDA-MB-231Cells=Red, MCF7 Cells=Blue.....</i>	<i>85</i>
<i>Table 10. Cell Distribution on Double-Coating Substrates. MDA-MB-231 Cells=Red, MCF7 Cells=Blue.</i>	<i>86</i>

List of Acronyms

<i>2D/3D</i>	<i>Two/Three-Dimensional</i>
<i>TME</i>	<i>Tumor Microenvironment</i>
<i>ECM</i>	<i>Extracellular Matrix</i>
<i>PDMS</i>	<i>Polydimethylsiloxane</i>
<i>ADSCs</i>	<i>Adipose-derived Mesenchymal Stem Cells</i>
<i>QDs</i>	<i>Quantum Dots</i>
<i>CdSe/CdS</i>	<i>Cadmium Selenide/Cadmium Sulfide</i>
<i>PMA</i>	<i>Poly(isobutylene-alt-maleic anhydride)-graft-dodecyl</i>
<i>FBS</i>	<i>Fetal Bovine Serum</i>
<i>Pen/Strep</i>	<i>Penicillin/Streptomycin</i>
<i>PBS</i>	<i>Phosphate-Buffered Saline</i>
<i>EDTA</i>	<i>Ethylenediaminetetraacetic Acid</i>
<i>RCF</i>	<i>Relative Centrifugal Force</i>
<i>TCPS</i>	<i>Tissue Culture Polystyrene Plate</i>
<i>CA</i>	<i>Contact Angle</i>
<i>SEM</i>	<i>Scanning Electron Microscopy</i>
<i>FTIR</i>	<i>Fourier-Transform Infrared Spectroscopy</i>
<i>DLS</i>	<i>Dynamic Light Scattering</i>
<i>TEM</i>	<i>Transmission Electron Microscopy</i>
<i>TCPS</i>	<i>Tissue Culture Polystyrene</i>
<i>HCl</i>	<i>Hydrochloric Acid</i>
<i>SD</i>	<i>Standard Deviation</i>
<i>H33342</i>	<i>Hoechst 3342</i>
<i>PEDOT</i>	<i>Poly(3,4-ethylene-dioxythiophene)</i>
<i>PSS</i>	<i>Poly(styrene sulfonate)</i>
<i>PMMA</i>	<i>Poly(methylmethacrylate)</i>
<i>DOX</i>	<i>Doxorubicin</i>
<i>GelMA</i>	<i>Gelatin Methacrylate</i>
<i>EMT</i>	<i>Epithelial-Mesenchymal Transition</i>

Chapter 1:
Introduction

Cancer, an intricate and multifaceted ailment, is characterized by the uncontrollable proliferation and dissemination of abnormal cells throughout the organism [1]. It encompasses a variety of disorders, each with unique attributes. Yet, all share the common trait of abnormal cell proliferation exceeding usual limits, potentially leading to invasion of neighboring tissues and metastasis to distant organs [2]. The extensive documentation of cancer's historical presence and its impact on human well-being spans centuries, evident in ancient skeletal remains exhibiting signs of the disease. Records from antiquity detail different types of cancer observed by early Greek and Roman medical experts [3]. Carcinoma, adenocarcinoma, sarcoma, lymphoma/leukemia, and myeloma are all categorized depending on their malignant cells' origin [4]. Tumor formation occurs due to multiple biological regulatory mechanisms at different levels, including cellular, molecular, and epigenetic. These mechanisms include disruptions in cell growth regulation and genetic alterations [5]. The progression of cancer is significantly shaped by external elements, such as lifestyle decisions and environmental factors, underscoring the importance of behaviors like smoking, alcohol consumption, and viral infections [6]. Despite its deadly nature, cancer can be effectively controlled, especially when detected early. This underscores the importance of continuous research and progress in diagnostic and therapeutic strategies[1]. Cancer management requires a comprehensive approach involving cooperation among oncologists, surgeons, and specialized nurses, all committed to providing holistic care to impacted individuals. Understanding the intricacies of cancer, from its genetic foundations to its societal impacts, remains a significant challenge and a key focus of present scientific inquiries.

Cell movement is a fundamental part of cellular biology, connecting to various processes like wound healing, cancer spread, and tissue creation. The mechanisms implicated in cell motility encompass cell protrusion, polarization, retrograde flow, and the reaction to external factors such as chemical gradients and variations in stiffness [2-4]. Cell motility can be viewed as a problem related to active phase transitions, where cells switch between static and motile states by minimizing a quasi-potential[5]. Cell migration is how living cells demonstrate motility, a process crucial for survival and development[6]. Delving deep into the complex aspects of cell motility enriches our fundamental knowledge of cellular biology and holds promise for creating biomimetic tissues with regulated and guided cell migration. In the lab, systems that explore cancer cell migration are vital for clarifying the underlying metastasis processes and shaping treatment options. These systems represent a variety of techniques, spanning from fundamental

2D¹ evaluations to sophisticated three-dimensional 3D² frameworks, each delivering unique observations regarding the movement of cancer cells. Wound healing or scratch assay is a prevalent 2D technique that offers a direct methodology for investigating cell migration by observing the closure of an artificially induced "wound" within a cell monolayer. This approach proves advantageous for evaluating the invasive characteristics of cancer cells. It has been utilized to construct computational frameworks, such as cellular automata, to model and forecast migratory tendencies predicated on in vitro findings[7, 8]. However, two-dimensional representations commonly fail to accurately depict the diverse TME that naturally exists in vivo. To mitigate these drawbacks, 3D culture methodologies have been instituted, providing a milieu that is more reflective of physiological conditions. The techniques involve multicellular spheroid invasion research, microfluidic device applications, and organoid design setups, which emulate the ECM³ and the TME more effectively. This enhances cancer cell mobility and invasion exploration within a more realistic in vivo-like context[7, 9, 10]. Considerable fascination surrounds microfluidic models for their potential to imitate the changing factors within the tumor microenvironment, enabling researchers to examine collective cell migration and the role of mechanical and chemical gradients in tumor evolution[10]. Innovative strides in microfluidic technology have produced vascularized cancer models that employ hydrophobic surfaces to foster pro-metastatic actions in cancer cells. These models assist in the analysis of extravasation, a crucial aspect of metastasis, by facilitating the observation of interactions among neoplastic cells, endothelial cells, and the extracellular matrix (ECM), within strictly managed environments [11]. Such models have illustrated their ability to link classic in vitro evaluations with in vivo studies, generating more valuable insights for judging therapeutic success. Comparative analyses of various 3D ECM systems have illuminated the significance of matrix composition and architecture in modulating cancer cell migration. For instance, matrices derived from cells, which closely emulate the natural ECM, have been shown to enhance directional persistence and migration efficacy in contrast to reconstituted matrices such as collagen hydrogels[12]. These observations emphasize the critical importance of selecting suitable 3D models that accurately reflect the specific TME under investigation to derive reliable insights into cancer cell behavior. Despite advancements in vitro modeling, challenges persist, including the necessity for

¹ Two-Dimensional (2D)

² Three-Dimensional (3D)

³ Extracellular Matrix (ECM)

standardization and incorporating diverse cell types to replicate the TME fully. Future inquiries should refine these models to augment their predictive capabilities and relevance to human malignancies, ultimately contributing to the development of targeted anti-metastatic therapies[13].

Cell imprinting, a technique that involves creating replicas or imprints of cell surfaces, has significant applications in cancer research. These applications include using bio-imprinted polymer membranes for tumor cell detection, maintaining stem cell stemness during expansion using imprinted substrates [15], enhancing cell-based studies through direct-cell photolithography and optical soft lithography [16], and patterning cells at sub-organelle scales using carbon nanoparticle-polymer composites [17]. These methods are instrumental in understanding cancer cell behavior and developing targeted anti-metastatic therapies.

1.1. Cell-Surface Interactions

Cell surface interactions are crucial for numerous biological processes and the further development of biomaterials for medical applications[14]. The surface's biochemical, physical, and mechanical properties influence these interactions and affect cell attachment, proliferation, migration, and differentiation. The material interface's physicochemical characteristics lead to focal adhesions' reorganization, activating integrin-dependent signaling molecules and eliciting phenotypic alterations, including modifications in the actin cytoskeleton[15]. The lack of ECM elements and specific chemical groups on the substrate surface might either support or hinder cell attachment, leading to cell death[16]. Surface properties such as chemistry and topography are intentionally modified to control the interaction between cells and material. This is critical in developing materials for orthopedic devices and other medical applications[17]. Different substrates, which differ in their material composition, surface stiffness, and energy, affect the rate of cell migration, highlighting the importance of substrate properties for cell behavior[18]. The fundamental processes that control cell adhesion on protein-coated substrates are crucial. The experimental methods available to study the interplay between cells and surfaces emphasize the importance of cell-matrix adhesion and the extracellular matrix in these interactions[19]. In particular, nanostructured surfaces have been observed to significantly influence cell behavior by modulating adhesion, proliferation, and differentiation through physical and chemical properties without introducing chemical functionalities[20]. Interactions between atoms and surfaces can

also become noticeable under certain conditions, influencing resonance lines through broadening and shifting, potentially affecting cell behavior at the atomic level[21]. Ultimately, the complex mechanisms that govern the interplay between synthetic surfaces and biological cells encompass the adsorption of proteins, establishing adhesive connections, and initiating particular cellular responses. Each of these processes is modulated by the nature and abundance of activating surface receptors, as well as the mechanical or topographical characteristics of the substrate.[22].

Cellular responses to mechanical pressures cover numerous important activities for upholding cellular and tissue balance. Cells can perceive and respond to mechanical forces by generating intracellular forces.[4]. Mechanical cues substantially influence fundamental cellular responses such as reorganization of the cytoskeleton, cell differentiation, and movement, thereby impacting tissue development and functionality[23]. Mechanotransduction pathways are initiated by physical elements like mechanical forces, cellular morphology, and properties of the extracellular matrix, which govern cellular activities, including cell proliferation, apoptosis, and differentiation[24]. Moreover, mechanical forces and resultant biochemical signals modulate the phenotype of vascular smooth muscle cells, underscoring the significance of accounting for the microenvironment of the extracellular matrix and the transmission of forces in investigations related to cellular functions[25]. In addition, short-lived mechanical inputs can initiate and adjust cellular movement at a single-cell dimension, yielding essential revelations about the basic mechanisms that govern cellular mobility when subjected to forces[26]. Figure 1 shows the cell response to mechanical and topographical features of different surfaces.

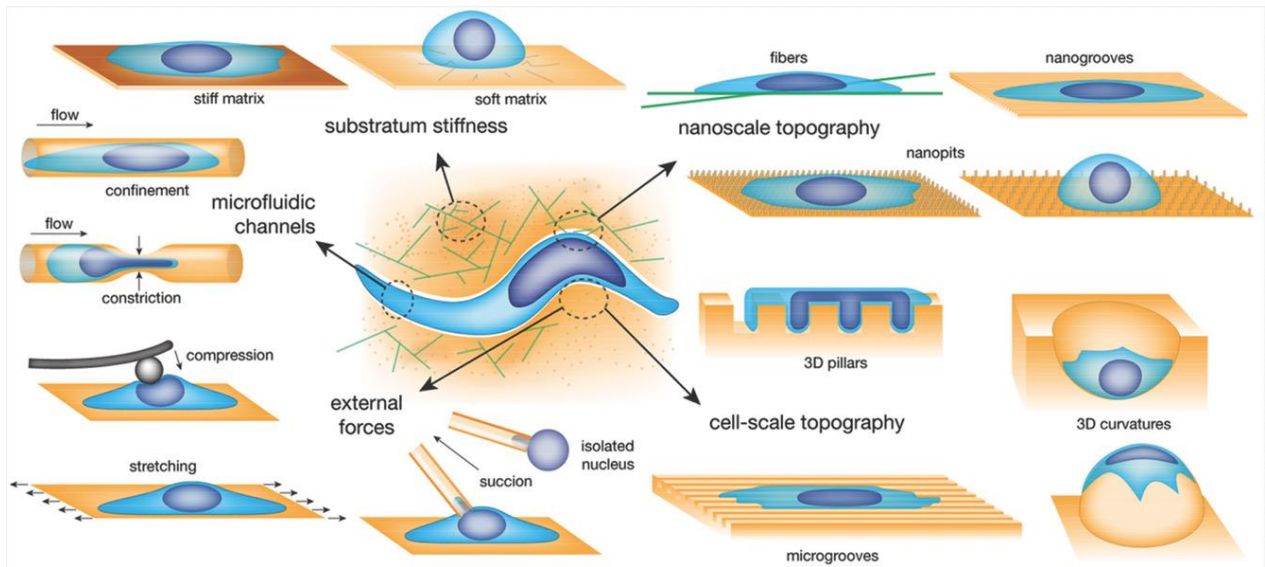


Figure 1. Cellular Responses to Mechanical and Topographical Cues. Numerous methodologies have been devised to investigate the cellular reactions to mechanical and topographical stimuli within their intrinsic milieu. The impact of substrate stiffness on cell behavior can be evaluated through alterations in the artificial matrix modulus. Cellular topographical sensitivity can be examined across various scales using patterned surfaces.[27]. (The image has been adapted with permission from ref.[27]).

1.1.1. Effects of Surface Topography on Cells

Surface topography is essential in determining cellular behavior, impacting various functions such as adhesion, proliferation, migration, differentiation, and gene delivery efficiency. Drawing inspiration from the ECM, contemporary bioprinting scaffold design strives to replicate the native tissue environment to imitate physiological functions, utilizing topographical elements to regulate these cellular behaviors[28]. Notably, alterations in surface topography can significantly influence cell responses, as evidenced by nano topography on rigid surfaces inducing comparable behaviors in neurons and stem cells as observed on softer hydrogels. This indicates that topographic cues may supersede the effects of substrate stiffness via mechanotransduction pathways[29]. Figure 2 schematically illustrates the effect of surface properties on stem cell behavior.

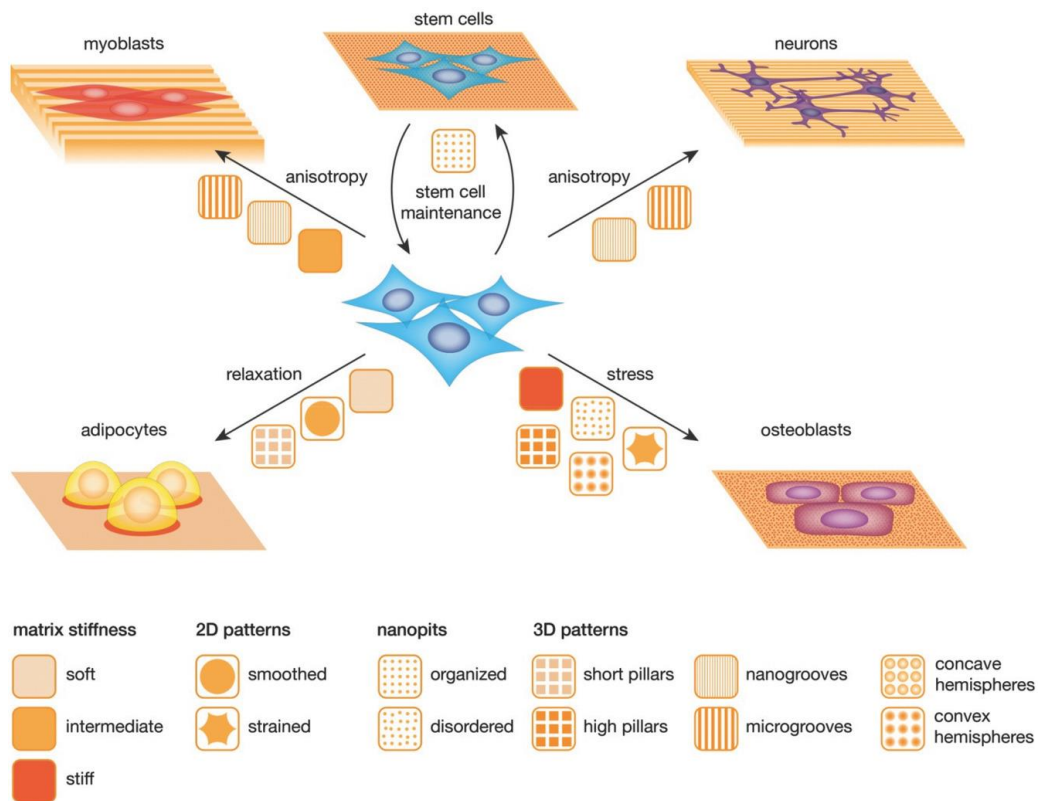


Figure 2. Effect of Matrix Stiffness and Topography. Matrix Stiffness and Topography are influential factors in regulating stem cell behavior. A variety of mechanical and topographical elements modulate stem cell behavior[27]. (The image has been adapted with permission from ref.[27].)

The impact of topography on gene delivery has emerged as an appealing strategy due to its minimal toxicity and localized delivery characteristics, with specific topographic substrates enhancing transfection efficacy depending on the cell type[30]. Moreover, distinct surface relief patterns have been shown to affect cell alignment, elongation, and differentiation, which are crucial for the progress of tissue engineering applications[31]. The intricate interplay between substrate stiffness and surface topography through mechano-transduction pathways underscores a complex regulatory role in cellular behavior[29]. Figure 3 demonstrates the impact of flat and nanostructured surfaces on the cytoskeleton and focal adhesion of cells, leading to variations in cell shape.

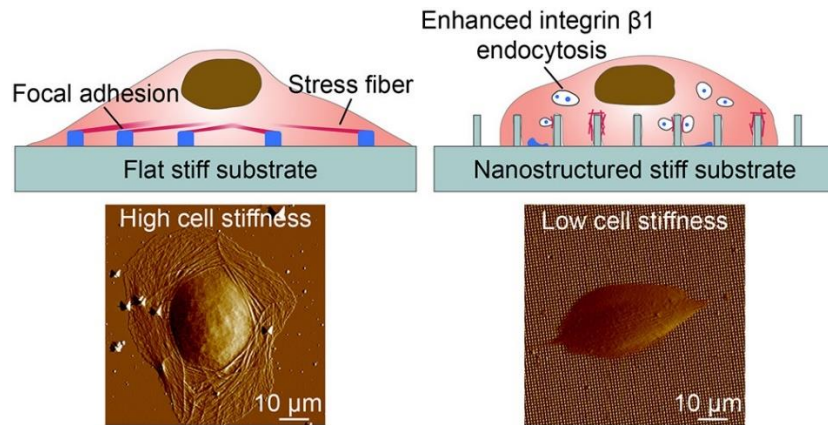


Figure 3. Effect of Mechanotransduction on Biological Mechanisms. The image depicts the biological mechanisms associated with mechanotransduction occurring on both planar and patterned substrates[29]. (The image has been adapted with permission from ref.[29].)

Exploration into surface design for biofilm prevention has revealed that topographical attributes influence the initial stages of biofilm formation by *Staphylococcus* spp., exhibiting bacteriostatic properties and disrupting microcolony morphology[32]. Electrospun scaffolds with controlled fiber surface topography have yielded diverse outcomes in cell-scaffold interactions, with nanopores and roughness promoting cell adhesion and proliferation[33]. Moreover, wrinkled material topographies have negatively influenced endothelial cell responses and monocyte adhesion, impacting inflammation and atherosclerosis development.[34]. Analyses focused on the interplay between mechanotransduction and TGF- β signaling have uncovered that surface designs augment protein phosphorylation and the activation of TGF- β target genes[35]. Lastly, the evolution of varied topographic structures has enriched the comprehension of cell-ECM interactions, emphasizing the substantial influence of surface topography on cellular behavior[36].

1.1.1.1. Nucleus as a Detector of the Cellular Environment

The cell nucleus serves a vital function as a sensor of the cellular environment's topography. It assimilates biophysical signals from the surrounding cellular environment to uphold homeostasis and carry out biological processes. This facet is particularly significant for tissue engineering and regenerative medicine, where comprehending how cells interpret external signals is crucial. The arrangement of nuclear components is essential in regulating gene expression (Fig.4) [27].

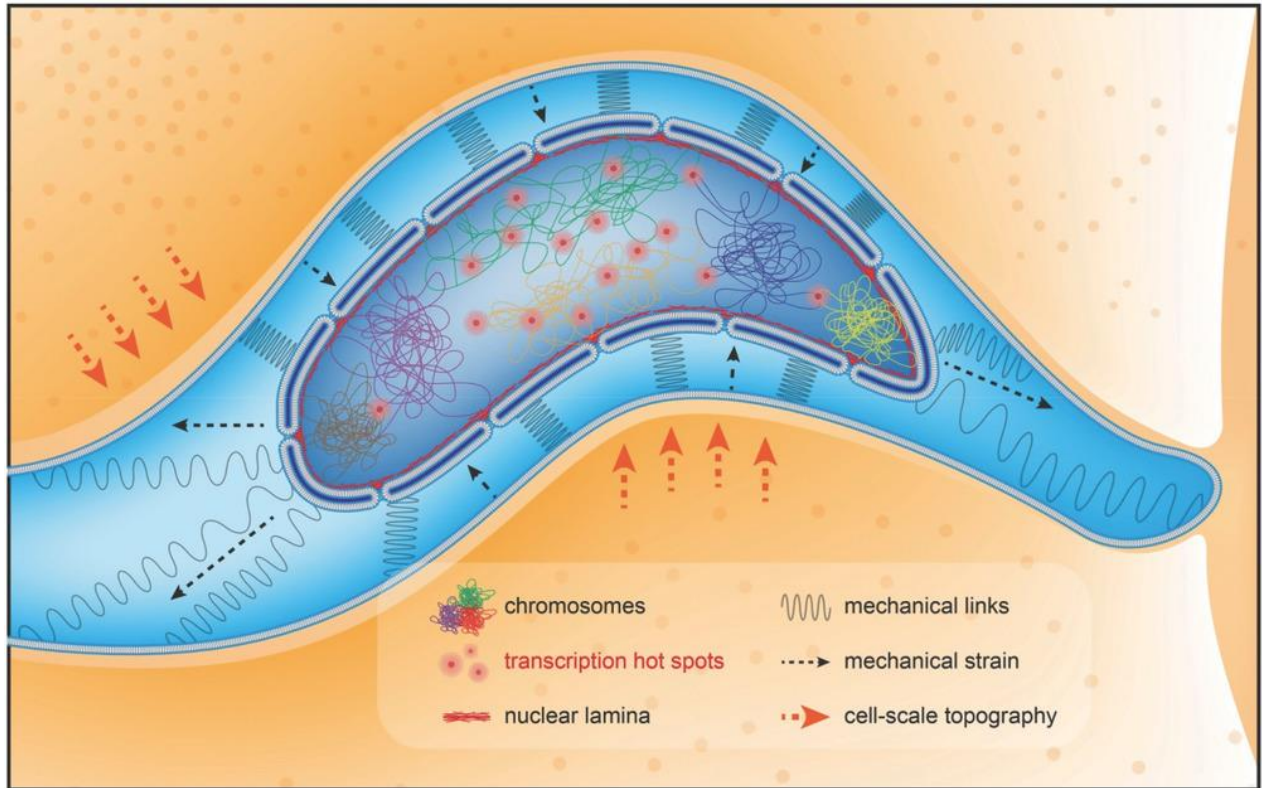


Figure 4. Effect of Mechanical Forces on Chromatin Transcription. Areas within the chromatin characterized by a more relaxed structure typically exhibit increased levels of transcriptional activity[27]. (The image has been adapted with permission from ref.[27].)

The nucleus serves as a non-dissipative gauge for alterations in cellular shape. It allows cells to assess shape changes and adapt their responses to the microenvironment by initiating a calcium-dependent mechano-transduction pathway that regulates actomyosin contractility and migratory flexibility[37]. Various environmental pollutants such as mercury and nanoparticles have been found to affect the nucleus and lead to changes in its configuration and functioning, ultimately negatively impacting cell viability and biodiversity[38]. Using fluorescent proteins targeting the nucleus, methods have been developed to quantify nuclear volume in multicellular 3D structures, indicating that mechanical pressures on the nucleus can influence cell behavior[39]. Mechanical signals transmitted to the nucleus can induce dynamic changes in the nuclear lamina and chromatin organization and thus affect gene expression[40]. The nucleus is acknowledged for its pivotal function in detecting and reacting to variations in the mechanical surroundings by swiftly relaying force through the cytoskeleton to adjust the transcriptional profile of the cell[41]. Studies in zebrafish models have further substantiated the role of the nucleus as an indicator of elastic deformation and shed light on how cells adapt to their physical microenvironment[42]. Abnormal

nuclear shape and lamin B1 displacement have been documented in cells cultured under 3D conditions, suggesting that the extracellular environment can cause significant changes in nucleus behavior and cellular functionality[43]. The role of the nucleus in mechano-sensing similarly encompasses the modulation of gene expression triggered by external factors, underscoring its significance in cellular adaptation. [44]. Ultimately, the nuclear DNA sensors in the innate immune system detect pathogenic DNA, activate antiviral responses, and showcase the nucleus's capability to perceive and react to environmental alterations at the molecular scale[45].

1.2. Cell Migration and Separation

Cell separation refers to isolating and sorting individual cells based on characteristics such as size, physical properties, or specific markers[46-50]. This method is crucial for biological investigations, tissue manipulation, regenerative medicine, and disease detection. Various techniques such as acoustic wave-driven segregation, electrokinetic systems based on insulators, and natural botanical processes such as abscission and dehiscence are used for cell isolation. The main goal of cell separation is to achieve high purity, recovery, and viability of the separated cells, which serve as a prerequisite for careful examination and possible therapeutic use. Advances in cell separation methods are driven by the need to study scarce cells for precision medicine, a practice that tailors treatments to individual patients based on specific characteristics[51]. In biomedical research and biotechnology, cell sorting is an essential process that involves separating different cell mixtures into homogenous populations[52]. Several methods have been developed to enable effective cell sorting, such as image-activated cell sorting using spatially resolved cell features, robotic manipulation in conjunction with microfluidic chip technology[53], and refinement of algorithms to optimize cell sorting[54]. Research shows that the procedures associated with cell sorting have minimal impact on downstream cellular applications, preserving the integrity of segregated cell populations for further investigation. The dynamics of cell sorting are highly influenced by differential adhesion and kinetic principles, with power-law scaling evident in the diffusion and fusion of cell domains during the sorting process[50]. These advances in cell sorting play a critical role in isolating specialized cell types with increased purity and efficiency used for various research and medical purposes.

Cell movement is a process in living organisms playing a role in various biological functions, like growth, healing, immunity, and disease development. The methods that manage cell migration

encompass the spatiotemporally regulated dynamics of the actomyosin cytoskeleton, the modulation of receptor expression, and the response to chemokine gradients[55, 56]. Cellular migration can occur individually or collectively as cells adjust their migratory strategies and interact with other cells and the extracellular matrix to address environmental challenges[57]. Migration is influenced by diffusible molecules, surface-bound molecules, mechanical forces, and electric fields, to which different cell types exhibit specific responses. It involves three crucial phases: cell polarization, protrusion, adhesion development, and rear retraction(Fig.5) [58]. This detailed process entails the organization of microtubule dynamics, actin-myosin contraction, and the recycling of adhesion complexes to support cell motion[59]. A thorough comprehension of cell migration is crucial for understanding various physiological phenomena and diseases, underscoring the necessity for further research in this domain.

Two types of cell migration, namely single and collective cell migration, represent fundamental processes in diverse biological phenomena. Individual cells exhibit independent movement within single-cell migration, while collective migration entails the coordinated motion of cell groups[60-63]. Research indicates that leader cells in collective migration play a pivotal role in guiding follower cells, thus enhancing the overall migratory capabilities of the cell populace. Besides, the mechanical traits of cells, including actin dynamics and intercellular adhesion, play a role in single-cell and collective migration. Additionally, the formation of collective sensory units could enhance chemotaxis efficiency in cell clusters, enabling them to surpass single cells in detecting signaling irregularities. Understanding the processes that control individual and group migration is crucial for exploring phenomena such as tissue formation, healing of wounds, and cancer metastasis [64].

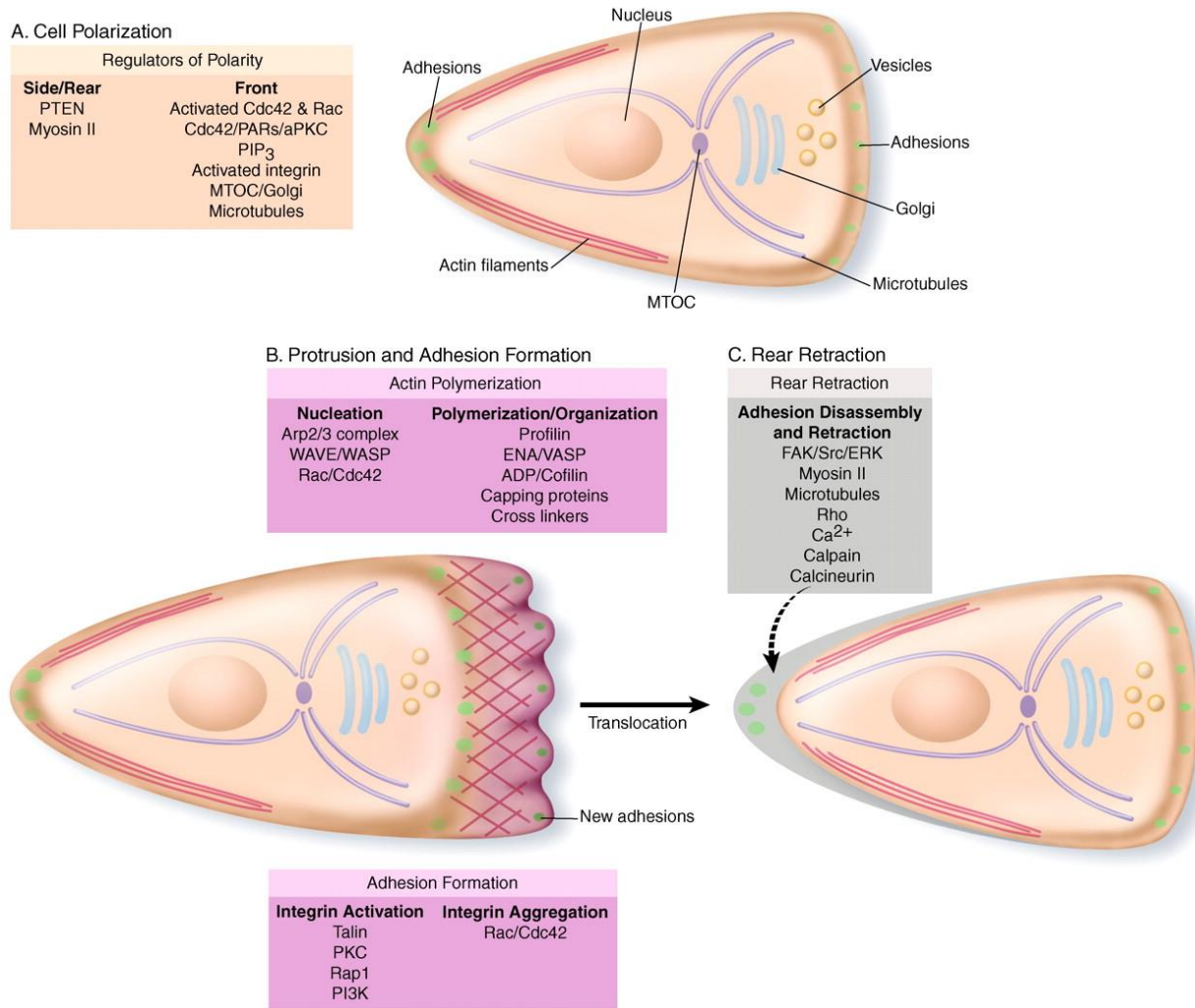


Figure 5. Cell Migration Steps. Cell migration has essential steps: **A)** Cell Polarization, **B)** Protrusion and Adhesion formation, and **C)** Rear Retraction. Inherent polarity plays a crucial role in guiding a migrating cell. Factors such as Cdc42, Par Proteins, and Protein kinase C are significant in establishing polarity, engaging various proteins that aid directed vesicle trafficking toward the leading edge, and organizing microtubules and organelles. The migration process is initiated by the formation of protrusions. Stabilizing adhesion is essential for the sustainability of protrusions, requiring the activation of integrins, their clustering, and the incorporation of necessary components. The activation of integrins is prompted by talin binding and is facilitated by Protein kinase C, Rap1, and Phosphoinositide 3-kinase. These pathways, along with other molecular interactions and microtubule-driven processes, are vital for the disassembly of adhesions at the rear and behind the leading edge at the front of the cell[58]. (The image has been adapted with permission from ref.[58].)

1.2.1. Single-Cell Migration

Single-cell migration is essential in various biological processes, including cancer biology, immune response, and embryonic development. Research has shown that single cells and cell clusters exhibit heterogeneous migration behavior[65, 66]. Studies have used advanced technologies like microfluidics and high-speed imaging to track and analyze individual cells' migration patterns[67, 68]. Comprehending the molecular mechanisms that govern the migration of individual cells is crucial for the examination of cancer metastasis, immune system responses, and tissue development[67]. By examining the intricate signaling pathways and the dynamics of protein interactions that govern cellular migration, scholars can understand the multifaceted relationships between molecular mechanisms and cell behavior at the individual cellular level. Such discoveries enhance our knowledge of the processes underlying cell migration and facilitate the formulation of innovative therapeutic approaches to modulate cellular migration in diverse pathological states.

1.2.2. Collective Cell Migration

The systematic relocation of interrelated cellular formations, called collective cell migration, is vital in various biological occurrences, encompassing embryonic development, tissue restoration, and cancer metastasis[69-72]. Cell populations possess the ability to migrate collectively in cohesive sheets, continuous streams, or dense clusters, with the dynamics of cell-environment interactions significantly influencing their migratory patterns[73]. The spatiotemporal gradients of extracellular signaling molecules, cell-cell adhesions, and environmental signals control this complicated phenomenon. Collective migration ensures the precise arrangement of tissues during the organism's development and can also contribute to pathogenic conditions such as tumor proliferation and spread [74]. A thorough comprehension of the fundamental molecular mechanisms and cellular dynamics that govern collective cell migration is critical for elucidating the processes associated with tissue development and disease advancement. Figure 6 illustrates how cells exhibit migration either individually or in collective arrangements.

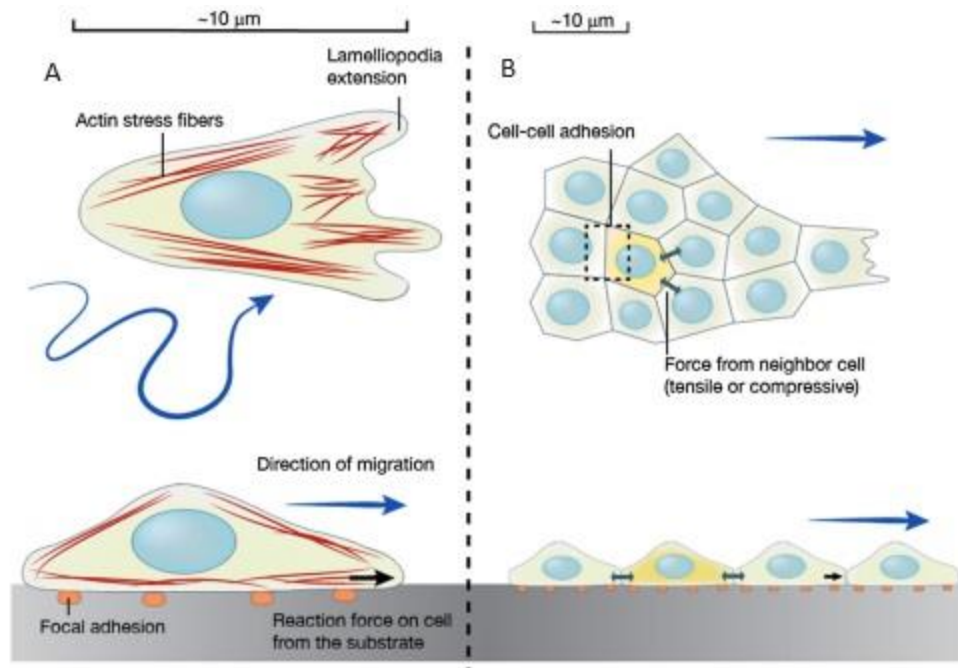


Figure 6. Single and Collective Cell Migration. Cells exhibit both single and collective migration patterns. **A)** single-cell migration is characterized by a persistent random walk, which includes processes such as lamellipodia extension, cell body contraction, and adhesion to the substrate via focal adhesions. **B)** Conversely, when cellular entities traverse in congregations, they exhibit a more purpose-driven locomotion. This collective translocation is modulated by the supplementary constraint of intercellular adhesion, which enhances the propagation of forces among adjacent cells[75]. (The image has been adapted with permission from ref.[75].)

1.2.3. Cell Migration in 3D

Cell migration in 3D environments entails intricate processes influenced by various factors. Empirical studies indicate that cellular entities within three-dimensional hydrogel environments demonstrate pronounced downward motility, a phenomenon attributable to self-induced chemotactic gradients orchestrated by the MAPK and TGF- β signaling cascades[76]. Analysis tools such as Migrate3D facilitate the assessment of cell migration by analyzing tracking data and providing biologically meaningful results[77]. The study of immune response and cell migration was performed using microfluidic methods, revealing differences in T lymphocyte velocity between restricted and 3D migration scenarios[78]. Understanding cellular migration in 3D environments compared to 2D surfaces is of utmost importance as it involves traversing different microenvironments that influence movement dynamics at both micro and macro levels[79]. Crucially, mechanisms such as non-muscle myosin II activity play a central role in maintaining 3D cell migration by generating essential mechanical forces[80].

1.2.4. Cell Migration and Surface Properties

The correlation between cell migration and surface characteristics is intricate, encompassing the interaction of mechanical, chemical, and topographical attributes that impact cellular activity. Cell migration is affected by surface features such as topography, material composition, and surface energy. These features impact cell speed, shape, spreading, and traction forces. For example, cells demonstrate distinct movement patterns on surfaces with different topographies, such as nanopillars, silicon oxide, and titanium oxide, where nanopillar surfaces enhance cell elongation and movement speed through heightened cell traction forces[81]. Similarly, the geometric configuration of three-dimensional printed surfaces significantly influences the behavior of mesenchymal stem cells, where concave surfaces facilitate cellular migration and convex surfaces enhance osteogenic differentiation, thereby implying that forces contingent upon curvature affect nuclear dynamics and cellular migration[82]. The intricacy of cellular migration is accentuated by the extracellular matrix's participation and the ambient environment's biomechanical characteristics, which may facilitate extensive mechanical linkages among cells and direct coordinated cellular migration by modifying substrate deformation patterns.[83, 84]. Surface and nano topography also guide cell movement, with specific designs aiding directional movement and influencing cell velocity[85, 86]. The impact of three-dimensional geometric cues, like surface curvature, on cell movement and differentiation behavior further demonstrates the intricate relationship between cell conduct and surface attributes, with notable implications for tissue repair and biomaterial development.[82]. In addition, the design of substrates replicating the ECM has revealed that tailored surface chemistries can prompt specific cellular responses, such as attachment and movement, crucial for various biological functions[87]. Lastly, establishing protein density gradients on surfaces shows promise in guiding cell movement, providing valuable insights into angiogenesis and the formulation of tissue-engineered structures[88]. These inquiries highlight the crucial importance of surface dynamics in shaping cellular behavior, affecting diverse sectors, including biomaterials science, tissue engineering, and regenerative medicine.

1.3. MCF7, MDA-MB-231 and 3T3 Cell Lines

The hallmark of cancer cells is the presence of genetic alterations that lead to irregular cellular activity, proliferation, and spread to distant sites. These malignant cells exhibit characteristics such as continuous growth, evasion of the immune system, and increased formation of new blood vessels[89]. Breast cancer is a neoplastic growth arising from cells within the mammary gland, predominantly impacting females but with potential occurrence in males as well. The process initiates when specific breast cells undergo aberrant changes, leading to uncontrolled proliferation and the formation of a tumor. Predominantly, the cells originating from breast malignancies are responsible for milk secretion and ductal transport, although a minority may stem from adipose or fibrous tissue[90, 91]. The classification of breast cancer hinges on its invasive nature; non-invasive forms confine themselves to the ducts or lobules, while invasive types infiltrate surrounding healthy tissues outside the breast parenchyma[92]. Ranking second in the mortality statistics of malignancies affecting women, next only to lung cancer, breast cancer manifests through diverse clinical signs like palpable masses, alterations in breast contour or dimensions, and nipple discharge[93]. Incidence and fatality rates of this disease exhibit considerable global disparity, with higher prevalence in developed nations compared to less affluent regions. It poses a substantial public health concern worldwide, with millions of fresh diagnoses reported yearly [94]. Factors contributing to the danger of developing breast cancer encompass advancing age, genetic predisposition, lifestyle choices, endocrine imbalances, and exposure to estrogenic compounds[95]. Diagnostic approaches typically entail radiographic assessments, clinical breast evaluations, imaging modalities, and histopathological sampling[96]. The choice of therapeutic measures depends on the histologic subtype and stage of disease and includes surgical procedures, cytotoxic agents, radiotherapy, and endocrine-disrupting drugs. Efforts to prevent health issues stress the importance of modifying lifestyle behaviors, like lowering alcohol intake, achieving a balanced body mass index, and embracing a diet high in fruits and vegetables. Breast Cancer Awareness Month constitutes an international campaign to enhance public understanding of the disease and obtain financial resources for its initiatives.

MCF-7 cells represent a well-established human breast cancer cell line that has been extensively studied for over 45 years. The pivotal role of these cells in shaping the landscape of breast cancer research, influencing both outcomes and progress within the discipline, cannot be overstated[97, 98]. Researchers have examined various aspects of MCF-7 cells, including their responses to

multiple stimuli. Findings propose that MCF-7 cells will likely face pyroptosis due to the action of substances released by mesenchymal stem cells harvested from human umbilical cords, resulting in their eventual demise [99]. In addition, the utility of MCF-7 cells extends to the study of resistance mechanisms associated with breast cancer therapy, as demonstrated by the photodynamic therapy studies in which resistant cell populations were developed and characterized[100]. Ultimately, the importance of MCF-7 cells as indispensable tools for understanding breast cancer biology, treatment responses, and resistance mechanisms cannot be overlooked.

MDA-MB-231 cells are triple-negative breast cancer cells, meaning they do not have estrogen, progesterone, or HER2 receptors. In other words, hormonal therapies and HER2-targeted therapies are not effective on them[101]. The unique features of these cells include a heightened ability to spread and renew themselves, both of which contribute to their aggressive nature and poor outlook in individuals with breast cancer[102, 103]. The transition from epithelial to mesenchymal phenotype identified in MDA-MB-231 cells is correlated with augmented migratory and invasive attributes, which is crucial for metastatic progression[104]. Additionally, these cells release exosomes, small vesicles implicated in intercellular signaling and capable of promoting both metastasis and resistance to chemotherapy. Their notable resilience to antineoplastic agents in 3D spheroid cultures, as opposed to 2D cultures, underscores the intricate microenvironment and drug resistance mechanisms they possess[105]. MDA-MB-231 cells collectively assume a pivotal position as a fundamental model for uncovering the biology of aggressive breast cancer and designing innovative therapeutic strategies.

3T3 cells represent a category of cell lines widely used in various research fields. These distinctive cells are derived from mouse embryonic fibroblasts. They are critical in cellular biological research owing to their capacity to proliferate in consistent monolayers, rendering them ideal for experimental cell culture applications[106, 107]. Research on 3T3 cells has been thoroughly conducted in various scenarios and has included studies on transformation processes, patterning of stress fibers, and their function as support cells for keratinocytes[108]. In addition, these cells are used in studies on calcium entry through various receptors, highlighting their importance in elucidating cellular communication pathways[109]. Overall, 3T3 cells represent valuable tools in biomedical research and provide useful insights into cell behavior, culture studies, and signaling mechanisms.

1.4. Cell Imprinting

Cell-imprinted substrates act as novel platforms that control cell behavior and differentiation by mirroring the topographical features of the cell membrane at the micro- and nanoscale (Fig.7). These substrates are fabricated using techniques such as photolithography and templating of cell morphology and mimic the physical conditions that cells encounter in their natural environment[110]. The surface morphology of these substrates, encompassing variables such as height, spatial characteristics, and composite roughness attributes, exerts a paramount influence on regulating stem cell differentiation into cellular lineages. This highlights the substantial impact of lineage-specific nanostructural topography on determining stem cell fate[111]. PDMS⁴ is extensively utilized in the fabrication of cell-imprinted surfaces owing to its capacity to replicate the natural environment, its economic efficiency in small-scale manufacturing, and its excellent compatibility with biological tissues. Nevertheless, plasma treatment, chemical customization, and ECM coating are crucial to increasing cell adhesion and imprinting efficiency[112]. Research has confirmed the potential of these components to maintain ADSCs' undifferentiated state over extended culture periods, reducing unwanted differentiation while preserving their ability to proliferate.[113]. In addition, cell-imprinted substrates have demonstrated their efficacy in preparing human adipose-derived stem cells for neural differentiation even without chemical inducers, demonstrating their potential in regenerative medicine[114]. The integration of cell-imprinted substrates into microfluidic systems has been investigated to improve the efficacy of imprinting and enable precise control of cell targeting and differentiation[115]. Ongoing investigations have broadened the application of cell-imprinted platforms to stimulate keratinocyte-like differentiation in mesenchymal stem cells. This exemplifies these substrates' adaptability in designing tailored microenvironments and surface characteristics for various cellular phenotypes[116]. In addition, using liquid crystalline networks with different surface topographies effectively influences cell orientation and differentiation and represents an alternative to traditional lithographic patterning[117].

⁴ Polydimethylsiloxane (PDMS)

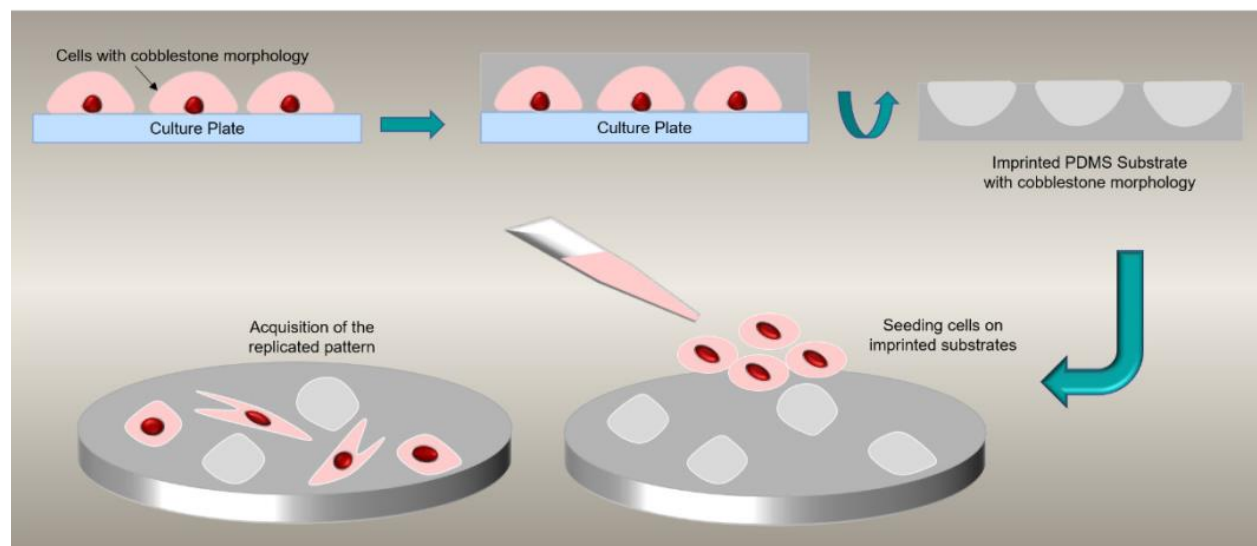


Figure 7. Cell Imprinting Schematic. A schematic representation of the cell imprinting process. The seeded cells obtain the replicated morphologies [118]. (The image has been adapted with permission from ref.[118].)

Cell imprinting is a versatile and innovative method in which the surface of a cell is replicated on a physical or chemical level to capture its topographical and molecular properties. This technique is used in various fields, e.g., cell culture, stemness, disease modeling, drug or particle toxicity assays, etc. (Fig.8). In the field of stem cell research, the employment of cell imprinting has revealed its effectiveness in upholding the undifferentiated characteristic of cells ADSCs⁵ through the creation of substrates that echo the original microenvironment of the cells. This secures their potential to proliferate without experiencing undesirable differentiation[113]. In a study by Mahmoudi and Parak, they successfully created surfaces that mimic the shapes of mature and dedifferentiated chondrocyte cells. When applied as templates, these substrates may steer the differentiation of rabbit ADSCs into defined cellular forms by reflecting their structure and gene activity profiles[119].

⁵ Adipose-Derived Stem Cells (ADSCs)

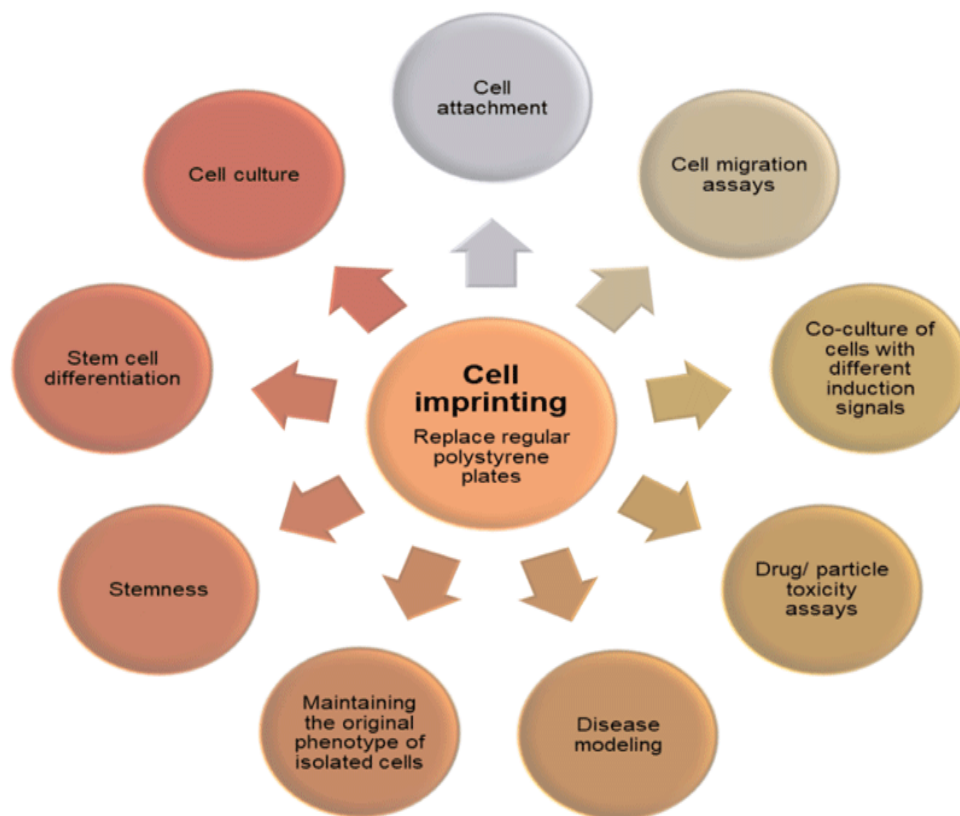


Figure 8. Cell Imprinting Applications[118]. (The image has been adapted with permission from ref.[118].)

Special cell imprinting techniques have also been developed in cancer diagnosis to accurately identify and detect tumor cells using bio-imprinted polymer membranes as sensors to differentiate cells based on subtle variations in surface proteins at the nanoscale. Another notable application of cell imprinting is cell imprinting lithography, which can be used to create biomimetic culture substrates capable of controlling cell adhesion and differentiation, essential for advances in tissue engineering and regenerative medicine[120]. In addition, cell imprinting has significantly enriched cell-based research by altering surface properties to control stem cell differentiation[121]. It also contributes to understanding genomic imprinting disorders such as Beckwith-Wiedemann syndrome by providing models for studying epigenetic control and gene expression in a parental-specific manner[122]. In tissue engineering, cell imprinting has facilitated the development of scaffold-free cell layers by mimicking the natural organization of tissues for applications in regenerative medicine[123]. The adaptability of this technique also extends to the production of specialized sensor materials for the detection of microorganisms or cells, highlighting its potential for diagnostic procedures and the monitoring of physiological functions[124]. The proposal of cell-imprinted biomimetic interfaces for effectively detecting

circulating tumor cells, integrating natural and synthetic antibodies to enhance detection capabilities, demonstrates the potential of this approach[125]. Furthermore, substrates imprinted with cellular structures possess the capacity to elicit distinct cellular characteristics, thereby presenting a novel avenue for the modulation of cellular phenotypes in vitro, which holds considerable ramifications for therapeutic strategies predicated on cellular applications[126]. Finally, imprinting extends to epigenetic gene regulation, influencing gene expression determined by parental origin and providing a framework for studying allelic variations in transcription and epigenetic processes[127]. In summary, the importance of ECM topography to cell behavior, including morphology, migration, adhesion, proliferation, and differentiation, underscores the significance of duplicating biomimetic topography in laboratory environments. It has been demonstrated that the effectiveness of contact guidance in aligning cells depends on the geometry of topographic cues, whereby sub-micrometer features on grooves can reduce the effectiveness of contact guidance by microgrooves by enhancing cell adhesion[128]. Therefore, cell-imprinted substrates play a critical role in controlling cells by providing physical cues that mimic the natural cellular environment and thus influence cell morphology, orientation, and differentiation by mimicking specific topographical features[129].

1.5. Quantum Dots

QDs⁶, are tiny semiconductor particles that exhibit unique optical and electrical properties due to quantum mechanical phenomena. These particles are characterized by their ability to confine excitons in three spatial dimensions, resulting in discrete energy levels similar to those in atoms, thus earning the nickname "artificial atoms"[130]. The dimensions of these quantum dots, ranging from a few nanometers to numerous micrometers, directly affect their emission color under Ultraviolet irradiation. Quantum dots of smaller dimensions exhibit violet luminescence in the electromagnetic spectrum, while those of greater dimensions radiate in the red spectrum[131]. This size-dependent emission is due to the quantum confinement effect, which allows precise modulation of the electronic and optical properties of QDs by adjusting their size, morphology, and material composition[132]. Quantum dots exhibit a core-shell configuration, where the core serves as the framework, and the shell enhances the photonic properties and durability of the QDs[133]. These nanomaterials are composed of various semiconductor elements, including

⁶ Quantum Dots (Qdots)

groups II-VI and III-V, which promotes their extensive applicability in domains including photovoltaic technology, electroluminescent devices, and biological and medical disciplines [134]. In the medical field, quantum dots are being investigated for their potential in imaging, diagnostics, and therapeutic delivery due to their intense luminosity, resistance to photobleaching, and customizable optical properties[135, 136]. Despite their promising applications, the toxicity associated with certain QDs materials hinders their clinical use. This highlights the need for further research into safer alternatives and surface modifications to address these concerns[133, 137].

1.5.1. Core/Shell Cadmium Selenide/Cadmium Sulfide QDs

CdSe/CdS⁷ QDs are unique semiconductor nanocrystals characterized by a layered core/shell structure with cadmium selenide at the center and cadmium sulfide surrounding it. This structural configuration significantly augments their optical and electronic attributes, rendering them particularly advantageous for various applications within quantum technologies and optoelectronics domains. The distinctive characteristics of CdSe/CdS QDs, including their emission contingent on size, elevated photoluminescence efficiency, and robust stability, are intrinsically linked to the core/shell framework. During our forthcoming dialogue, we will explore the combination, traits, and functions of CdSe/CdS QDs and review the likely difficulties and opportunities for upcoming inquiries. Recent breakthroughs have facilitated the emergence of colossal CdSe/CdS QDs, exhibiting dimensions that range from 30 to 100 nm. These QDs are synthesized stepwise using a continuous injection at elevated temperatures, which fosters the development of substantial CdS shells surrounding the CdSe cores. This approach culminates in QDs possessing a hexagonal diamond morphology, enhancing their photoluminescence lifetimes while mitigating blinking phenomena at ambient temperature [138]. The thickness of the CdS shell is a pivotal determinant of the stability and the optical characteristics of the QDs. Increased shell thickness contributes to the reversibility of alterations in optical properties when subjected to electron injection while also averting lattice degradation during hole injection, thereby augmenting the stability and luminescence efficiency of the QDs [139]. Recognized for their enduring photoluminescence and outstanding single-photon emission characteristics, CdSe/CdS quantum dots are perfect for implementation in quantum photonics. The emission characteristics can be finely adjusted through variations in the size and composition of the QDs, thereby allowing for meticulous control over their optical properties[138]. The electronic states inherent to CdSe/CdS QDs are shaped

⁷ Cadmium Selenide/Cadmium Sulfide (CdSe/CdS)

by the core/shell configuration, which can be conceptualized as layered systems possessing distinct energy band gaps. This structural arrangement enables the establishment of electronic states characterized by two energy gaps, thereby amplifying their applicability in optoelectronic realms[140].

1.5.1.1. CdSe/CdS QDs Bioimaging Applications

Due to their pronounced and stable fluorescence characteristics, CdSe/CdS quantum dots are widely utilized in cellular imaging. They can be meticulously engineered to emit light at defined wavelengths, thereby facilitating the high-resolution visualization of cellular architectures and dynamic processes[141, 142]. The biosynthetic production of CdSe quantum dots utilizing recombinant bacterial systems has demonstrated promising outcomes in generating quantum dots with commendable biocompatibility and fluorescence attributes, rendering them appropriate for applications in cellular imaging[141]. Integrating CdSe quantum dots into bio-nano hybrid systems, including gelatin-based matrices, significantly enhances their potential as contrast agents for cellular labeling, establishing a straightforward and efficacious methodology for cellular imaging[142]. By engaging with metallic nanoparticles like gold, the photoluminescent traits of CdSe quantum dots can see considerable enhancement. This enhancement emanates from the interaction phenomena between the excitonic states of the quantum dots and the surface plasmon resonance fields of the metallic substrate, which serves to augment the photoluminescence intensity and refine imaging efficacy. Such enhancements are pivotal for advancing more effective bioimaging devices, as they facilitate improved signal detection and imaging resolution[143].

Biocompatibility and Safety The cytotoxicity associated with CdSe quantum dots constitutes a paramount consideration for their application in bioimaging. Empirical studies have indicated that hybrid nanocomposites comprising CdSe and silver demonstrate diminished toxicity compared to pure CdSe quantum dots, rendering them safer for biological applications. The capacity to synthesize CdSe quantum dots characterized by low toxicity and high luminescence is critical for their deployment in medical diagnostics and therapeutic interventions, ensuring minimal adverse effects on living cells during imaging procedures[144]. The distinctive optical characteristics of quantum dots, such as their resilience to photobleaching and stable emission profiles, endow them with advantages over conventional fluorophores, thus providing prolonged imaging capabilities

that are essential for single-molecule investigations[145]. In bioimaging, incorporating CdSe/CdS quantum dots provides substantial benefits, yet the questions about their biocompatibility and the threats posed by heavy metals like cadmium remain. Ongoing investigative efforts address these concerns by developing safer synthetic methodologies and exploring alternative materials, such as carbon quantum dots, which proffer analogous optical properties with diminished environmental and health hazards. These initiatives are vital for extending the applicability of quantum dots in bioimaging and ensuring their safe utilization in medical and biological research[145].

1.6. Fluorophores

Fluorophores are many compounds that exhibit fluorescence, characterized by light absorption at a particular wavelength and subsequent re-emission at another, often longer, wavelength. These compounds include inorganic variants of elements dissolved in an inorganic crystal lattice, including Mn, Ce, Pr, Nd, Sm, Eu, Tb, Dy, and Yb, implying a wide range of potential fluorophores with different emission properties.[146]. Conversely, organic fluorophores encompass a broad spectrum of molecules ranging from simple organic dyes to complicated biological compounds. Cyanine dyes, for example, known for their use in photography and as fluorescent markers in biological studies, form a category of organic fluorophores with tunable absorption properties that cover the visible spectrum[147]. Fluorophores are indispensable in fluorescence spectroscopy and imaging. They serve as fundamental components that interact with light to elicit fluorescence. This interaction is essential to understanding the behavior of substances that exhibit coloration or luminescence when excited[148].

1.6.1. Cell Staining with Fluorophores

Fluorescent dyes are used extensively in biological and medical research to stain cells. Their unique properties are used to observe and study cellular and molecular processes with precision and specificity. A significant cause is the visualization of living cells with a resolution beyond the diffraction limit. This facilitates tracking individual biomolecules within cells using single-molecule localization microscopy[149]. This method is enhanced using fluorophore-labeled antibodies for cell staining, surpassing conventional microscopy's resolution limitations by detecting the light emitted by excited fluorophores, enabling the detailed study of subcellular components[150]. In addition, enzyme-based self-labeling tags have been developed to label

proteins in living cells with synthetic small molecules, allowing visualization of protein distribution in the cells by fluorescence microscopy. This labeling methodology further facilitates the ensuing segregation of proteins and exemplifies the myriad applications of fluorophores in the realms of visualization and biochemical assessment[151]. In addition, carbocyanine dyes have the potential to be used as fluorescent markers for nucleic acids. They offer high resistance to photobleaching and high cell compatibility. This is crucial for in vivo applications and possibly targeted cancer therapy due to their selective toxicity towards certain cancer cell lines[152]. The combination of aptamers with fluorophores in super-resolution microscopy, such as Stimulated Emission Depletion, enables the exploration of receptor nanodomain arrangements and the endocytic pathway, highlighting the role of small, monovalent affinity probes in overcoming limitations imposed by steric hindrances in traditional staining methods[153]. Fluorescent cell labeling also benefits high-content imaging assays that enable systematic and precise evaluation of drug candidates by evaluating specific cellular and molecular signals[154]. Labeling neurons in vivo using genetically targeted membrane-binding fluorescent dyes covalently provides a rapid and efficient approach to observing neuronal structure in living brains. It facilitates anatomical comparisons and studies of brain function[155]. Photoactivatable fluorophores allow spatial and temporal fluorescence control, enabling real-time monitoring of dynamic cellular events and visualization of structural details with nanometer precision. These are critical for understanding cellular processes and structures at the molecular level[149]. The extensive use of fluorescence in diagnostics and basic life science research is demonstrated by its role in monitoring living cells and analytical methods for detecting and quantifying nucleic acids and proteins[156]. The development of rhodamine dyes for light-sensitive staining represents a new method for the microscopic examination of biological tissue and enables the optical detection of specific features in biological samples and the visualization of intracellular transport[157]. These different applications underline fluorophores' versatility and importance for better understanding biological systems and developing diagnostic and therapeutic tools.

This research seeks to examine the influence of substrates that are imprinted with cellular structures on the migration of MCF7, 3T3, and MDA-MB-231 cells to assess the potential of cell imprinting techniques for cell separation and sorting in laboratory settings (in vitro). To track the movement of the cells, they were tagged with PMA⁸-Coated CdSe/CdS QDs (Red) and Hoechst

⁸ Poly(isobutylene-alt-maleic anhydride)-graft-dodecyl (PMA)

fluorophores (Blue), and their migratory behavior and selection of pathways were examined over various surfaces.

Chapter 2:
Experimental Part

2.1. Materials

Dulbecco's Modified Eagle Medium (DMEM)-High Glucose (D6429-500ML, SIGMA, United Kingdom) which was supplemented with 10% FBS⁹ (F9665, Gibco, United Kingdom), and 100U/mL Pen/Strep¹⁰ (15140-122, Gibco, United States) was used to culture MCF7, MDA-MB-231 and 3T3 cells. PBS¹¹ (18912-014, Gibco, UK) was employed for cell washing pre-dissociation, and the cell detachment from the culture flasks was carried out using Trypsin-EDTA¹² (25300-054, Gibco, United Kingdom). The cells were immobilized for cell imprinting and imaging using Glutaraldehyde (G6257, SIGMA, Germany) and Paraformaldehyde (158127-500G, SIGMA, Germany) at a concentration of 4%. Distinguishing between dead (blue labeled) and live (colorless) cells was achieved using Trypan Blue solution 0.4% (15250061, Invitrogen, United States). Also, PDMS (1673921, SYLGARDTM184 Elastomer 1.1 Kg Kit, Dow Corning, Germany) was utilized for imprinting the cells' morphology. To facilitate more effective cell tracking, cells were discriminated by employing Hoechst 33342 (H1399, Invitrogen, United States) and CdSe/CdS QDs solutions at 5 µg/ml and 5nM concentrations. To coat the QDs with the polymer, Poly (isobutylene-alt-maleic anhydride) was dissolved in chloroform (Roth, Germany), and then the anhydride rings were hydrolyzed using sodium hydroxide (Roth, Germany) buffer. The materials' information summary is presented in Table 1.

⁹ Fetal Bovine Serum

¹⁰ Penicillin/Streptomycin (Pen/Strep)

¹¹ Phosphate-buffered Saline (PBS)

¹² Ethylenediaminetetraacetic acid (EDTA)

Table 1. Materials' Information Summary.

Reagent Name	Supplier	Country	CAT No.	Stock Solution	Final Concentration
DMEM-High Glucose	SIGMA	United Kingdom	D6429-500ML	1x	1x
FBS	Gibco	United Kingdom	F9665	10x	1x
Trypsin-EDTA	Gibco	United Kingdom	25300-054	0.05%	0.05%
Pen/Strep	Gibco	United States	15140-122	10,000U/mL	100U/mL
PBS Tablets	Gibco	United Kingdom	18912-014	-	0.01 M
SYLGARD™184 Elastomer 1.1 KG Kit	Dow Corning	Germany	1673921	-	-
Sodium Hydroxide Powder	Roth	Germany	6771.1	-	0.1M
Glutaraldehyde	SIGMA	Germany	G6257	25%	4%
Paraformaldehyde Powder	SIGMA	Germany	158127-500G	-	4%
Trypan Blue	Gibco	United States	15250061	0.4%	0.4%
Hoechst 33342 (Bisbenzimidazole)	Invitrogen	United States	H1399	10 mg/mL	5µg/ml
CdSe/CdS QDs	Fraunhofer IAP	Germany	Cd-0-288-2fz	100nM	5nM
Crystal Violet	SIGMA	Germany	548629	-	0.5%
Presto Blue	Invitrogen	Germany	A13261	10x	1x
Poly (isobutylene-alt-maleic anhydride)	SIGMA	Germany	531278	-	-
Hydrochloric Acid	Roth	Germany	7647-01-0	37%	2%
Chloroform	Roth	Germany	67663	99%	-

2.2. Methods

2.2.1. Cell Culture

In summary, 1×10^6 MCF7 (ATCC HTB-22), MDA-MB-231 (ATCC HTB-26), and NIH/3T3 (CRL-1658) cells were cultured in two T75 cell culture flasks (Thermo Fisher Scientific) with 10ml DMEM-high glucose, supplemented with 10% FBS and 100 U/mL Penicillin-Streptomycin and every four days the medium was changed. Once the cells had grown to 80% confluency, they were dissociated using 1 ml of 0.05% Trypsin-EDTA for 3 minutes. Then, the cells were neutralized with 5ml of complete medium (DMEM+10%FBS). Next, the cell

suspension underwent centrifugation at a rate of 120 RCF¹³, and then the cells were resuspended in 5 ml of complete DMEM. Finally, a volume of 20µl of a 1:1 mixture of Trypan Blue Solution 0.4% and the cell suspension was applied onto a hemocytometer for cell counting and calculation utilizing a specific formula:

$$\text{Cell Number/ml} = \frac{(\text{Total number of counted cells})}{4} \times 2 \times 10^4$$

2.2.2. PDMS Preparation

To produce PDMS, the curing agent and the base silicone elastomer (SYLGARD 184) were combined in a 1:10 ratio and subjected to a thorough blending process; nonetheless, this blending technique resulted in the formation of bubbles (Fig. 9. A). Subsequently, the resulting composite was subjected to centrifugation at a relative centrifugal force of 300 RCF for 5 minutes within a centrifuge tube to facilitate the removal of these gas bubbles (Fig. 9. B).

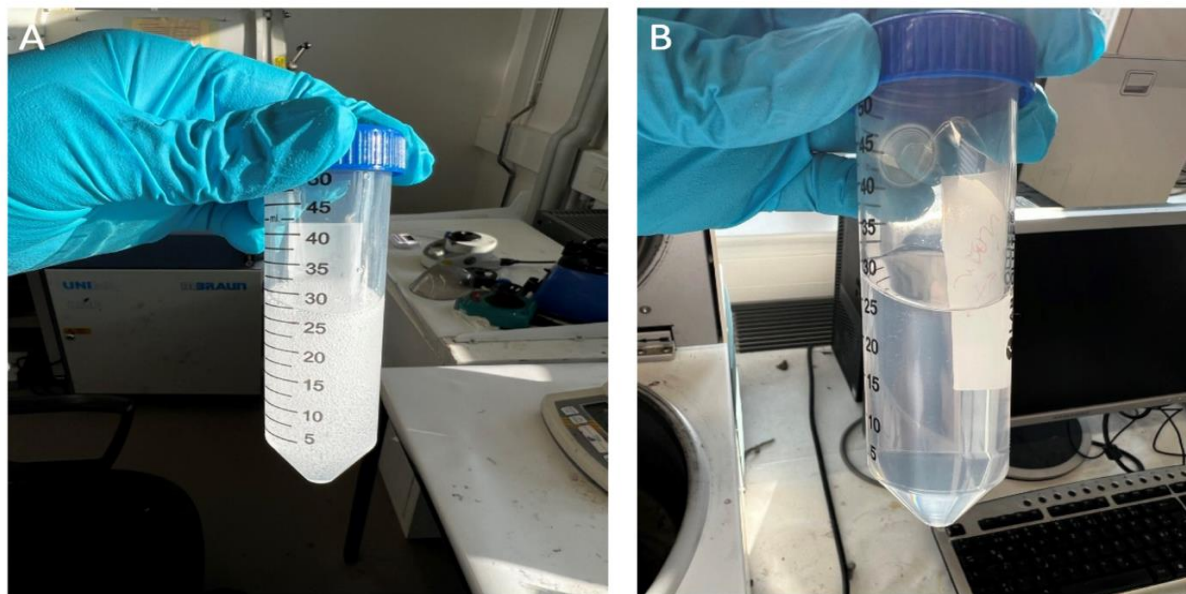


Figure 9. PDMS-Curing Agent Mixture. The 1:10 mixture of the silicone base and the curing agent of PDMS: **A)** Before and **B)** After centrifuging at 300 RCF for 5 minutes.

¹³ Relative Centrifugal Force (RCF)

2.2.3. Template Preparation

2.2.3.1. Single-Coating Templates

To create templates with a single coating, 5×10^4 MCF7, 3T3, and MDA-MB231 cells in 500 μ l of DMEM-high glucose were placed in each well of a 24-well plate (Fig. 10). After incubating overnight, the medium was removed, and the cells were washed with 0.1M PBS once. The cells were then immobilized using a Glutaraldehyde 4% solution for 20 minutes. Subsequently, the 4% Glutaraldehyde solution was eliminated, and the immobilized cellular structures underwent a thorough washing with MiliQ water three times.

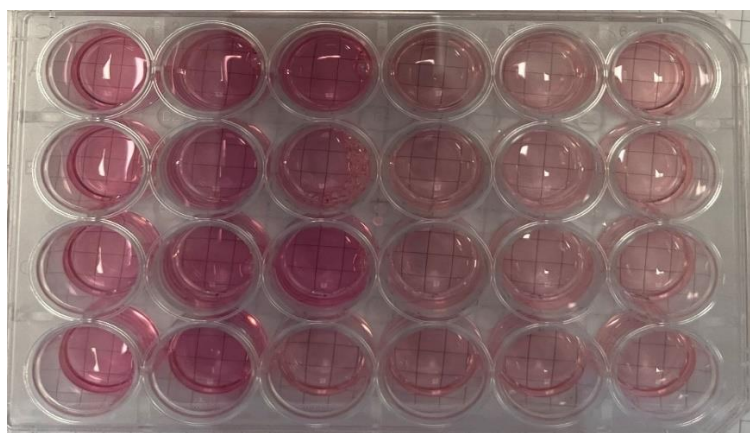


Figure 10. Single-Coating Substrates. 5×10^4 MCF7 cells per well in 500 μ l DMEM in a 24-well plate

2.2.3.2. Double-Coating Templates

2.2.3.2.1. Semi-Circle Blockers

A 24-well plate was used as a template to make the semi-circle blockers and filled with 0.2 gr of PDMS per well (Fig. 11. A). The plate was then heated to 80°C for an hour to cure the PDMS. After the curing step, the circular discs were removed from the plate (Fig. 11. B) and cut into halves to create semi-circular plugs (Fig. 11. C). These plugs were then placed in the wells of another 24-well plate to block half of its surface area (Fig. 11. D).

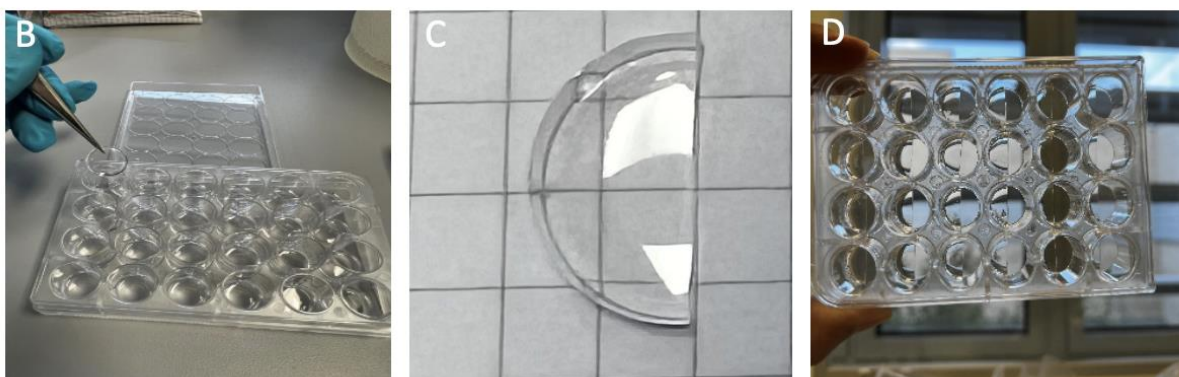
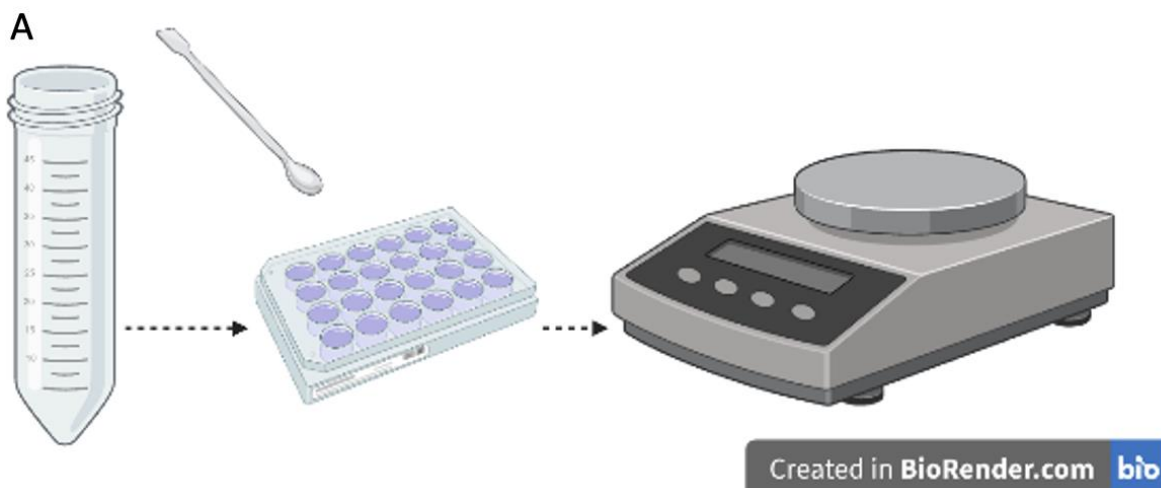


Figure 11. Semi-Circle Blockers Preparation. **A)** 0.2gr PDMS per well of a 24-well plate. **B)** Removing the circular blockers after heating at 80°C for an hour **C)** Cutting the blockers into two halves **D)** Attachment of semi-circle blockers inside a 24-well plate.

2.2.3.2.2. Cell Addition

In order to provide double-coating substrates, the plate with semi-circle blockers was sterilized by UV-type C irradiation for 30 minutes. Subsequently, 25×10^3 MCF7, 3T3, and MDA-MB-231 cells in 250 μ l of DMEM were introduced into half of the wells (Fig. 12). Similar to the Single-Coating templates, the cells were immobilized using Glutaraldehyde 4% in 20 minutes. They underwent three cycles of washing with MiliQ water.

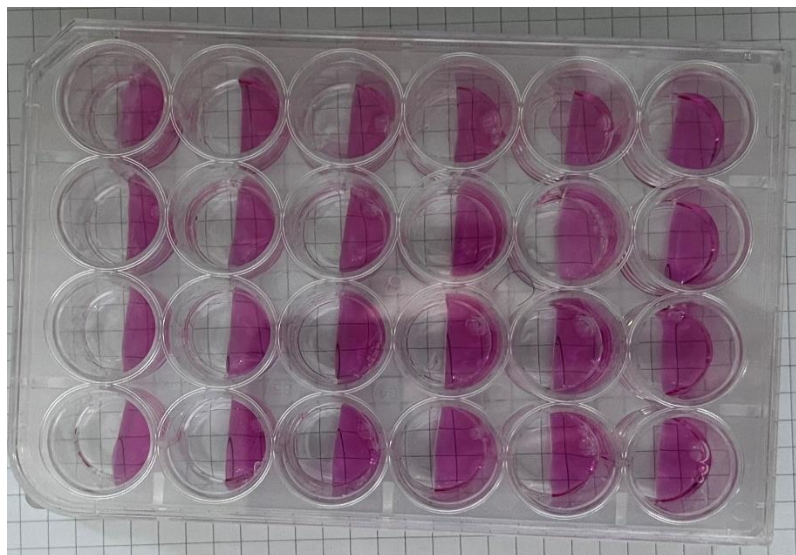


Figure 12. Double-Coating Substrates. 25×10^3 MCF7 cells in 250 μ l DMEM in half of a well while using blockers.

To create MCF7-MDA MB 231 or 3T3 patterned substrates, the MCF7 cells were cultured in one half, immobilized, and covered with semi-circle blockers. Afterward, MDA-MB231 or 3T3 cells were introduced into the other half and left to settle overnight before immobilizing with Glutaraldehyde 4%. The remaining steps are similar to those used for other Double-Coating substrates.

2.2.4. Substrates Development

2.2.4.1. Casting

0.2 grams of PDMS were added to each template well to cast the PDMS.

2.2.4.2. Curing

The template containing PDMS was incubated overnight at 37°C in the oven to cure PDMS and imprint the cellular morphology onto PDMS. The resulting solid PDMS substrates were detached from the template and subjected to a further curing process at 100°C for 10 minutes.

2.2.4.3. Preparation

The PDMS substrates were punched into 1cm circular samples (Fig. 13).

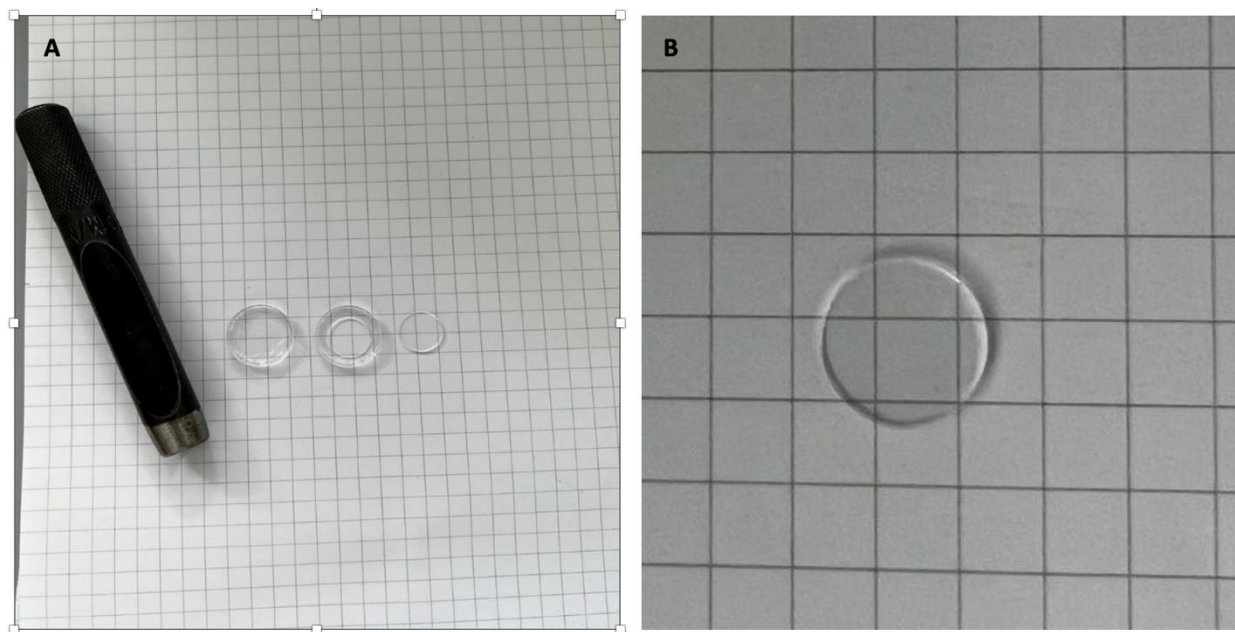


Figure 13. Sample Preparation. A, B) Preparation of 1cm circular substrates using a punch.

For each type of substrate, three samples were attached to the underside of a 24-well plate. The resultant combinations were as follows: MCF7 Pattern, MDA-MB 231 Pattern, Plain PDMS, TCPS¹⁴, MCF7 Pattern-Plain PDMS, MDA-MB 231 Pattern-Plain PDMS, and MCF7 Pattern-MDA-MB 231 Pattern.

2.2.5. PMA Coating of CdSe/CdS QDs

PMA is a graft copolymer made of alternating copolymer of isobutylene and maleic anhydride and dodecyl groups linked to the polymer's backbone. The grafting process entails replacing maleic anhydride units with dodecyl groups, significantly modifying the resultant polymer's physical and chemical characteristics. Research on the synthesis and analysis of analogous graft copolymers has demonstrated that the extent of substitution and the type of grafted groups can impact the polymer's structure, stability, and behavior toward solvents and temperature[158]. The protocol for coating the QDs with PMA has already been described[159]. In summary, CdSe/CdS QDs were uniformly mixed in chloroform with PMA-g-dodecyl using a stirrer for 5 minutes at ambient temperature. The solution was then evaporated using a rotary evaporator (Heidolph, Germany) at 40°C to coat the amphiphilic polymer onto the QDs. The resulting dry layer was

¹⁴ Tissue Culture Polystyrene Plate (TCPS)

dissolved again in a small amount of anhydrous chloroform, and this desiccation procedure was repeated twice more to guarantee the development of a consistent layer. Ultimately, the wholly dried layer was dissolved in Sodium Hydroxide 0.1M with vigorous stirring and kept overnight in the fridge (3-5 °C). This procedure led to the hydrolysis of anhydride rings, resulting in the generation of carboxyl groups that assist in stabilizing the particles and promoting the establishment of a colloidal solution in water. Next, the solution was centrifuged (Thermo Fischer Scientific Megafuge 8R with a MicroClick 24×2 rotor, Germany) at 3×10^4 RCF for 45 minutes. Subsequently, the supernatant was discarded, and the particles underwent a washing and centrifugation process three times utilizing MilliQ water to eliminate any residual buffer components. Finally, the particles were resuspended in 200µl water, and the concentration was determined using ICP-MS (7700 Series, Agilent Technologies, Germany). To prepare the particles for ICP-MS analysis, 10µl of the QDs were diluted in Aqua regia overnight at room temperature. Then, the solution was diluted in 2ml of 2% HCl¹⁵[159].

2.2.6. Substrate Characterization

2.2.6.1. Light Microscopy

Light microscopy has diverse practical uses across multiple scientific disciplines. It capitalizes on its capacity to observe living specimens and perceive color, which is pivotal in comprehending biological processes and diagnosing diseases. Light microscopy plays a crucial role in visualizing tissue structure and nuclear characteristics within clinical environments, contributing to diagnosing and comprehending cancer development by delivering detailed, three-dimensional volumetric views of tissue formations[160]. Historically, light microscopy has constituted a fundamental element in scientific breakthroughs, with notable contributions from pioneers like Robert Hooke and Antony Leeuwenhoek. It is an essential instrument in diverse investigative fields due to its adaptability and effectiveness in addressing routine scientific inquiries.[161]. In essence, the advancements in light microscopy techniques have significantly expanded its scope of applications, establishing it as an indispensable implement in both fundamental and practical sciences. Substrates were observed under the light microscope (Axiovert 40 C, Zeiss) equipped with a camera (MikroCam SP 5.0, BRESSER) using a 10x objective lens and 1x zoom. The

¹⁵ Hydrochloric Acid (HCl)

substrates included Plain PDMS, TCPS, MDA-MB-231 Pattern, MCF7 Pattern, MCF7 Pattern-Plain PDMS, MDA MB 231-Plain PDMS, and MCF7 Pattern-MDA-MB-231Pattern.

2.2.6.2. Contact Angle Measurement

The CA¹⁶ measurement is a critical technique for investigating the interactions between cells and biomaterials, as it is a straightforward way to retrieve data on the surface properties and the wettability of biomaterials valuable in many applications across tissue engineering, medical implants, and other fields related to blood interaction with biomaterials. The wettability of biomaterials, typically measured through CA, significantly influences cell adhesion, proliferation, and differentiation. Therefore, this influences biomaterial products' biocompatibility and therapeutic efficacy [162-164]. For example, porous and hydrophilic scaffolds are typically built to promote cell and tissue penetration in tissue engineering, though CA examination on such surfaces is more challenging[165]. CA serves as an instrument for investigating the dynamic processes of protein adsorption and desorption on biomaterial surfaces, which subsequently relates to cellular adhesion and proliferation, as evidenced by studies concerning stent coatings aimed at enhancing endothelialization[166]. The interaction between cells and biomaterials involves specific and nonspecific interactions, where CA is a tool to help significantly predict nonspecific interactions through wettability investigation[167]. Material wettability also affects the interface between biomaterials and bodily fluids, such as blood, and CA can also be beneficial in predicting how the material will perform in vivo by its wettability[168]. In summary, these processes indicate that CA investigations represent a robust method to design and appraise biomaterials, aiming to help construct materials that can effectively interact with biological systems[169]. The sessile drop technique is frequently utilized to measure the contact angles between a liquid droplet and a solid substrate, thereby providing essential insights into surface tension and wettability characteristics. An integral aspect of this approach entails carefully examining the configuration assumed by a droplet positioned on a surface to ascertain the contact angle (Fig. 14)[170, 171].

¹⁶ Contact Angle (CA)

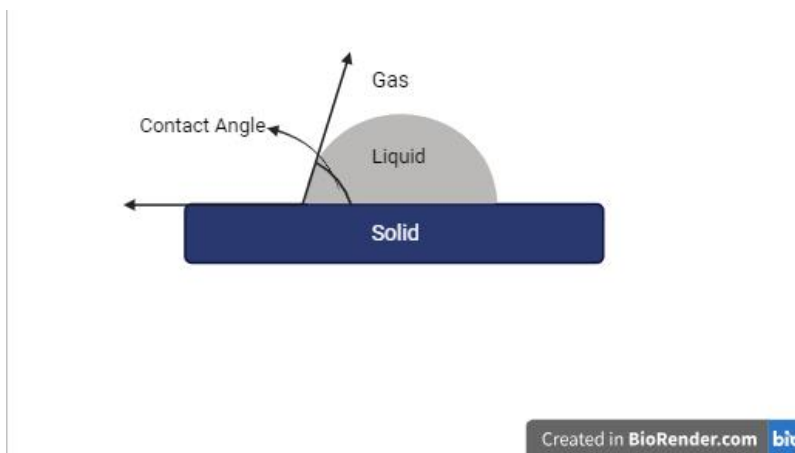


Figure 14. Schematic Illustration of Contact Angle.

The sessile drop technique was utilized with a Drop Shape Analyzer device (DSA25E, Krüss, Germany) to analyze how surface topography affects the wettability properties of various substrates. Three substrates were prepared: TCPS, Plain PDMS, and Patterned PDMS. Initially, it was ensured that the samples lacked contamination, scratches, or physical damage. Following this, the drop analyzer machine was carefully calibrated based on the manufacturer's instructions, and the lighting and focus of the machine's camera were adjusted. Subsequently, a droplet of MiliQ water (10 μ l) was gently deposited onto the sample surface. Once the water droplet was stabilized, an image was captured using the high-resolution camera with an appropriate zoom to obtain a clear droplet profile. The captured image was then analyzed using the machine's software (Advance, V.1.8.0.4, Krüss) to identify the baseline of the droplet over the substrate. Subsequently, the angle delineated between the tangent line and the droplet at the contact point was quantified in relation to the baseline. The experiment was conducted at three distinct locations to guarantee precision and reproducibility. Finally, the average contact angles and the standard deviations from multiple measurements were reported.

2.2.6.3. Scanning Electron Microscopy

SEM¹⁷ Scanning Electron Microscopy (SEM) features an intricate imaging technique that harnesses high-energy electrons targeted at a sample to develop images distinguished by excellent resolution and depth of field. The engagement of the electron beam with the specimen results in the production of signals, including secondary and backscattered electrons, thus substantially

¹⁷ Scanning Electron Microscopy

enhancing the imaging potential[172]. SEM is versatile for in-depth surface analysis and elemental identification across various scientific domains. SEM was used to study three types of substrates: MCF7 Patterned PDMS, Plain PDMS, and Tissue Culture Polystyrene samples to analyze the surface topography and cell interactions. First, 1cm circular samples were cut from the mentioned substrates using a 1cm punch. The substrates were subsequently subjected to sterilization utilizing UV/C for 30 minutes after being immersed in 70% ethanol for 20 minutes. After that, the specimens were rinsed three times with sterile PBS. After the preparation of the samples, 2000 MCF7 cells in 100µl of complete DMEM were seeded on the samples overnight. The medium was removed, and the cells were immobilized with 4% Glutaraldehyde for 20 minutes. Subsequently, the samples were washed twice with PBS and once with MiliQ water to remove Glutaraldehyde and any unattached cells. After permitting the specimens to undergo air drying at ambient temperature, they were coated with a fine layer of gold utilizing a sputter coater apparatus (K550, EMITECH). Finally, SEM characterization images of the substrates were taken using a GEMINISEM machine (ZEISS, Germany) at 5 kV and an SE2 detector with 500-, 100-, and 1500-time magnifications. The images were captured with SmartSEM Version 6.00, Service Pack 5 software (ZEISS, Germany).

2.2.6.4. Fourier-Transform Infrared Spectroscopy

FTIR¹⁸ analysis is an effective analytical technique for investigating the infrared spectrum and illustrating solids, liquids, or gases' absorption, emission, or photoconductivity. It collects an interferogram of a sample signal using an interferometer, which is then transformed into a spectrum via Fourier transformation[172]. FTIR spectroscopy's flexibility is impressive because it can analyze various materials, such as biological samples, plastics, polymers, and organic compounds. It identifies their molecular structures and functional groups through vibrational modes.[173, 174]This non-destructive and swift technique accurately represents the analyzed material, rendering it indispensable in food verification, environmental surveillance, and pharmaceuticals[175]. The extensive applicability and accuracy of FTIR spectroscopy establish it as a fundamental technique in both scholarly research and industrial practices. The PDMS and TCPS disc-shaped samples (1cm diameter) were prepared and analyzed using the FTIR instrument (Cary 630 FTIR Spectrometer, Agilent, Germany) in the transmission mode, and the

¹⁸ Fourier-Transform Infrared Spectroscopy

results were analyzed in the software (MicroLab, Agilent Technologies) to analyze the substrates chemically.

Siloxane bonds are crucial components in the design of PDMS, functioning as the foundational architecture of the polymer. This bond is generally detected in the FTIR spectrum at approximately 1100 cm^{-1} , signifying the existence of the silica network within the composite material. The methyl groups covalently bonded to the silicon atoms in PDMS are integral to their hydrophobic characteristics. Identifying peaks near 1250 cm^{-1} in the FTIR spectrum makes these groups noticeable, as they relate to the Si-C bond [176]. On the other hand, the FTIR spectrum characteristic of TCPS typically exhibits pronounced absorption bands attributed to aromatic C-H stretching vibrations occurring at approximately 3000 cm^{-1} . These absorption features serve as a strong indicator of the presence of phenyl groups, which constitute a fundamental component within the structural framework of polystyrene[177, 178]. Furthermore, the C-H out-of-plane bending vibrations are discernible within the spectral region of $870\text{--}820\text{ cm}^{-1}$, particularly highlighted by a prominent peak located at 841 cm^{-1} , which correlates with the amorphous phase of syndiotactic polystyrene[179]. The existence of aromatic rings within the polystyrene matrix is corroborated by the C=C stretching vibrations, which manifest as distinct absorption bands around 1600 cm^{-1} . These spectral features are pivotal for elucidating the aromatic characteristics inherent to the polymer[178, 180]. The spectral profile also reveals bands corresponding to C-H bending vibrations, especially within the $1450\text{--}1500\text{ cm}^{-1}$ spectral range. These absorption bands are associated with the bending motions of the methylene and methine groups in the polymer backbone [178, 181].

2.2.7. CdSe/CdS QDs Characterization

2.2.7.1. Dynamic Light Scattering

DLS¹⁹ constitutes a frequently utilized photonic methodology for examining size distribution, hydrodynamic radius, ζ -potential, and polydispersity of nanoparticles, polymers, and cellular entities in either suspension or solution. This technique identifies the fluctuations in the intensity of scattered light engendered by the Brownian motion of particles, which is subsequently converted into temporal autocorrelation data to evaluate particle size distribution and

¹⁹ Dynamic Light Scattering (DLS)

diffusivity[182, 183]. Within various domains, such as nanomaterial synthesis, DLS proves to be highly advantageous as it offers prompt, non-invasive evaluations of particle size and stability, which are essential for comprehending the distinct characteristics of nanomaterials arising from surface and quantum size effects.[184] The particle size analysis apparatus was employed to ascertain the dimensions of the PMA-coated QD nanoparticles. The PMA-QD stock solution underwent dilution in Milli-Q water to achieve a concentration of 10nM. It was then sonicated for 30 minutes to separate the agglomerated particles before being transferred into a plastic cuvette. Finally, the cuvette was analyzed using the instrument (Malvern Panalytical Ltd, United Kingdom).

2.2.7.2. Fluorescence Emission Spectroscopy

Fluorescence spectroscopy assumes a pivotal role in a variety of applications related to nanoparticles. It is employed in assessing biodistribution and accumulating fluorescent agents conjugated to drugs for therapy control[185]. Moreover, fluorescence sensing, especially using carbon nanoparticles, facilitates the creation of intelligent sensor devices by detecting analytes based on alterations in color or emission[186]. In nanomaterials, fluorescence polarization techniques, combined with inorganic nanomaterials such as quantum dots, enhance biosensing capabilities for early disease detection, food safety inspections, and environmental monitoring[187]. These varied applications underscore the adaptability and importance of fluorescence spectroscopy in nanoparticle research and advancement. To find the emission wavelength of the PMA-QDs, they were first diluted 100 times in MiliQ water, transferred to a crystal cuvette, and analyzed using a Fluorescence Spectrometer (Cary Eclipse, Agilent, Germany).

2.2.7.3. Cytotoxicity and Endocytosis

The Presto Blue cytotoxicity assay, a metabolic assessment tool based on resazurin, is extensively utilized for evaluating cell viability and cytotoxicity in various biological and medical research fields. This assay functions on the premise that metabolically active viable cells can convert non-fluorescent resazurin into highly fluorescent resorufin, inducing a detectable color alteration that can be quantitatively assessed[188]. The Presto Blue assay has demonstrated a rapid and easily distinguishable color change, simplified visual interpretations, and established itself as a

convenient instrument for qualitative and quantitative evaluations. In tissue engineering and regenerative medicine, this assessment has demonstrated significant promise for monitoring cellular proliferation over time within three-dimensional bioreactor systems. More specifically, a direct relationship has been established between the rate of Presto Blue conversion and cell quantity, enabling the establishment of optimal signal detection ranges during the growth phase of human periosteal cells in 2D and 3D environments[189]. When nanoparticles are absorbed through endocytosis, it reflects a sophisticated occurrence affected by different variables, including their physical and chemical features, the pathways within the cells, and the external environmental aspects. A comprehensive comprehension of these determinants is imperative for optimizing nanoparticle architecture for biomedical applications, encompassing drug delivery systems and diagnostic methodologies. This discourse investigates the underlying mechanisms and variables that affect nanoparticle endocytosis, extracting insights from contemporary scholarly research. Although the predominant emphasis often lies in augmenting nanoparticle uptake for therapeutic objectives, addressing the possibility of inadvertent cellular interactions and resultant toxicity remains equally critical. A detailed comprehension of the mixed pathways and determinants that regulate nanoparticle endocytosis can enhance the formulation of nanomedicines that are not just safer but also more powerful, thereby reaching a careful balance between therapeutic benefits and related hazards.

Cell viability and emission analysis of the endocytosed particles were performed to assess the suitable concentration of the PMA-coated QDs. For an overnight, 1×10^4 MCF7 cells in 100 μ l of complete medium were seeded in a 96well plate in nine columns for each concentration, with six replicas for each group. Then, the medium was removed, and QDs with 0, 0.01, 0.1, 1, 5, 10, 20, 50, and 100nM in complete medium were added to the MCF7 cells for 24 hours. Afterward, the extra particles were removed, and the cells were washed three times with PBS to remove extra particles. Finally, 100ml/well of the presto blue dye, which was diluted in serum-free medium, was added to each group, and the plate was kept for an hour in the incubator before analyzing using a plate reader machine (FLUOstar Omega, BMG LABTECH, Germany). Then, the plate was analyzed for the QDs endocytosis and Cytotoxicity, and the tests were repeated three times. QDs composed of cadmium selenide demonstrate optical characteristics that are contingent upon their size, a phenomenon attributable to quantum confinement effects. Quantum dots that are smaller in size are generally observed to emit light at shorter wavelengths, a phenomenon referred

to as a blue shift. In contrast, their larger counterparts are characterized by emissions at extended wavelengths, known as red shift[190]. This tunability based on size facilitates an extensive spectrum of emissions, spanning from the visible spectrum into the near-infrared range[191]. The emission spectrum associated with CdSe quantum dots frequently broadens due to surface trap states responsible for emissions ranging from 450 nm to 800 nm [192]. These trap states are intrinsically linked to surface imperfections and can be strategically manipulated to modify the emissions' characteristics. For example, applying a zinc selenide (ZnSe) shell over CdSe quantum dots can transform the broad emissions linked to trap states into narrow and intense emissions within the blue spectrum[193]. Based on the size and surface features of the PMA-coated QDs, 355 nm for excitation and 620 nm were set to detect the endocytosed QDs in the cells.

On the other hand, the active ingredient of PrestoBlue, resorufin, exhibits fluorescence upon reduction by cells exhibiting metabolic activity. This fluorescence is typically quantified within the wavelength spectrum of 570-590 nm, a distinctive emission range attributed to resorufin assays [194, 195]. For the Cytotoxicity assay (Prestoblue), excitation and emission of 560 and 590 nm were taken, respectively.

2.2.7.4. Transmission Electron Microscopy

TEM²⁰ is a highly efficient and versatile technique widely employed in physical and life sciences for examining materials at the nanoscale, focusing on morphology, crystal structure, and chemical composition. TEM operation transmits electron beams through fragile specimens, enabling precise imaging and thorough structural analysis. This approach is valuable in characterizing nanostructures spanning 0D, 1D, and 2D materials. It plays a crucial role in establishing correlations between structural analysis and the distinctive properties exhibited in nanomaterials, thereby enabling more controlled synthesis and enhanced device performance[196]. Modern TEM instruments have sophisticated features like aberration correctors, rapid cameras, and highly sensitive spectrometers to augment their functionalities. The precise determination of the gap in the objective lens pole-piece holds crucial significance, as it impacts the instrument's resolution and adaptability for diverse applications, including tomography and in-situ experiments.[197]. TEM is indispensable for the ultrastructural characterization of cells and organelles in biological and pathological investigations, often in conjunction with molecular analyses to provide a

²⁰ Transmission Electron Microscopy (TEM)

comprehensive understanding[198]. TEM is used to assess morphology, crystalline structure, and elemental composition in membrane materials, utilizing bright-field and dark-field imaging modes to obtain detailed micrographs.[199]. TEM imaging of the PMA-QDs was performed at a voltage setting of 100 kV using a JEOL JEM-1011 TEM microscope. 10 μ L of the diluted (10 times) nanoparticle solutions were applied on a carbon-coated TEM grid as a part of the sample preparation for the TEM. Finally, the particles' dimensions were assessed using the software FIJI ImageJ version 1.46, based on the acquired TEM micrographs.

2.2.8. Migration Assay

2.2.8.1. Crystal Violet Assay

Crystal violet staining is commonly employed in different biological and medical research environments due to its capability to specifically attach to nucleic acids and proteins, facilitating the observation and measurement of cellular and microbial elements. This particular staining method is commonly employed in cell culture experiments to standardize data based on the number of adherent cells, giving a dependable option to the bicinchoninic acid assay for measuring protein content[200]. In oncological pathology, the application of crystal violet staining has demonstrated significant efficacy in identifying mitotic figures within pathological states such as oral squamous cell carcinoma and oral epithelial dysplasia. Crystal violet is more cost-efficient and cost-effective than advanced technologies such as flow cytometry and immunohistochemistry [201, 202]. Furthermore, it is utilized to indirectly assess cell death by staining adherent cells; those undergoing cell death lose adherence and remain unstained, decreasing staining within a culture[200]. Generally, crystal violet staining is widely recognized as a simple, quick, and cost-effective method with numerous applications in various fields like cell biology, virology, cancer research, and microbiology.

There are seven types of substrates (3 replicas for each type), including Single-Coating (Coating A): TCPS²¹, Plain PDMS, MCF7 Pattern, and 3T3 Pattern. Double-Coating (Coating A+B) patterns include MCF7 Pattern-Plain PDMS, 3T3 Pattern-MCF7 Pattern, and 3T3 Pattern-Plain PDMS. Subsequently, 500 MCF7 or 3T3 cells suspended in 25 μ l of medium were carefully placed at a 5mm circular area in the center of disc-shaped samples with a diameter of 10mm (Fig.

²¹ Tissue Culture Polystyrene (TCPS)

15). Following a duration of 3 hours, an additional 75 μ l of medium was uniformly dispensed onto every individual substrate. After overnight, which was less than the doubling time of the cells, the cells were meticulously immobilized using a 4% paraformaldehyde solution for 20 minutes, followed by thorough washing with PBS twice and MiliQ water once. Ultimately, the immobilized ed cells underwent staining with crystal violet solution at a concentration of 0.5%, followed by three subsequent washes with MiliQ water. The stained cells were examined under the light microscope (Axiovert, Zeiss, Germany) with a 10x objective. To quantify the migration, the density of the cells (MCF7 or 3T3 cells) is calculated in the seeding and outside the seeding area based on the number of cells per surface area (cell/mm²), and results are reported as Mean Values \pm SD²². Also, three photos per sample were captured, one from the cell seeding area and two from outside the seeding areas.

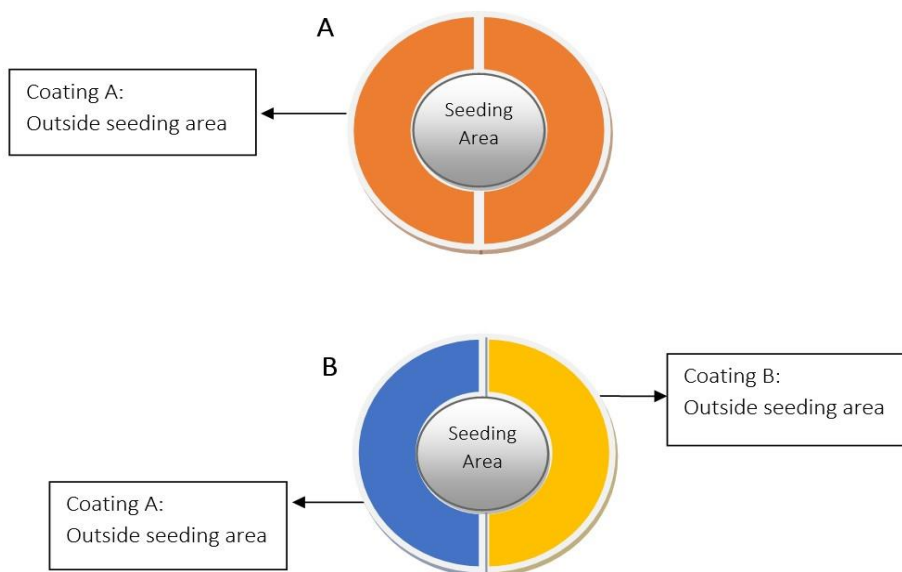


Figure 15. Cell Seeding Schematic. The Schematic view of cell seeding on the substrates: **A)** Single-Coating Substrates and **B)** Double-Coating Substrates.

2.2.8.2. Red/Blue Ratio Assay

To determine whether the MCF7 and 3T3 (or MDA-MB-231) cells were within or outside the seeding area overnight later, PMA-coated CdSe/CdS core-shell type quantum dots (QDs) and Hoechst 33342 (Invitrogen) were used to stain the cells.

²² Standard Deviation (SD)

2.2.8.2.1. *Hoechst Staining*

H33342²³ is a fluorescent dye extensively employed for DNA staining within viable cells. Its capability to permeate cellular membranes and stain DNA makes it a valuable instrument in diverse biological and medical research realms. [203, 204]. It has significant utility in live cell imaging and flow cytometry for evaluating cell proliferation, viability, and apoptosis. Assessments include discriminating between healthy, apoptotic, and necrotic cells by noting nuclear condensation. [205, 206]. The ionization states of H33342 can vary depending on the pH, thereby influencing its interaction with lipid bilayers and the rate at which it permeates through cellular membranes.[207, 208]. Furthermore, this dye acts as a substrate for multidrug transporters, which can actively eliminate or accumulate it, impacting its intracellular concentration and fluorescence characteristics[209, 210]. Despite its wide-ranging utility, H33342 may exhibit cytotoxicity at elevated concentrations, thereby influencing cell proliferation and viability and inducing DNA harm, necessitating meticulous calibration of its concentration for specific purposes.[211, 212]. Moreover, it has been revealed that H33342 labels DNA and transmembrane proteins like P-glycoprotein (P-gp), which can assist in observing specific cellular structures in immobilized samples[213]. Metabolic inhibitors can influence cells' uptake of this dye, which is employed to analyze membrane transport rates and mechanisms of drug resistance.[214]. In summary, Hoechst 33342 emerges as a versatile and potent instrument in cell biology; however, its application mandates thoughtful deliberation concerning its concentration and potential cytotoxic impacts to ensure the attainment of precise and dependable outcomes. In this study, the MCF7 (or MDA-MB 231) cells were subjected to Hoechst staining at 5 μ g/ml concentration in PBS for 10 minutes. Following this, the cells were washed three times with PBS before being detached and counted.

2.2.8.2.2. *QD Labeling*

MCF7 (3T3 or MDA-MB-231) cells were treated with PMA-Coated CdSe/CdS core-shell type quantum dots (QDs) at a concentration of 5nM for 24 hours to get endocytosed by the cells. Then, the cells were washed three times with PBS to remove any excess particles before separation and counting.

²³Hoechst 33342

2.2.8.2.3. *Cell Dissociation*

As previously described, to detach the stained cells, a procedure involving incubation with 1 ml of 0.05% Trypsin-EDTA for 3 minutes and subsequent neutralization with 5 ml of DMEM+10% FBS was carried out. The resulting cell suspension underwent centrifugation at 120 RCF, following which the cells were resuspended in 5ml of complete DMEM. Cell counting was done using a hemocytometer under an inverted light microscope (Primovert, Zeiss, Germany), and the cell concentration was adjusted to a diluted value of 20,000 cells/ml.

2.2.8.2.4. *Cell Seeding*

An equal number of MCF7 and 3T3 (or MDA-MB 231) cells were mixed to obtain 20,000 cells/ml concentration. 25 μ l of this mixture, while containing 500 cells (MCF7+3T3 (or MDA-MB 231)), was introduced into the seeding area in the center, a 4 mm circle for the PDMS and 5mm for the TCPS substrates. Due to the different wettability properties of PDMS and treated polystyrene plates, it is advisable to widen the seeding area in the plate to ensure that the cells remain within the seeding circle, as the treated polystyrene plate is more hydrophilic than PDMS. For samples with Double-Coating, the seeding area was positioned on the border between the two substrate types (Fig. 16. A-B). After allowing for a 3-hour incubation period, each sample received an additional 75 μ l of medium to cover the substrate surface (Fig. 16. C).

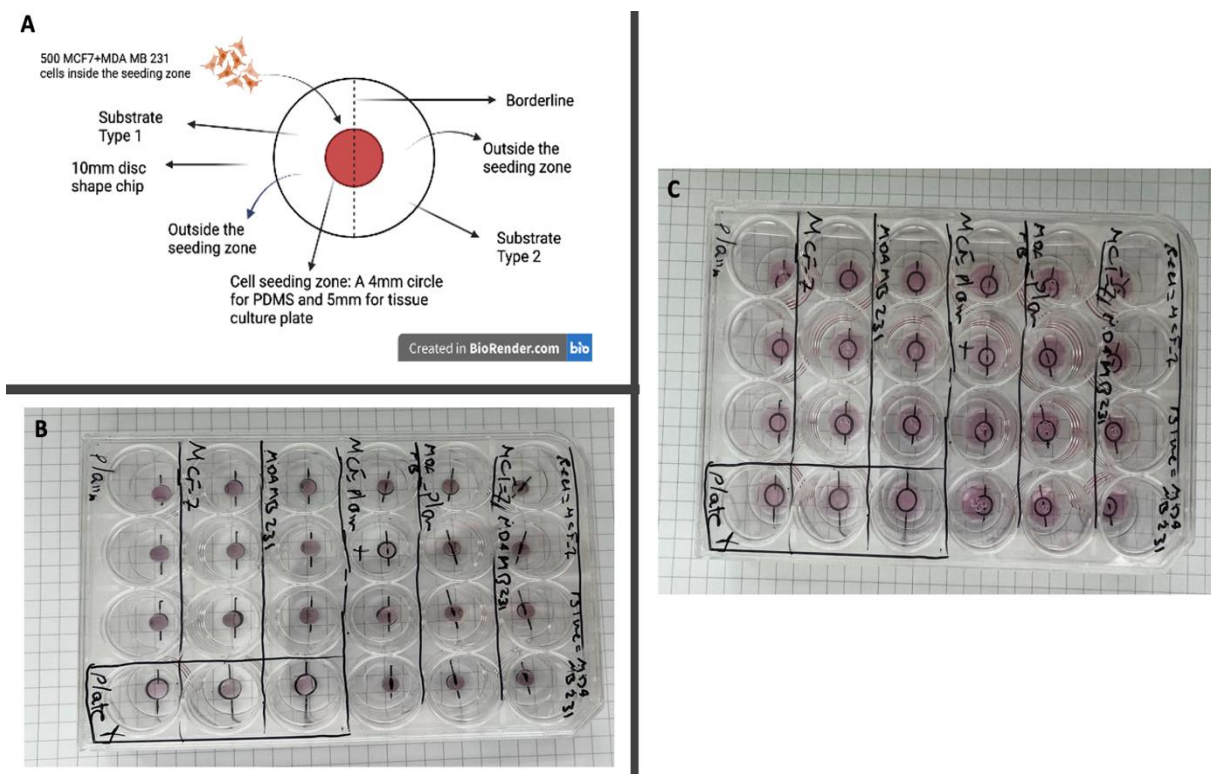


Figure 16. Cell Seeding. A) Schematic view of the cell seeding B) 500 MCF7+MDA-MB-231 cells in 25 μ l DMEM in the seeding area C) The substrates were covered with 75 μ l of DMEM after 3 hours.

2.2.8.2.5. Immobilization (Fixation)

After overnight incubation, the medium was removed, and the cells were immobilized using 4% paraformaldehyde for 20 minutes. Then, the paraformaldehyde was removed, and the samples were washed twice and covered with 100 μ l of PBS.

2.2.8.2.6. Calculation

To quantify the cell migration, the proportion of red-stained (PMA-QDs) cells to blue-stained (Hoechst) cells was determined using an inverted fluorescent microscope (Axiovert 200M, Zeiss, Germany), both inside and outside the seeding area of Single-Coating substrates and outside of Double-Coating substrates. To determine whether swapping these fluorescent markers within the cells influences the results, the two cell types were dyed in both red and blue during distinct assays, each conducted with a minimum of three repetitions. The number of red and blue-stained cells was determined using ImageJ and confirmed by manually counting the cells under a fluorescent microscope. Lastly, the ratio of each cell type in each area was calculated using formula 1.

$$(1) \text{Red/Blue Ratio} = \frac{\text{Total Number of Red stained cells}}{\text{Total Number of blue stained cells}}$$

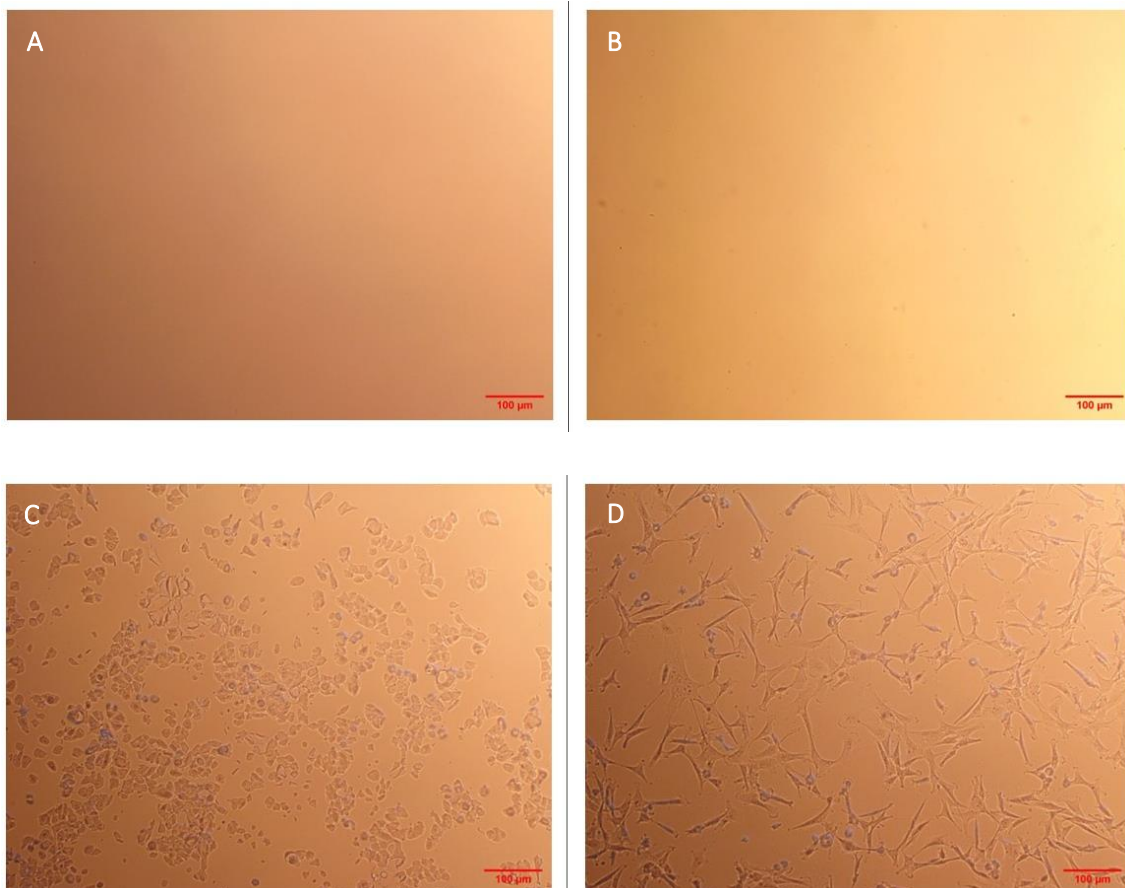
The calculation was performed for three replicates of each substrate type in each assay repetition, and the average value was obtained. In the case of Single-Coating substrates, the ratio of cells within and outside the seeding area was recorded. The cells outside the seeding area were analyzed for both substrates for the Double-Coating samples. The results were reported using the format Mean Values \pm SD. The assay used two methods: MCF7 cells were tagged with the PMA-QDs (Red), and 3T3 cells were stained with the Hoechst (Blue). In the second approach, the opposite was done, i.e., MCF7 cells were stained with Hoechst, 3T3 (Or MDA MB 231 Cells) cells were tagged with the PMA-QDs, and the assay was repeated. The test was also repeated for the MCF7 (Blue) mixture and MDA-MB-231(Red) cells.

Chapter 3:
Results and Discussion

3.1. Substrates Characterization

3.1.1. Light Microscopy Images

The images in Figure 17 show a variety of substrates, including Plain PDMS, TCPS, MDA-MB-231 Pattern, MCF7 Pattern, 3T3 Pattern, MCF7 Pattern-Plain PDMS, MDA-MB-231 Pattern-Plain PDMS, and MCF7-MDA-MB-231 Patterns. Images were captured using an Axiovert 40C (Zeiss, Germany) microscope and a MicroCam SP 5.0 camera (BRSSER) with a 10x objective and 1x zoom. These images clearly show the morphology of the cells on the PDMS.



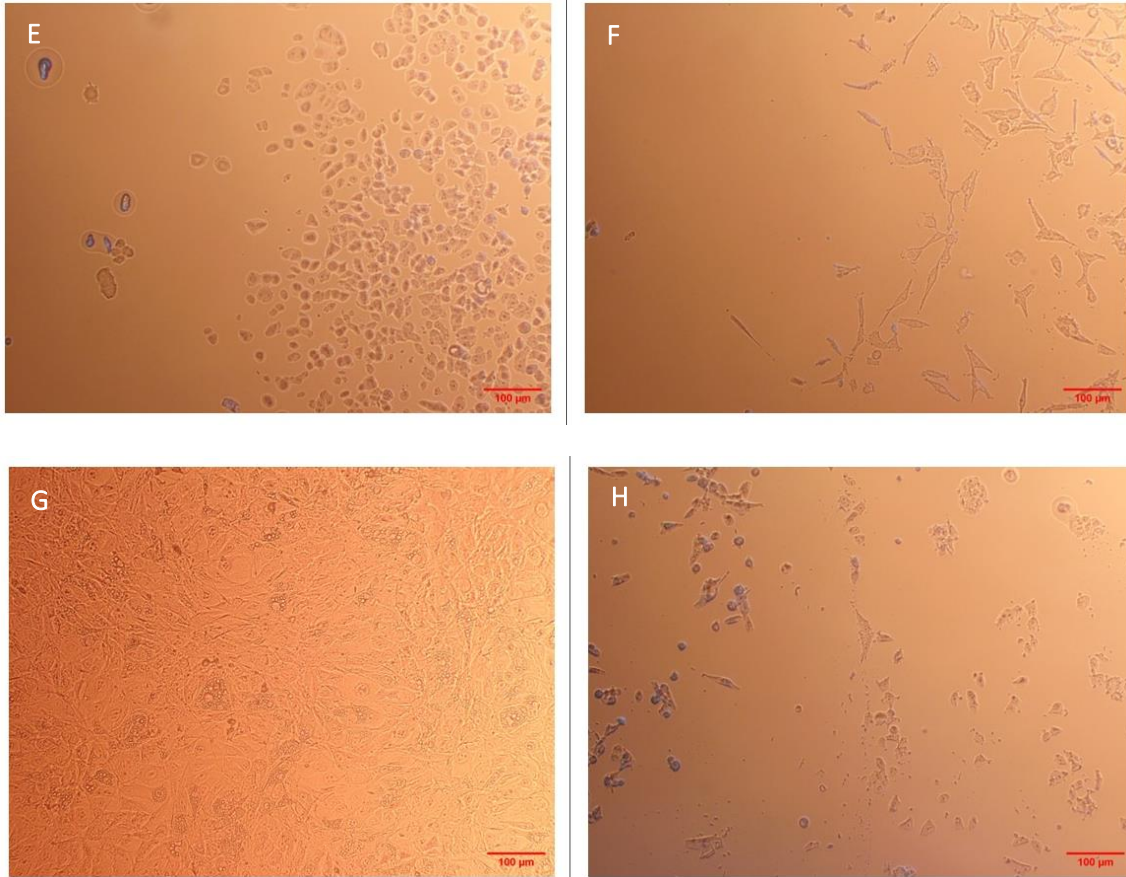
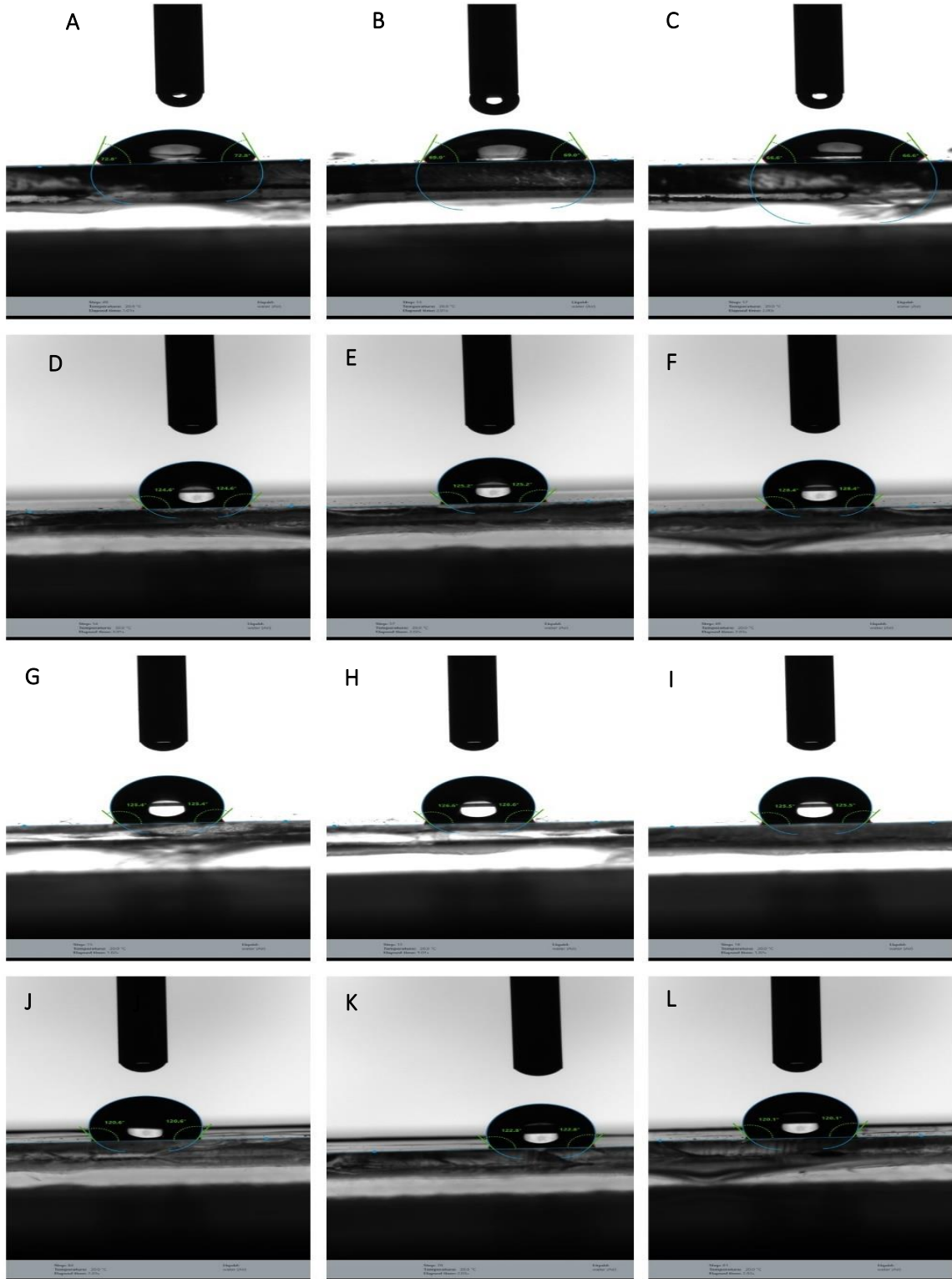


Figure 17. Light Microscopy Images of the Substrates. Substrates under the light microscope with the camera with 10x objective, zoom 1x. **A)** TCPS, **B)** Plain PDMS, **C)** MCF7 Pattern, **D)** MDA MB 231 Pattern, **E)** MCF7 Pattern-Plain PDMS, **F)** MDA MB 231-Plain PDMS, and **G)** 3T3 Pattern **H)** MCF7 Pattern-MDA MB 231Pattern.

3.1.2. Contact Angle Measurement

To explore the influence of the cell imprints on the wettability of the substrates, the sessile drop method was employed using a Drop Shape Analyzer machine (DSA25E, Krüss, Germany). Three substrates were prepared: TCPS, Plain PDMS, MCF7, MDA MB 231, and 3T3 Patterned PDMS. A 10 μ l droplet of MiliQ water was gently deposited onto each sample surface. Once the water droplet had stabilized, three images per substrate were captured using a high-resolution camera with an appropriate zoom level to obtain a clear droplet profile (Fig. 18). Finally, the contact angles were measured using the machines' software (Krüss Advance 1.08.04).



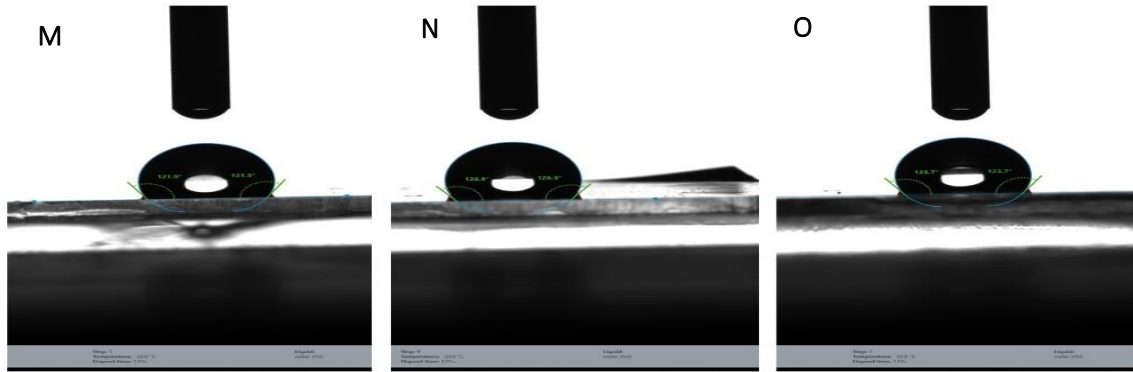


Figure 18. Contact Angle Measurement. Three areas on **A-C)** Polystyrene Plate, **D-F)** Plain PDMS, **G-I)** MDA-MB-231 Patterned PDMS, **J-L)** MCF7 Patterned PDMS, **M-O)** 3T3 Patterned PDMS.

By definition, when θ (Contact Angle) is $<90^\circ$ the surface is hydrophilic, and when θ is $>90^\circ$ it is considered a hydrophobic substrate[215]. As shown in Fig. 18 and Table 2, the treated TCPS has a hydrophilic contact angle with a value of around 69.42° , while this value for unpatented PDMS is 121.20° , which is hydrophobic. These values for other substrates with cell imprinting are higher up to 5 degrees. This shows that cell imprinting with changing the surface topography can slightly increase the surface hydrophobicity. PDMS is hydrophobic mainly due to its unique chemical arrangement and surface features. The hydrophobic characteristics of PDMS introduce both obstacles and benefits in cell imprinting. Although its hydrophobic properties may impede cellular adhesion, they simultaneously provide distinctive prospects for targeted cellular attachment and molecular retention, which prove advantageous in various biomedical contexts. This bifunctional aspect of PDMS's hydrophobicity can be harnessed to augment the efficacy of devices designed for cell imprinting. For instance, regarding circulating tumor cell isolation strategies, the hydrophobic features of PDMS can be strategically used to enhance capture outcomes. By incorporating boronate affinity principles and localized post-imprinting alterations, PDMS can proficiently isolate target cells from intricate biological matrices, improving cellular capture systems' efficiency and specificity[216]. PDMS and hydrogels are commonly employed in cell imprinting because of their remarkable traits. Nevertheless, PDMS presents numerous advantages over hydrogels, especially in cell imprinting applications. These advantages encompass superior mechanical properties, simplified fabrication processes, and targeted functionalization capabilities, rendering PDMS a preferred selection in various biomedical applications. The siloxane group in PDMS is pivotal in characterizing its special attributes, involving flexibility, formability, elasticity, and biocompatibility, which are essential for cell

imprinting. For example, PDMS nanosheets can elongate at a breakpoint of 338% alongside Young's modulus of 0.46 MPa, signifying pronounced flexibility and moderate rigidity[217]. Additionally, PDMS elastomers can be crafted to demonstrate elongations beyond 3,000% using solvothermal polymerization, thereby increasing their stretchiness and softness[218]. Moreover, the mechanical properties of PDMS can be modulated by changing the mixing ratios of the elastomer and curing agent. An increase in the quantity of the curing agent leads to a reduction in tensile strength. At the same time, the hardness is contingent upon the base-to-curing agent ratio, as evidenced by Shore A hardness values ranging from 37.2 to 43.2[219]. PDMS is recognized for its mechanical resilience and stability, which are vital for preserving micro/nano topographies' integrity over extended periods. This stability is advantageous in applications such as cell imprinting, microfluidic devices, and organ-on-chip systems, where consistent operational performance is paramount[220]. Furthermore, PDMS can be readily molded and cured, facilitating the swift and economically viable production of intricate micro- and nano-patterns. This simplicity in fabrication represents a notable superiority over hydrogels, which typically necessitate more complicated synthesis and molding methodologies[221]. Moreover, PDMS is biocompatible, allowing its application in numerous biomedical fields, like tissue engineering and pharmaceutical assessments. Its capacity to replicate the physiological niche and sustain cell viability is extensively documented[112, 222]. As a further point, integrating PDMS with carbon nanotubes allows for the creation of multifunctional substrates that confer additional benefits like electrical conductivity. This adaptability facilitates the innovation of advanced scaffolds for tissue engineering and other biomedical applications[223]. Alternatively, even though hydrogels showcase benefits, including modifiable mechanical features and reactions to environmental influences, they are not free from limitations. Hydrogels may encounter challenges for cell imprinting associated with mechanical strength and stability, which can compromise the durability and reliability of imprinted patterns. Furthermore, hydrogel fabrication methodology can be more intricate and less reproducible than PDMS[224, 225].

The hydrophobic characteristics of PDMS arise from many interconnected factors, as demonstrated by numerous research. To begin with, the chemical architecture of PDMS is pivotal in its hydrophobicity. PDMS is a silicone-derived polymer comprised of recurrent units of dimethylsiloxane, which feature a silicon-oxygen backbone accompanied by two methyl groups bonded to each silicon atom. This arrangement yields a minimal surface energy, which is a

fundamental determinant of hydrophobicity. The existence of methyl groups, characterized by their non-polar nature, enhances the water-repellent qualities of PDMS by reducing interactions with polar water molecules [228, 229]. Furthermore, the flexibility of the siloxane backbone permits PDMS to adopt configurations that further diminish surface energy. Such adaptability enables the restructuring of polymer chains to showcase the hydrophobic methyl groups at the surface, consequently boosting the material's hydrophobic properties [230, 231]. The low surface energy of PDMS, generally ranging from 20-24 mN/m, is markedly lower than that of water, which is approximately 72 mN/m, resulting in elevated contact angles and reduced wettability [232]. The surface features of PDMS, together with its basic chemical attributes, could impact its hydrophobic properties during application. Surface roughness, which may be introduced during the manufacturing process or via post-processing treatments, can intensify the hydrophobic effect of the Cassie-Baxter model. This theoretical model elucidates how air pockets trapped beneath water droplets on a rough surface can enhance the contact angle, thereby improving hydrophobicity. In simpler terms, the Cassie-Baxter model helps us understand how the surface roughness of PDMS contributes to its hydrophobicity. Therefore, the air pockets trapped inside the patterns justify the slight increase in the hydrophobicity of the Cell-Patterned PDMS compared to Plain PDMS. The contact angles observed for MCF7 and MDA MB 231 patterned PDMS exhibit a statistically significant difference compared to those associated with Plain PDMS ($P < 0.05$). Conversely, the disparity between 3T3 patterned and Plain PDMS does not achieve statistical significance ($P > 0.05$). This shows that the morphology of imprinted cells can manipulate the hydrophobicity of PDMS (Table 2).

Table 2. Contact Angle Values. The values for the contact angles of different substrates.

Surface Type	Contact Angle \pm SD
TCPS	69.42 \pm 3.16 $^\circ$
Plain PDMS	121.20 \pm 1.49 $^\circ$
MDA-MB-231 Patterned PDMS	125.76 \pm 0.65 $^\circ$
MCF7 Patterned PDMS	125.89 \pm 1.92 $^\circ$
3T3 Patterned PDMS	124.22 \pm 2.52 $^\circ$

Polystyrene exhibits an intrinsic hydrophobic nature attributable to its molecular architecture, characterized by extensive hydrocarbon chains that exert a repulsive force against water molecules. Conversely, tissue culture plates are hydrophilic through specific surface modifications that integrate polar functional groups, augmenting their water interaction capacity and facilitating cellular adhesion. The conversion from a hydrophobic to a hydrophilic state is accomplished via a spectrum of surface treatment methodologies. The hydrophilicity of polystyrene surfaces can be enhanced through plasma treatment techniques, such as electron cyclotron resonance plasma utilizing argon, which facilitates the incorporation of polar groups onto the surface. This treatment reduces the water contact angle, signifying improved wettability; however, meticulous control is essential to prevent surface degradation[226]. Ion-Assisted Reactions: An alternative approach involves ion-assisted reactions, wherein polystyrene is subjected to ion irradiation in the presence of oxygen. This treatment engenders the formation of hydrophilic groups such as C-O and -(C=O)-O- on the surface, substantially diminishing the contact angle and promoting cellular proliferation on the modified surfaces[227]. Using grafting techniques to bond hydrophilic polymers with polystyrene enhances its ability to attract water. This technique permits meticulous regulation of the hydrophilic layer's thickness, which is paramount for applications such as cell sheet engineering[228]. The application of silica films to polystyrene surfaces can yield super-hydrophilic characteristics. These coatings significantly boost wettability and simultaneously stimulate cell adhesion and proliferation by enhancing serum protein absorption, which is vital for cell culture[229]. Plasma Deposition Isopropyl Alcohol Plasma enables the deposition of a thin hydrophilic film onto polystyrene, thereby increasing the surface oxygen content and introducing carbonyl and alcohol/ether functional groups. Such modifications enhance the surface's suitability for cell attachment and proliferation[230].

The hydrophilic properties of TCPS are crucial as they affect cell attachment to the plate's surface. Surfaces exhibiting hydrophilicity have been shown to enhance cellular attachment by their capacity to engage with the aqueous surroundings and various proteins in the culture medium. Such interactions play a pivotal role in facilitating the binding of proteins that ultimately govern cell adhesion[231]. However, the impact of other surface characteristics of materials utilized in tissue culture on cell adhesion is of great significance. Hickman et al.'s study brings to light the essential importance of surface chemistry alongside topographical traits in affecting how cells respond. The discussion revolves around the ability of specific surface modifications to

improve cell attachment and growth, which are essential for tissue engineering purposes[232]. This viewpoint is further supported by Bain and Hoffman, who emphasize that surface hydrophilicity and charge can impact protein adsorption, subsequently influencing cell adhesion and proliferation[233]. Moreover, the mechanical attributes of the surface, such as stiffness, also hold a crucial position. Brecher et al. study how alterations to the substrate's mechanical features can influence stem cells' differentiation pathways, a vital aspect in regenerative medicine[234]. This perspective aligns with the discoveries of Kasper et al., who observe that the mechanical signals provided by the substrate can replicate the natural cellular surroundings, thus fostering desired cellular functions[17]. Apart from chemical and mechanical properties, surface micro- and nano-scale topography is paramount. Sivanesan et al. delve into how micro-patterned surfaces can steer cell alignment and organization, a critical aspect in fabricating tissue constructs necessitating specific cellular architectures[235]. Similarly, Hsieh's research underscores the significance of nano-topographical characteristics in elevating cell-surface interactions, potentially leading to enhanced tissue integration and function[236]. Although the PDMS is intrinsically hydrophobic, creating micro patterns with the cell imprinting technique can make it a desirable substrate for cell adhesion since it improves cell-substrate interactions.

3.1.3. Fourier-Transform Infrared Spectroscopy

FTIR spectroscopy constitutes a sophisticated analytical methodology for identifying organic compounds, polymeric materials, and, occasionally, inorganic entities. The samples of PDMS and TCPS, fabricated in the form of circular discs measuring 1 cm in diameter, were meticulously prepared and subjected to FTIR analysis (Cary 630 FTIR Spectrometer, Agilent, Germany) in transmission mode to facilitate the identification of chemical substrates, with the resultant data processed utilizing the spectrometer's FTIR software (MicroLab, Agilent Technologies). Subsequently, the FTIR spectra, depicting %Transmittance as a function of Wavenumber (cm^{-1}), were generated and plotted utilizing OriginPro. (Fig 19). Polystyrene, a thermoplastic polymer, demonstrates specific FTIR spectral characteristics that can be employed to verify its identity and evaluate its structural attributes. The FTIR spectrum of polystyrene (Fig. 19. A) generally, reveals distinct absorption bands that correlate with its chemical architecture. The analysis shows distinct absorption peaks at approximately 3026 cm^{-1} , which are linked to the aromatic C-H stretching vibrations, alongside peaks near 1602 cm^{-1} and 1490 cm^{-1} , tied to the C=C stretching vibrations of

the aromatic ring. Furthermore, the spectrum frequently exhibits bands around 1446 cm^{-1} and 752 cm^{-1} , which signify the C-H bending vibrations within the aromatic ring[237, 238].

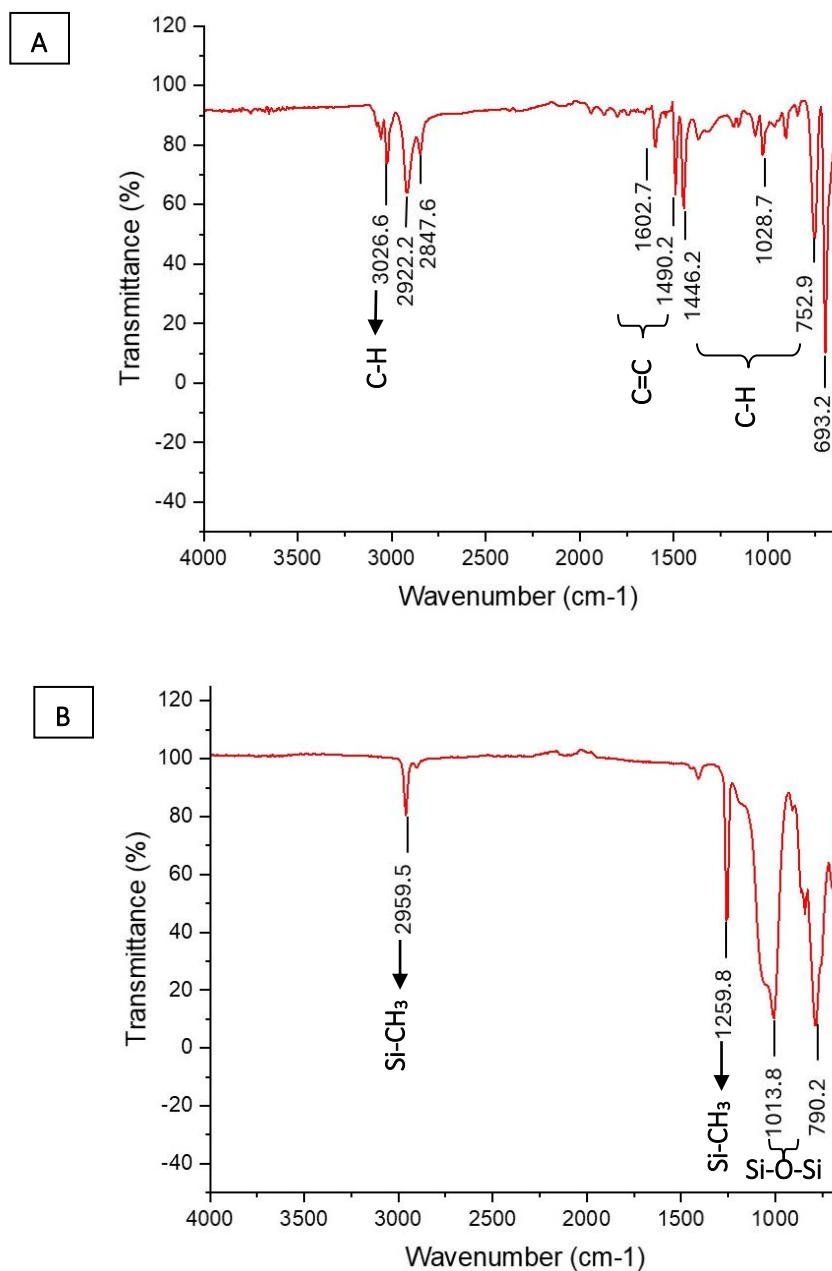


Figure 19. FTIR Analysis. A) Polystyrene B) PDMS.

On the other hand, PDMS showcases its FTIR spectral traits (Fig. 19. B), incorporating numerous significant absorption bands. The most conspicuous is the Si-O-Si stretching vibration, which manifests in the $1000\text{-}1100\text{ cm}^{-1}$ region. This absorption band is a definitive marker of the

siloxane backbone inherent to PDMS. It plays a critical role in verifying the presence of the polymer within a given sample [239, 240]. Furthermore, the Si-CH₃ stretching vibrations are detected near 2960 cm⁻¹, indicating the methyl groups covalently bonded to the silicon atoms within the PDMS molecular framework[241, 242]. An additional salient feature in the FTIR spectrum of PDMS pertains to the Si-CH₃ bending vibration, which characteristically emerges around 1260 cm⁻¹. This spectral band, in conjunction with the Si-O-Si and Si-CH₃ stretching vibrations, aids in differentiating PDMS from other silicone-derived materials and polymers [243, 244]. Observing these absorption bands substantiates the structural integrity of PDMS and may be employed to evaluate the purity and compositional attributes of the material.

3.2. Characterization of CdSe/CdS QDs

3.2.1. Dynamic Light Scattering

The particle size analyzer instrument (Malvern Panalytical) was used to assess the size of the PMA-QDs. The initial PMA-QD stock solution with a concentration of 100nM was diluted in Milli-Q water to achieve a concentration of 10nM, followed by a 30-minute sonication process to disperse any agglomerated particles before transfer into a plastic cuvette. Subsequently, the cuvette was subjected to analysis using the instrument. The size of the particles was measured five times, and the size distribution of the particles by intensity was plotted as Average±SD on OriginPro (Version 9.9.0.225, Academic) (Fig.20). The results show that the average size of the PMA-Coated QDs is around 41nm. The dimensional characteristics of polymer-encapsulated CdSe/CdS QDs represent a pivotal variable affecting their optical attributes and utility across diverse disciplines, including optoelectronics and biomedical imaging. The dimensions of CdSe/CdS QDs exhibit variability contingent upon the methodologies employed for synthesis and coating. CdSe/CdS quantum dots generally exhibit dimensions spanning from 1.5 nm to more than 10 nm. For example, CdSe quantum dots synthesized within a 6-12 nm size range demonstrate pronounced alterations in their optical spectra as a function of size variation[245]. The core-shell configuration, exemplified by CdSe/CdS, may possess diverse shell thicknesses, affecting the overall dimensions and optical characteristics. For instance, shell thicknesses varying from 0 to 8 monolayers have been investigated, revealing that increased shell thickness enhances the reversibility of optical property modifications following electron injection[139]. In a

study by Mansoor Ani Najeeb et al., CdSe QDs integrated within a PEDOT²⁴: PSS²⁵ matrix were fabricated, yielding an average size within the range of 5 to 7 nm[246]. This dimensional range is representative of QDs utilized in optoelectronic contexts, where diminutive sizes are frequently favored for their size-dependent optical characteristics. An additional investigation by Rashmi Singh et al. documented CdSe QDs exhibiting sizes spanning from 4 to 7 nm when incorporated within a Poly(1,8 diamionaphthalene) matrix[247]. The observed consistency in size across various polymer matrices implies a shared methodology in synthesis or aligns with specific application prerequisites, such as the preservation of elevated quantum efficiency and stability. Conversely, the research conducted by Ki-Heon Lee et al. delineated larger CdSe/ZnS QDs, with dimensions extending up to 12.7 nm, after applying an additional ZnS shell[248]. This augmented size is ascribed to the overcoating procedure, which bolsters the stability and operational efficacy of the QDs in electroluminescent devices. The enlargement in size attributable to supplementary shell layers underscores the inherent trade-off between size and enhanced optical characteristics, including increased luminance and efficiency. In addition, the analysis by Young-Tae Kwon and others centered around CdSe/ZnSe quantum dots that were covered with a PMMA²⁶ film, which granted improved stability and a limited size range[249].

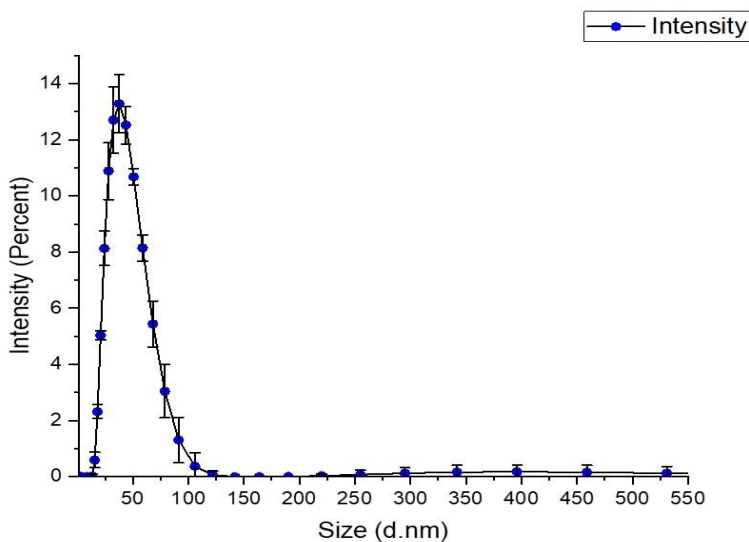


Figure 20. Size Distribution by Intensity. The graph shows the size distribution of the PMA-Coated QD particles. The average size of the particles is about 41nm.

²⁴ Poly(3,4-ethylene-dioxythiophene) (PEDOT)

²⁵ Poly(styrene sulfonate) (PSS)

²⁶ Poly(methylmethacrylate) (PMMA)

3.2.2. Fluorescence Spectroscopy

The emission wavelength of the PMA-QDs was determined by diluting the stock solution in MilliQ water to reach 10nM of concentration and transferring the solution to a crystal cuvette (Hellma Analytics, Switzerland), followed by analysis using the Fluorescence Spectrometer (Cary Eclipse, Agilent Technologies, Germany), and the normalized intensity was plotted against the wavelength on OriginPro. (Fig. 21). The results show that the emission peak is on 620nm wavelength. The fluorescence properties of CdSe QDs display elevated quantum yield and narrowly defined emission bands, which are beneficial for applications that necessitate accurate optical attributes. Still, these precisely outlined bands create obstacles that demand extensive emission spectra. Alterations, such as introducing defect-state emissions, can facilitate broadening the emission spectrum, thereby augmenting their functionality in such applications[250]. The emission characteristics of CdSe QDs can be deeply influenced by their surface conditions and the ambient surroundings. For example, the existence of surfactants can influence emission characteristics, a phenomenon that can be alleviated by the application of a shell around the quantum dots[250]. By enhancing the fluorescence of plasmonic structures like gold nanorods, one can markedly elevate the fluorescence of CdSe QDs via a plasmon-enhanced fluorescence mechanism. The degree of enhancement is critically contingent upon the interstitial distance between the quantum dots and the plasmonic substrate, with optimal spatial configurations resulting in considerable amplifications in fluorescence intensity[251].

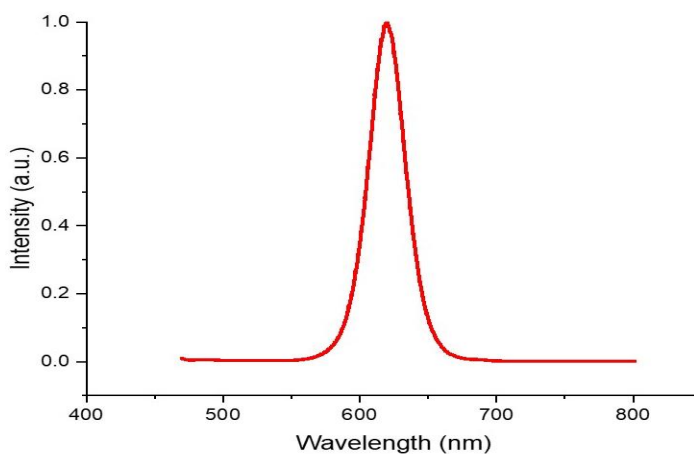


Figure 21. PMA-QDs Emission Spectrum. The normalized emission spectrum of the PMA-QDs.

3.2.3. Endocytosis Assay

The fluorescent emission of particles was measured after 24 hours to find the endocytosis of PMA-coated QDs. First, MCF7 cells at a concentration of 1×10^4 in $100 \mu\text{l}$ of complete DMEM were seeded in a 96-well plate across nine columns overnight, with six replicates for each concentration group. Following this, the medium was removed, and various concentrations of QDs (0, 0.01, 0.1, 1, 5, 10, 20, 50, and 100 nM) in a complete medium were added to the MCF7 cells for 24 hours. After removing the QDs, the cells were washed three times with sterile PBS and then covered with 100 ml/well of DMEM. Finally, the plate was analyzed using the microplate reader instrument (FLUOstar Omega, BMG LABTECH, Germany) for the fluorescent emission analysis (Ex/Em 355/620nm). As demonstrated in Fig. 23, the emission intensity increased from around 40,000 in the control group to more than 220,000 in the group with 100 nM of QD concentration. In other words, expanding the QD concentration has led to a higher uptake of the particles. However, the Presto blue assay was conducted to find a non-toxic concentration of the particles.

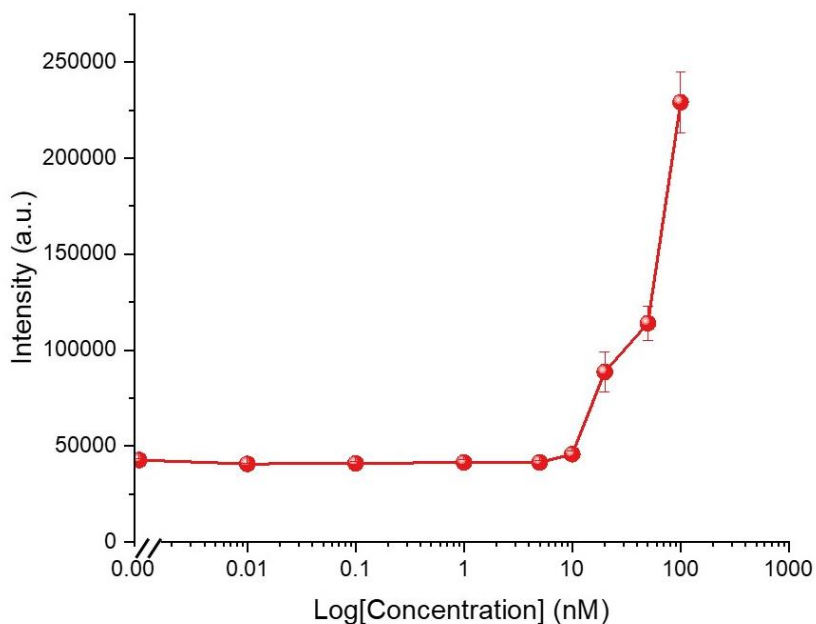


Figure 22. Endocytosis. The PMA-QD intensity emission from MCF7 cells exposed to various concentrations of the QDs ranged from 0.01 to 100 nM .

The intricate uptake of CdSe/CdS QDs via endocytosis is shaped by numerous cellular pathways along with the core physicochemical attributes of the QDs. Investigations have demonstrated that

these nanoparticles can penetrate cellular areas through different endocytic strategies, with clathrin-mediated endocytosis identified as a significant channel. Research has corroborated that CdSe/CdS QDs endocytosis transpires through clathrin-mediated endocytosis, a mechanism governed by the adapter protein HIP-55. This specific protein engages with clathrin and F-actin, promoting the endocytic uptake of QDs. The inhibition of HIP-55 or its interaction with F-actin markedly diminishes the uptake of QDs, thereby underscoring its pivotal function within this cellular pathway[252]. Furthermore, research with yeast models has disclosed that QDs can modify receptor-mediated endocytosis and pinocytosis, causing issues in the maturation of endocytic patches and shifting intracellular trafficking dynamics[253]. The internal movement of CdSe/CdS quantum dots is also distinguished by their accumulation at the cell exterior, which is later accompanied by their entry through clathrin-receptor-mediated endocytosis. Upon their entry, QDs are disseminated to the late Golgi/trans-Golgi network, thereby influencing cellular dynamics, including growth rate and the organization of actin filaments[254]. This implies that quantum dots might influence cellular mechanisms by adjusting the actin cytoskeleton, which is essential for endocytic processes and other cellular functions. Moreover, the surface characteristics of QDs, particularly their coatings, play a significant role in determining their endocytic pathways. For instance, carboxylic-acid-coated quantum dots (COOH-QDs) utilize lipid raft and caveolin pathways for cell entry, subsequently sequestered in multivesicular bodies to bypass lysosomal degradation. In another light, quantum dots bonded with biologically active proteins, such as platelet-derived growth factors, are absorbed via clathrin-mediated endocytosis and gathered in lysosomes, highlighting how surface characteristic alterations can reshape intracellular transport mechanisms and affect biological operations[255]. The endocytic uptake of QDs is additionally contingent upon their interaction with cellular membranes and the ensuing intracellular transport mechanisms. Research has indicated that QDs can be internalized and subsequently processed by endosomes and lysosomes, with variances in surface functionality influencing their toxicity profiles. For example, COOH-QDs undergo continuous internalization and transport, culminating in more significant toxicity than NH₂-QDs, which predominantly reside within lysosomes[256].

3.2.4. Presto Blue Cytotoxicity Assay

To determine the non-toxic concentration of PMA-coated QDs, the Presto Blue assay was performed on the samples from the previous step. After QDs removal, the cells were washed three times with PBS, and then 100ml/well of the presto blue dye 1x, pre-diluted in the serum-free DEMEM, was administered to each group. Finally, the plate was incubated for one hour before being analyzed using the microplate reader (Fluostar Omega, BMG Labtech, Germany) for the fluorescent emission analysis (Ex/Em 560/590nm) of Resorufin (Fluorescent Converted Resazurin). As shown in Figure 24, the QD concentration between 0.01 and 10nM does not show significant cytotoxicity; however, the emission intensity drops significantly for concentrations higher than this, which means they are unsuitable for cell tagging. Research demonstrates that CdSe/CdS quantum dots can elicit considerable cytotoxicity through mechanisms involving oxidative damage and inflammatory responses.

The cytotoxicity of CdSe QDs may be appreciably diminished by modifying their surface characteristics. For instance, CdSe QDs coated with ZnS shells exhibit lower toxicity than uncoated QDs. This is attributed to the ZnS shell acting as a barrier, reducing the release of toxic cadmium ions[257, 258]. In the same manner, CdSe QDs that are confined within biocompatible agents like polyethylene glycol or polyvinyl alcohol portray increased biocompatibility and decreased cytotoxic outcomes, thereby making them appropriate for bioimaging applications[259]. The cytotoxicity manifested by CdSe QDs is contingent upon dosage levels. Empirical studies have demonstrated that at concentrations reaching up to 100 $\mu\text{g/mL}$, CdSe QDs display minimal toxicity; however, elevated concentrations decrease cellular viability [260, 261]. Furthermore, extended durations of exposure correlate with an increase in cytotoxicity, as evidenced by investigations where QDs were subjected to testing over intervals ranging from 24 to 72 hours[259]. The cytotoxicity of CdSe QDs exhibits variability across diverse cellular types. As an illustration, the impact of CdSe QDs has shown a capacity to hinder the growth of HeLa cells, the human cervical cancer type, while not greatly elevating the generation of reactive oxygen species when used in minimal concentrations[257]. Conversely, investigations involving human embryonic kidney cells (HEK293) and human colorectal carcinoma cells (HCT-116) have indicated that CdSe QDs may be non-toxic at specific concentrations, particularly when modified with biocompatible coatings[261-263].

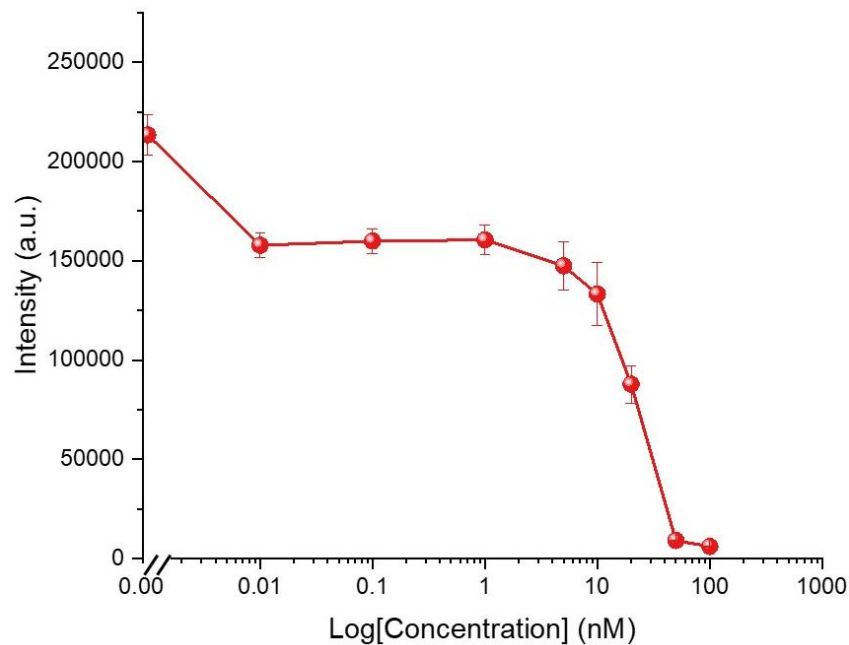


Figure 23. Cytotoxicity by Presto Blue. Resorufin intensity emission of MCF7 cells exposed to various concentrations of QDs ranging from 0.01 to 100nM.

3.2.5. Transmission Electron Microscopy

TEM imaging is a critical method in exploring the structural aspects of QDs, delivering a significant understanding of their dimensions, morphological traits, and core-shell formats. The diminutive dimensions of QDs present significant obstacles to TEM sample preparation, necessitating meticulous methodologies to guarantee site-specific examination. This is fundamental for revealing the microstructural aspects and particular chemical qualities of QDs at the nanoscale[264]. As already explained, TEM imaging of the CdSe/CdS QDs was performed at a voltage setting of 100 kV for the 10 times diluted QD solution and on a carbon-coated TEM grid. The particles' dimensions were calculated using ImageJ version 1.46, based on the TEM images (Fig. 25). The estimated size of the QD after analyzing these images with ImageJ is 15.23 ± 1.19 nm. Figure 26 shows the histogram and distribution curve of the particles' size. The difference between the results from DLS, which was around 41 nm, is due to the inability of the TEM to image the ligand (PMA) around the particles. Meanwhile, DLS provides the hydrodynamic size of the particles. In other words, the size of QDs without the PMA coating is around 15 nm, while the actual size of the coated QDs is around 41 nm.

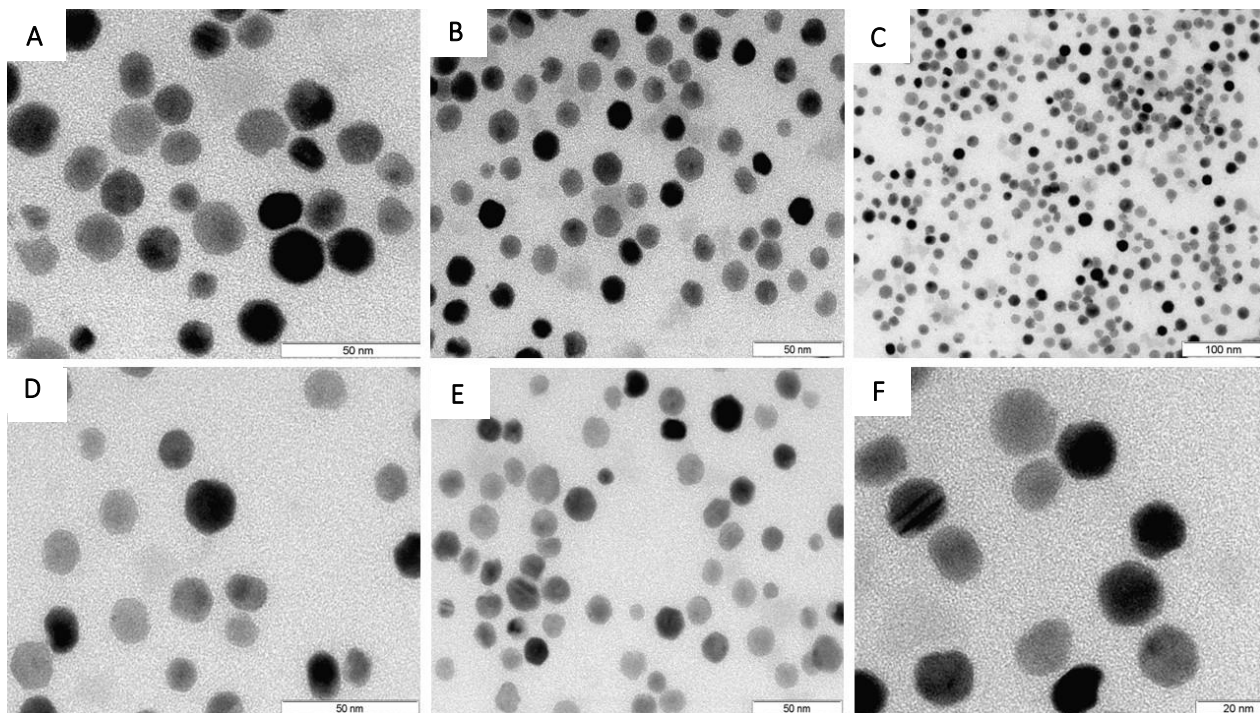


Figure 24. TEM Micrographs of PMA-QDs. A-F) TEM images with various magnifications.

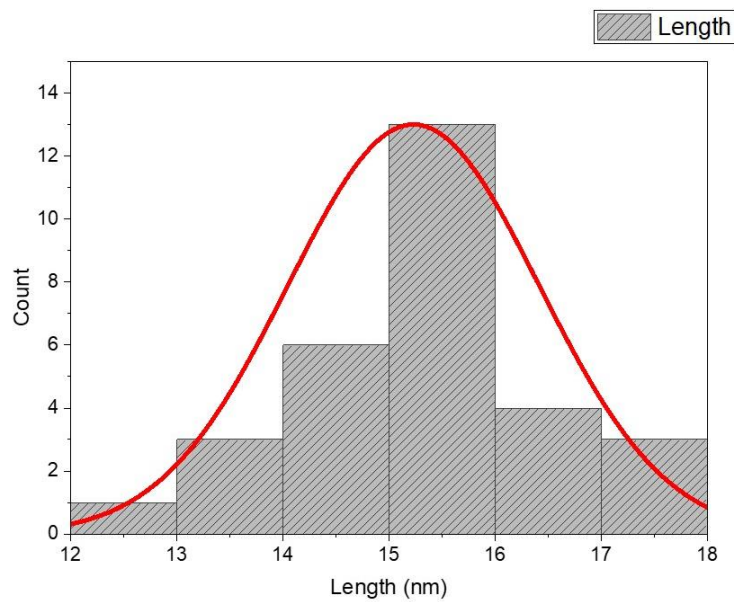
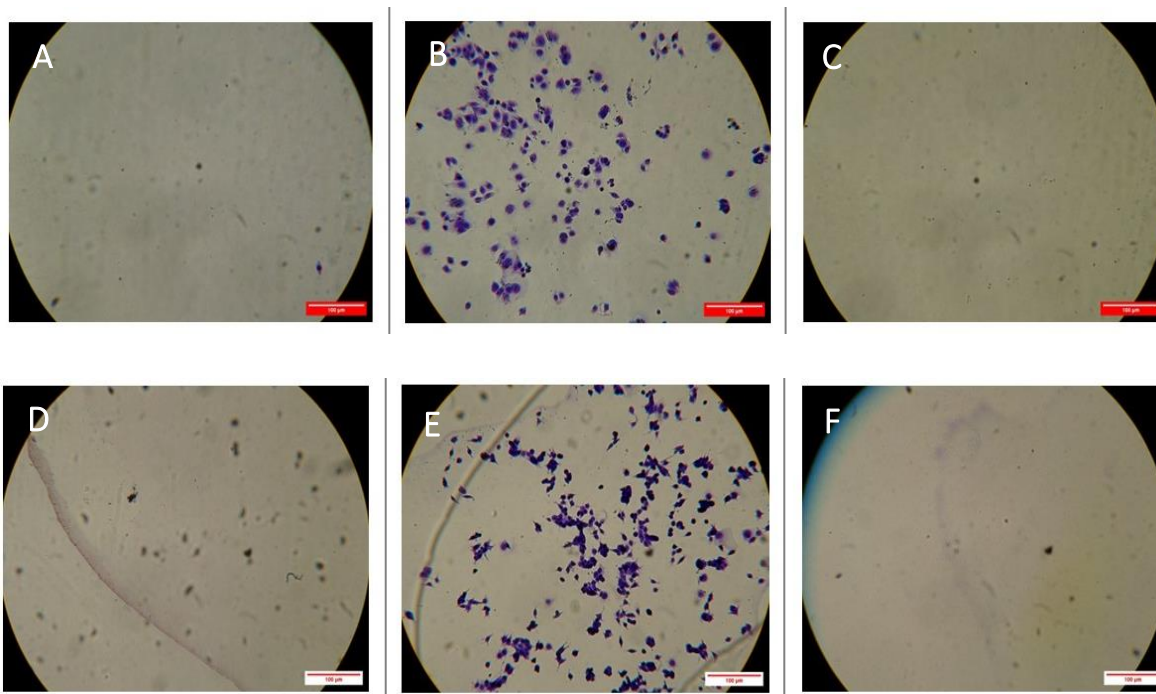


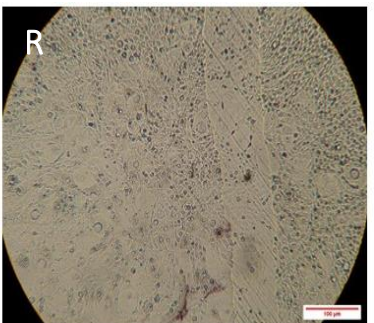
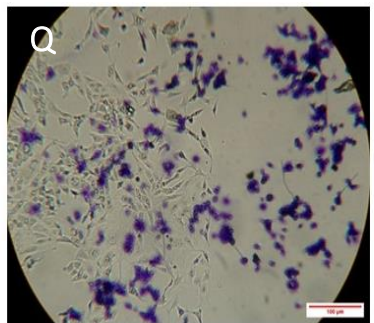
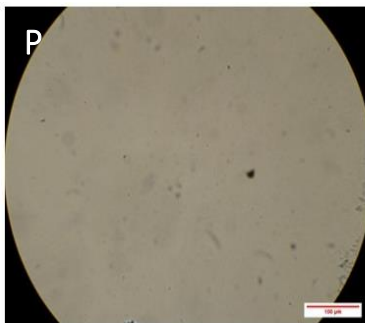
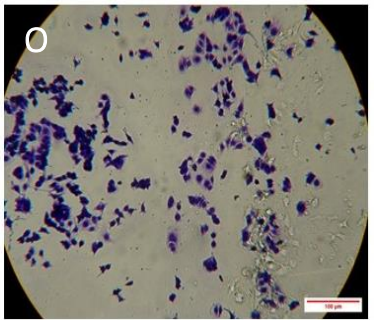
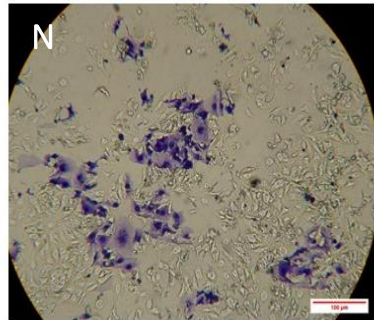
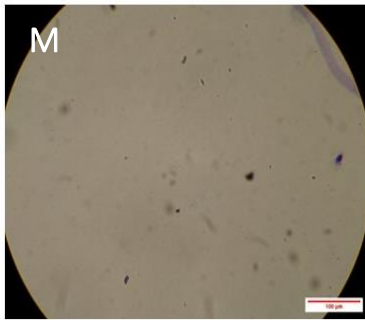
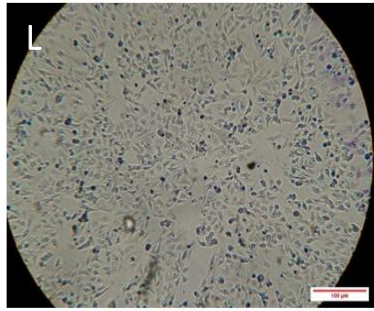
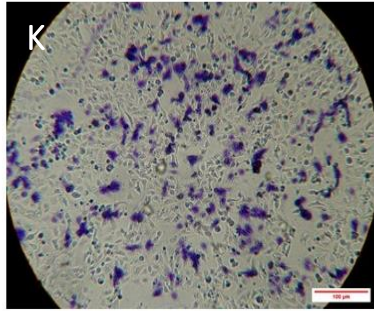
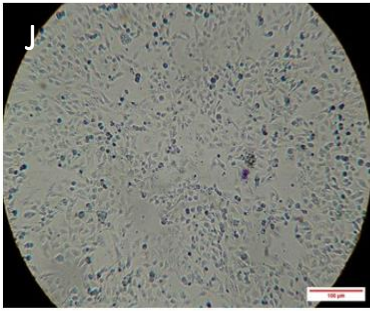
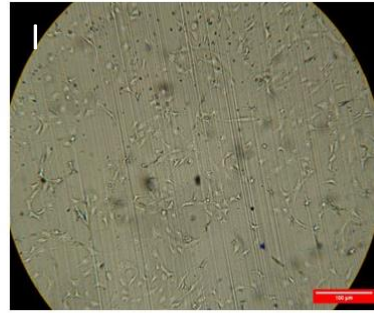
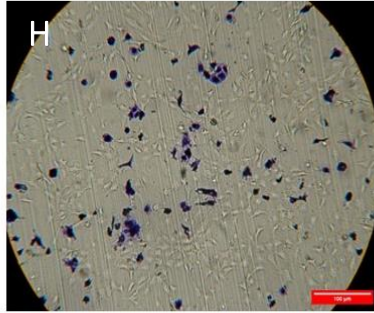
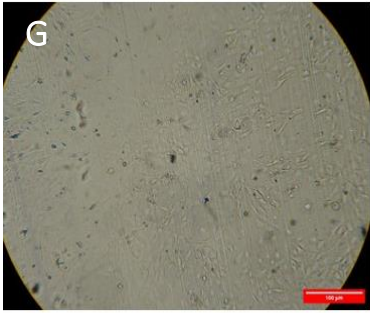
Figure 25. The Histogram and Distribution Curve of CdSe/CdS QD Particles' Size.

3.3. Migration Assay

3.3.1. Crystal Violet Assay

Seven different substrates were prepared, with three replicas for each type. These included MCF7 Pattern, MCF7 Pattern-Plain PDMS, Plain PDMS, 3T3 Pattern, 3T3 Pattern-MCF7 Pattern, 3T3 Pattern-Plain PDMS, and TCPS. Subsequently, 500 MCF7 or 3T3 cells suspended in 25 μ l of medium were carefully placed at the center of disc-shaped samples measuring 10mm in diameter. After 3 hours, an additional 75 μ l of medium was evenly distributed onto each sample. Following 21 hours, shorter than the cells' doubling time, the cells were immobilized using a 4% paraformaldehyde solution for 20 minutes. The immobilized cells were then stained with a crystal violet solution at a concentration of 0.5% and subsequently examined under the light microscope (Axiovert, Zeiss, Germany) with a 10x objective after three subsequent washes with MiliQ water. Figures 27 and 28 show the distribution of the MCF7 and 3T3 cells on different substrates, respectively.





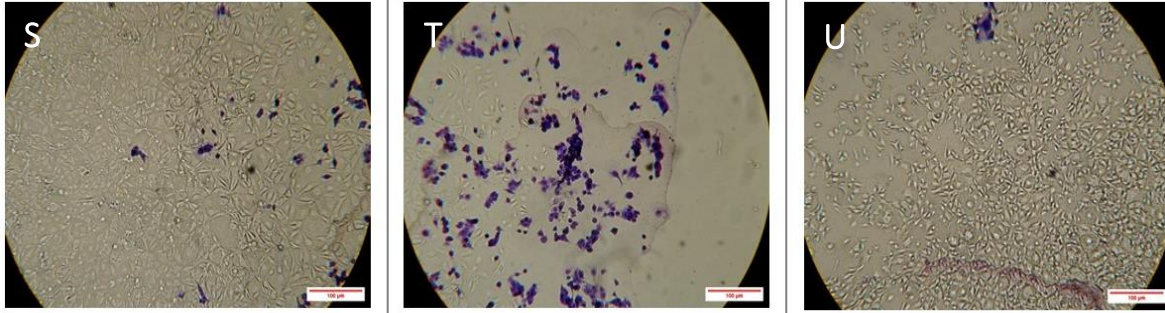
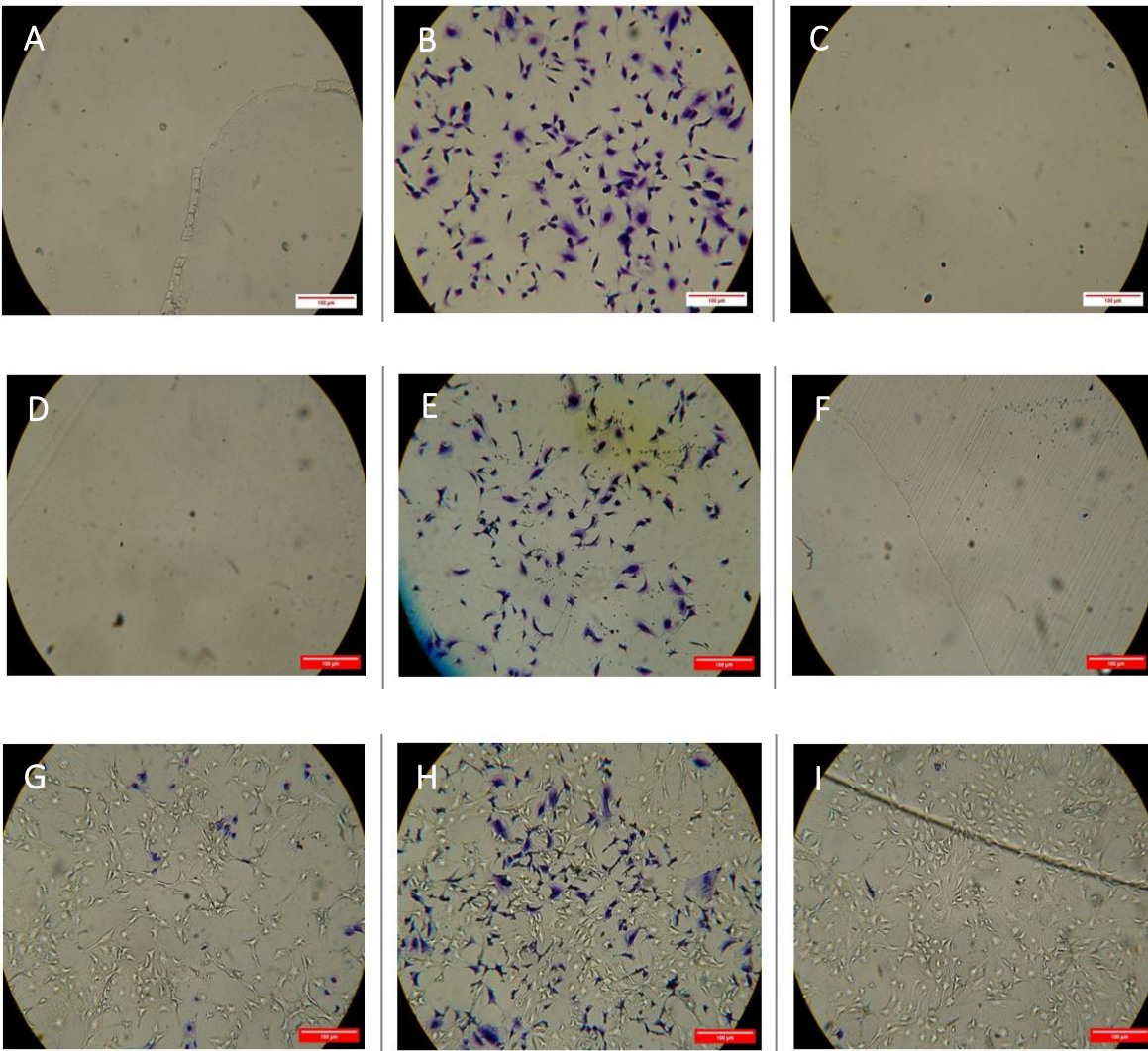


Figure 26. MCF7 On Different Substrates. TCPS: **A)** Outside Seeding Area **B)** Seeding Area **C)** Outside Seeding Area. Plain PDMS: **D)** Outside Seeding Area **E)** Seeding Area **F)** Outside Seeding Area. 3T3 Pattern: **G)** Outside Seeding Area **H)** Seeding Area **I)** Outside Seeding Area. MCF7 Pattern: **J)** Outside Seeding Area **K)** Seeding Area **L)** Outside Seeding Area. MCF7 Pattern-Plain PDMS: **M)** Plain Area **N)** Seeding Area **O)** Patterned Area. 3T3 Pattern-Plain PDMS: **P)** Plain Area **Q)** Seeding Area **R)** Patterned Area. MCF7 Pattern-3T3 Pattern: **S)** MCF7 Patterned Area **T)** Seeding Area **U)** 3T3 Patterned Area.



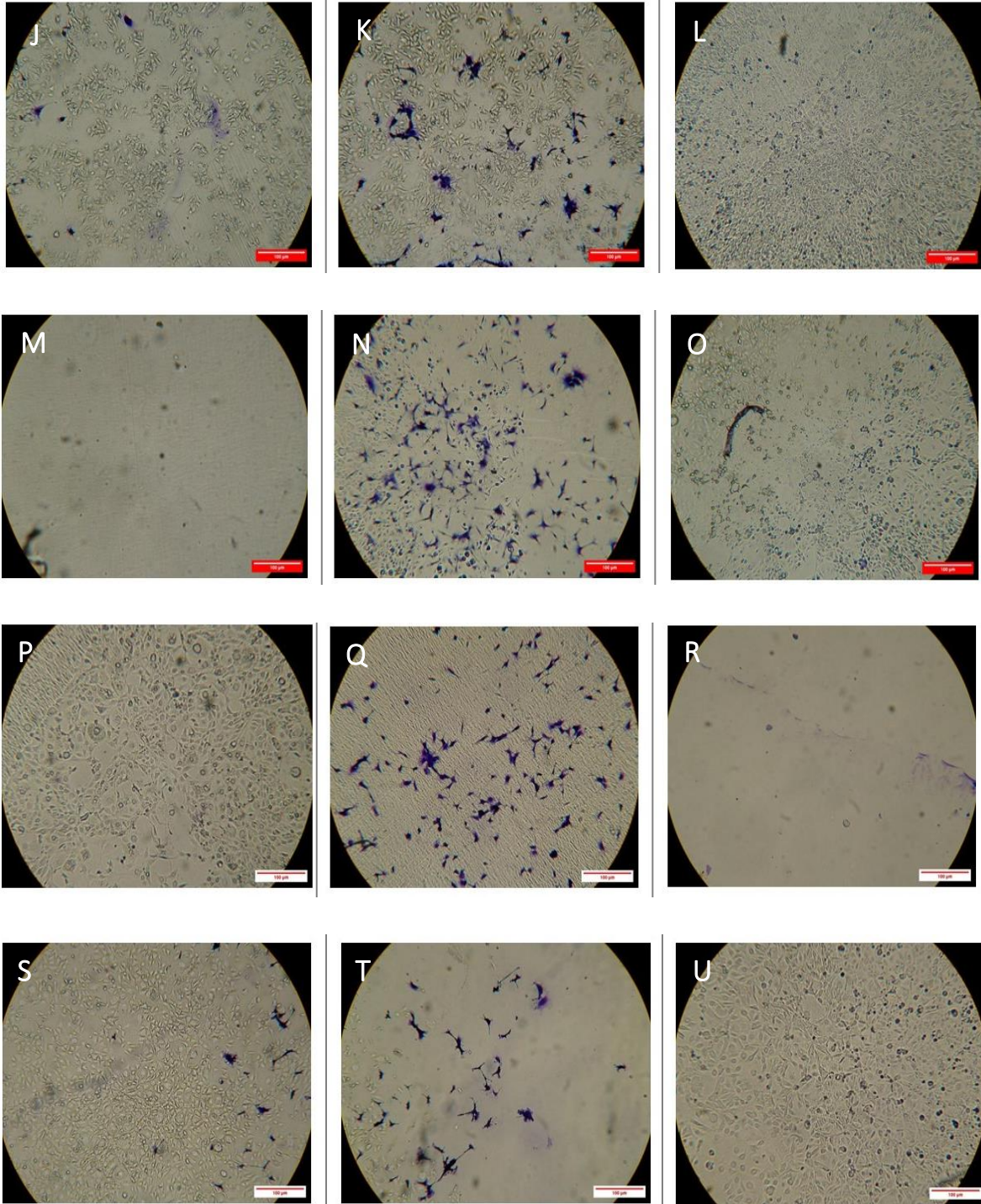


Figure 27. 3T3 On Different Substrates. TCPS: **A)** Outside Seeding Area **B)** Seeding Area **C)** Outside Seeding. Plain PDMS: **D)** Outside Seeding Area **E)** Seeding Area **F)** Outside Seeding Area. 3T3 Pattern: **G)** Outside Seeding Area **H)** Seeding Area **I)** Outside Seeding Area. MCF7 Pattern: **J)** Outside Seeding Area **K)** Seeding Area **L)** Outside Seeding Area. MCF7 Pattern-Plain PDMS: **M)** Plain Area **N)** Seeding Area **O)** Patterned Area. 3T3 Pattern-Plain PDMS: **P)** Patterned Area **Q)** Seeding Area **R)** Plain Area. MCF7 Pattern-3T3 Pattern: **S)** 3T3 Patterned Area **T)** Seeding Area **U)** MCF7 Patterned Area.

In Figures 27 and 28 A-L, it is evident that MCF7 and 3T3 cells on Single-Coating substrates, such as TCPS, Plain PDMS, MCF7 Patterned PDMS, and 3T3 MCF7 Patterned PDMS, exhibit less migration outside the primary seeding area compared to Double-Coating substrates, namely Plain PDMS-MCF7 or 3T3 Patterned PDMS and MCF7-3T3 Patterned PDMS. This means that cells migrate toward their patterns rather than Plain surfaces or those with a different pattern. Specifically, Figures 27 and 28-S demonstrate a significant migration of MCF7 and 3T3 cells towards their pattern outside the seeding area, as opposed to Figures 27 and 28-U, where a different cell pattern is observed outside the seeding area. Tables 3-4 and Figures 29-30 show the quantified results of cell distribution on Single and Double-Coating substrates.

Table 3. Cell Density on Single-Coating Substrates.

Coating A	Type of Seeded Cells	Average Density of Cells in the Seeding Area [cells/mm ²] ±SD	Average Density of Cells Outside the Seeding Area [cells/mm ²] ±SD
TCPS	MCF7	21.92±4.40	0.08±0.03
Plain PDMS		32.84±7.60	0.23±0.16
MCF7 Pattern		32.46±7.61	0.33±0.26
3T3 Pattern		29.70±8.00	0.86±0.77
TCPS	3T3	22.46±4.71	0.45±0.61
Plain PDMS		33.12±7.65	0.18±0.09
MCF7 Pattern		32.32±7.97	0.49±0.23
3T3 Pattern		31.14±7.81	0.54±0.40

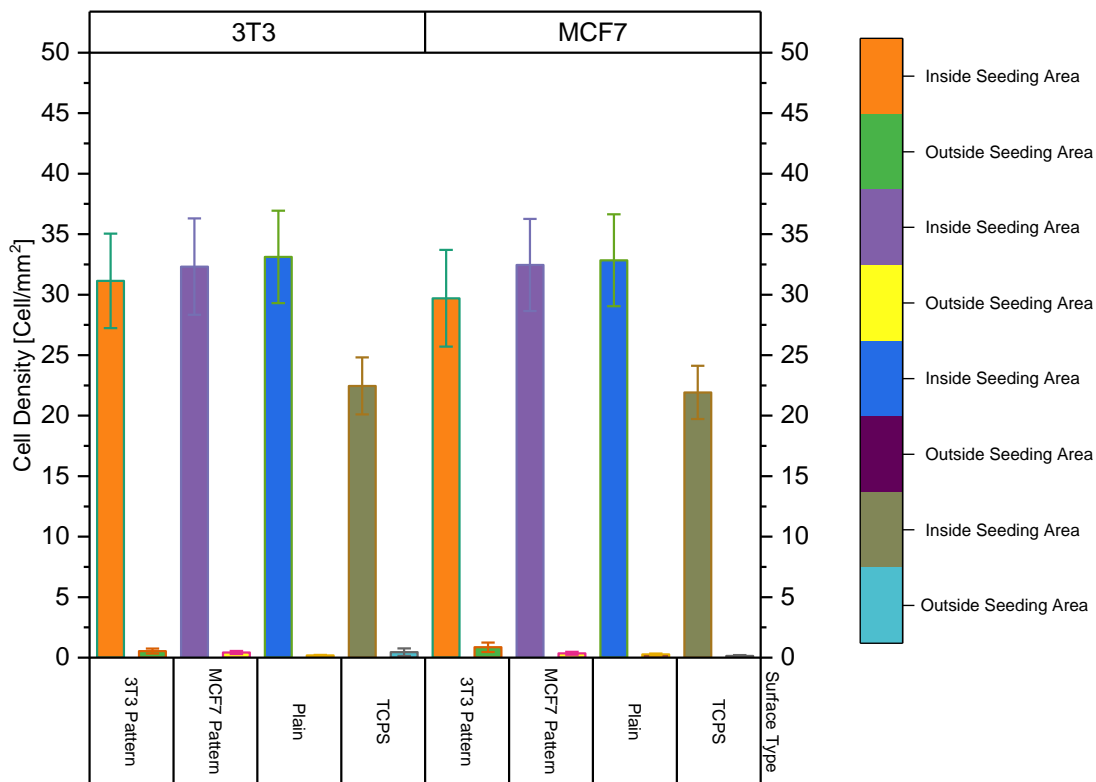


Figure 28. Diagram of Cell Density on Single-Coating Substrates.

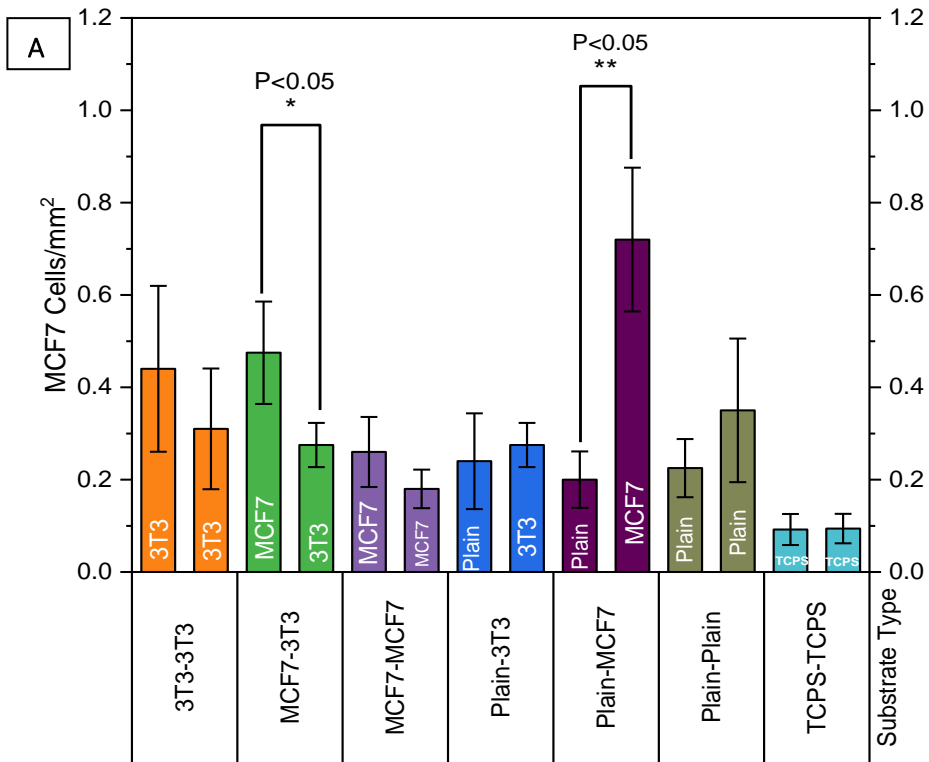
As shown in Table 3 and Figure 29, both MCF7 and 3T3 cells have high density inside the seeding zone compared to the outside seeding zone in Single-Coating substrates. In other words, the cells have a low migration rate when cultured on single-type substrates. Considering Table 4 and Figure 30, when Coating A is Similar to Coating B, e.g., TCPS-TCPS, there is no significant difference between the cell density on both substrates. Nevertheless, when Coating A is not similar to Coating B (Table 4, Figure 30), the cells demonstrate a significantly elevated density on their identically configured patterned surfaces compared to the heterogeneous substrates. For example, MCF7 cell density is more than three times higher on the MCF7 patterned side than on the plain side of the MCF7 Pattern-Plain PDMS. Similarly, the 3T3 density population is 2.5 times higher in the 3T3 patterned area than in the plain area. This proves the cell's tendency toward patterns rather than plain regions. Interestingly, the cells prefer a similar pattern for double-patterned substrates, i.e., MCF7 Pattern-3T3 Pattern. For instance, the MCF7 cell density on the MCF7 patterned area is 2.1 times higher than the 3T3 patterned side. Likewise, 3T3 cell density is 2.3 times higher in the 3T3 patterned zone than in the MCF7 patterned area. This

clearly demonstrates how smartly cells select and prefer their pattern over a different cell pattern for migration. However, the sole exception pertains to 3T3 cells cultured on Plain PDMS-MCF7 Pattern substrates, wherein the 3T3 cells exhibited a higher density on the patterned side in comparison to the Plain side, even though the pattern type diverges from their inherent morphology.

Table 4. Cell Density on Double-Coating Substrates.

Coating A	Coating B	Type of the Seeded Cells			
		MCF7		3T3	
		Average Cell Density outside Seeding area (coating A) [cells/m ²] ±SD	Average Cell Density outside Seeding area (coating B) [cells/m ²] ±SD	Average Cell Density outside Seeding area (coating A) [cells/m ²] ±SD	Average Cell Density outside Seeding area (coating B) [cells/m ²] ±SD
TCPS	TCPS	0.09±0.07	0.09±0.06	0.42±0.36	0.30±0.24
Plain PDMS	Plain PDMS	0.22±0.13	0.35±0.31	0.17±0.05	0.15±0.06
Plain PDMS	MCF7 Pattern	0.20±0.12	0.72±0.31	0.36±0.24	0.72±0.38

Plain PDMS	3T3 Pattern	0.15±0.06	0.28±0.09	0.22±0.13	0.55±0.40
MCF7 Pattern	MCF7 Pattern	0.18±0.08	0.26±0.15	0.29±0.12	0.32±0.13
MCF7 Pattern	3T3 Pattern	0.47±0.22	0.27±0.09	0.40±0.28	0.93±0.66
3T3 Pattern	3T3 Pattern	0.44±0.36	0.31±0.26	0.22±0.05	0.22±0.09



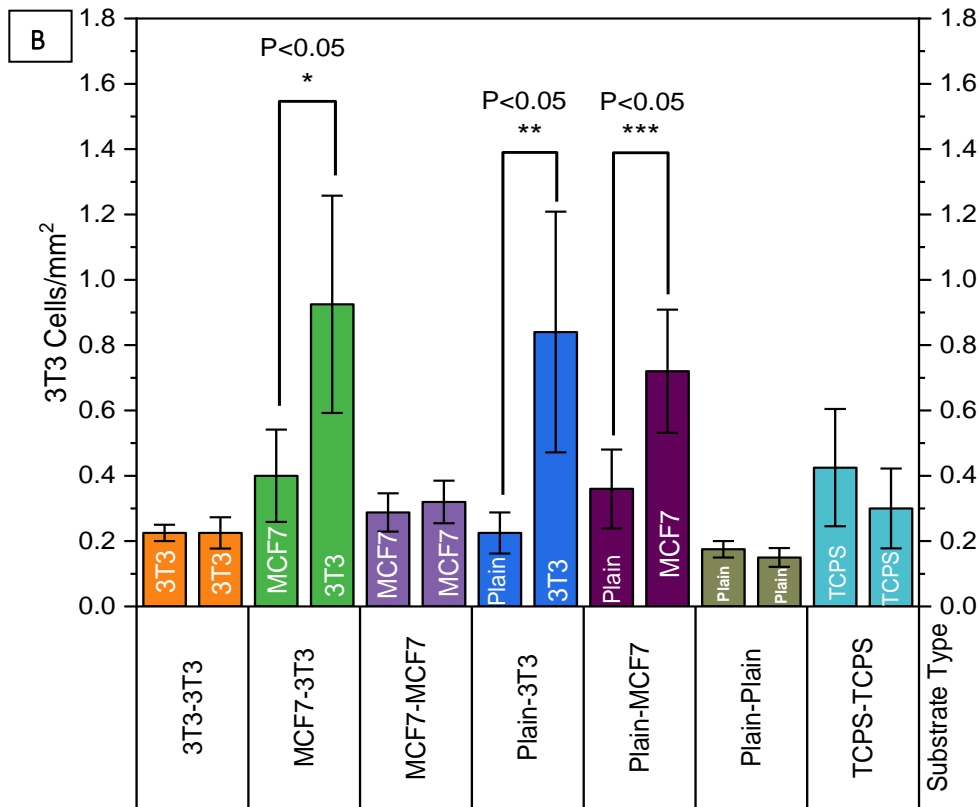


Figure 29. Diagram of Cell Density on Double-Coating Substrates. A) MCF7 cells B) 3T3 Cells

Crystal violet staining is a prevalent methodology for evaluating cancer cell motility, particularly in in vitro experimental paradigms. This technique is applied across diverse experimental frameworks to assess neoplastic cells' migratory and invasive attributes. In cancer cell motility, crystal violet is employed in the scratch Wound Healing Assay, which functions as a dye to visualize and quantify cellular migration across a deliberately induced "scratch" in a monolayer of cells. This methodological approach is particularly beneficial due to its straightforwardness and economic viability, enabling researchers to modify experimental parameters with relative ease to investigate various facets of cell migration[265]. Furthermore, crystal violet is incorporated into a refined assay designed to assess tumor cell invasion and migration, wherein it stains cells that have traversed through a microporous membrane within a Transwell chamber. This technique facilitates a colorimetric evaluation of cellular invasion, furnishing a quantitative metric of migratory capability that aligns with conventional cell-counting methodologies. Applying this unique strategy is especially relevant for analyzing possible inhibitors that affect the invasion and migration of cancer cells, illustrated by recognizing the anti-invasive attributes of substances such as doxorubicin and caffeic acid[266].

3.3.2. Scanning Electron Microscopy (SEM)

SEM is a powerful tool for assessing surface topography, providing detailed and quantitative insights into the microstructural elements of various materials. The micrographs generated by SEM offer both qualitative and quantitative data on surface topography, which is crucial for understanding material properties and performance. SEM's ability to perform three-dimensional reconstructions further enhances its efficacy in surface topography analysis[267]. For instance, high-temperature SEM can capture a series of tilted images to reconstruct three-dimensional representations of a sample's surface, enabling the examination of variations in material roughness and topography across different thermal conditions. SEM's rapid and non-destructive three-dimensional metrology capabilities make it an indispensable tool for evaluating the topography of microstructures and ensuring the quality and reliability of manufactured components[268].

To examine the surface topography and cell interactions of three different substrates, including MCF7 Patterned PDMS, Plain PDMS, and TCPS, the SEM characterization was performed on a GEMINISEM (Zeiss, Germany) with an acceleration of 5kV and an SE2 detector. The process involved obtaining 1cm circular samples from the substrates and sterilizing them with UV/C for 30 minutes, followed by a 20-minute immersion in 70% ethanol. The samples were then rinsed three times with sterile PBS. Next, 2000 MCF7 cells in 100 μ l of complete DMEM were seeded on the samples and left overnight. The medium was removed, and the cells were immobilized with 4% Glutaraldehyde for 20 minutes. The samples were washed twice with PBS and once with MiliQ water to eliminate Glutaraldehyde and unattached cells. Once air-dried at room temperature, a thin layer of gold was applied to the samples using a sputter coater machine (K550, EMITECH). Finally, SEM micrographs of the samples were captured at magnifications of 500-, 1000-, and 1500 times (SmartSEM 6.00 with Service Pack 5, Zeiss), as shown in Figure 29. D-F shows that when the MCF7 cells are cultured on the patterned substrates, they tend to reside in their pattern, while in Plain PDMS (Fig 29. A-C) and TCPS (Fig 29. G-I), the cells randomly attach to the surface. Moreover, the cell morphology in PDMS-based substrates is different from that of TCPS, and this is due to the difference in surface properties between TCPS and PDMS, including topography and hydrophilicity. Since PDMS is intrinsically hydrophobic, cells typically shape a rounded morphology when cultured on PDMS; however, when cultured on a TCPS, they spread entirely on the surface[269, 270].

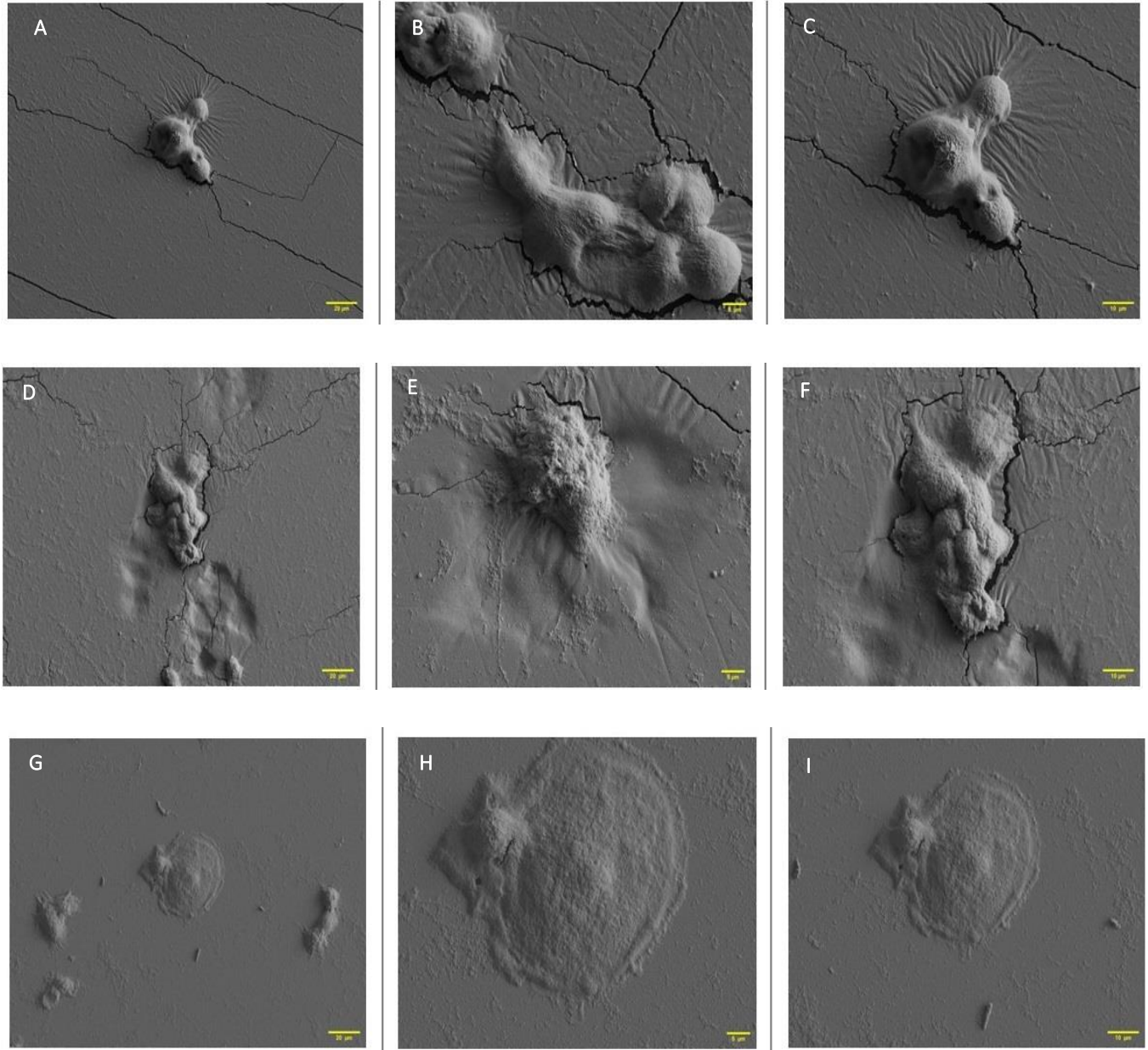


Figure 30. SEM Micrographs. The SEM images show MCF7 cells on different substrates. On Un-patterned PDMS: **A)** 500x, **B)** 1000x, and **C)** 1500x magnifications. On Patterned PDMS: **D)** 500x, **E)** 1000x, and **F)** 1500x magnifications. On Polystyrene Plate: **G)** 500x, **H)** 1000x, and **I)** 1500x magnifications.

To have a cross-sectional view of the cells residing inside their patterns, with the help of a 45°-tilted SEM clip holder, SEM micrographs with different magnifications from 1000-3500 times were captured from the MCF7 cells on MCF7 imprinted substrates (Fig. 30. A-D). These images demonstrate how smartly the MCF7 cells have detected their pattern on the surface and accommodated within.

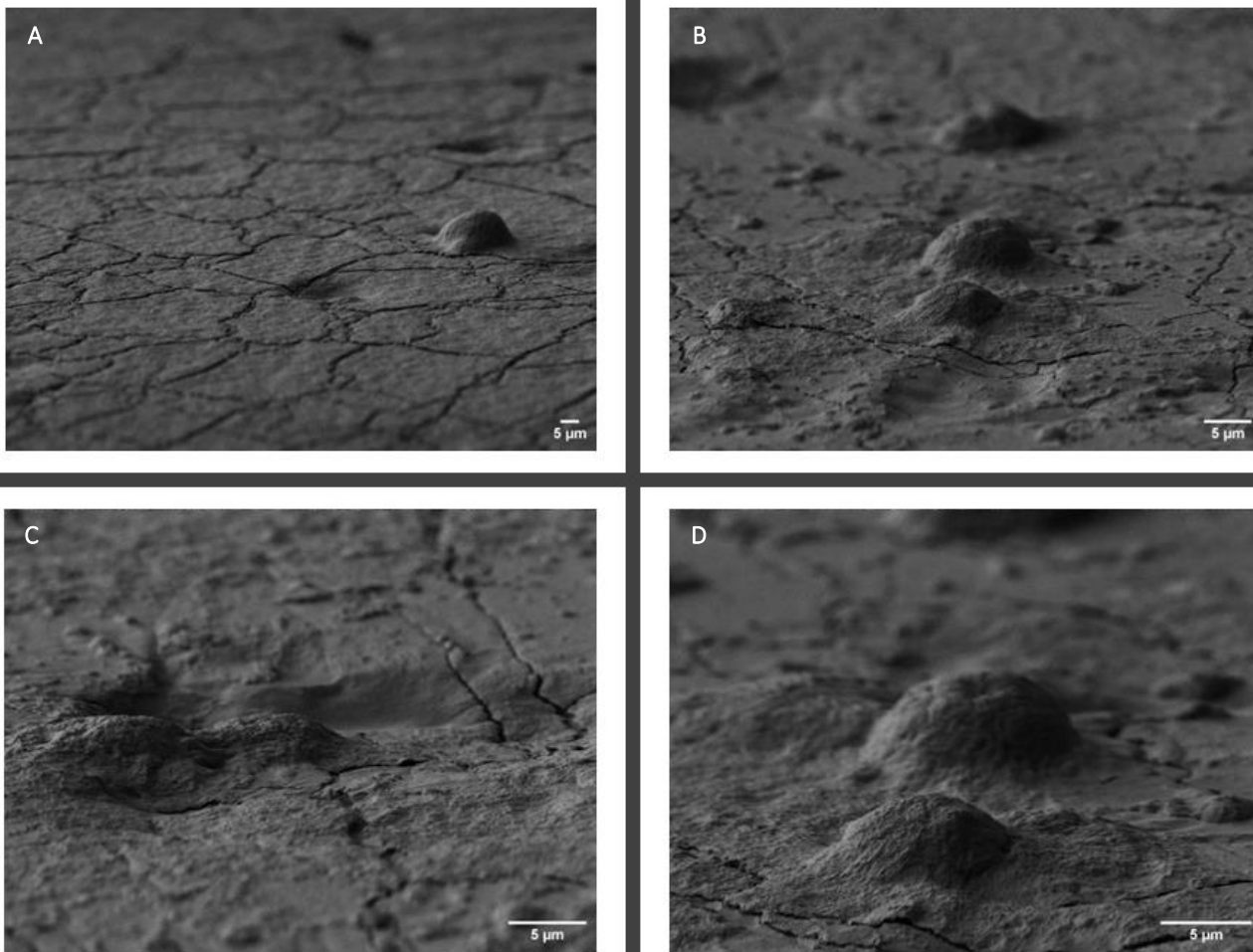


Figure 31. Cross Section View. Cross-section view of MCF7 cells in their patterns. **A)** 1000x **B)** 2000x **C)** 3000x and **D)** 3500x magnification.

3.3.3. Red/Blue Ratio Assay

To assess cell migration, the ratio of red-stained cells to blue-stained cells was quantified utilizing an inverted fluorescent microscope (Axiovert 200M, Zeiss, Germany) inside and outside the seeding area for Single-Coating substrates and outside Double-Coating substrates. An example of this analysis is presented in Figure 31, which exhibits a combination of MDA-MB-231(Red) and MCF7 (Blue) cells in three distinct areas on three different surfaces overnight.

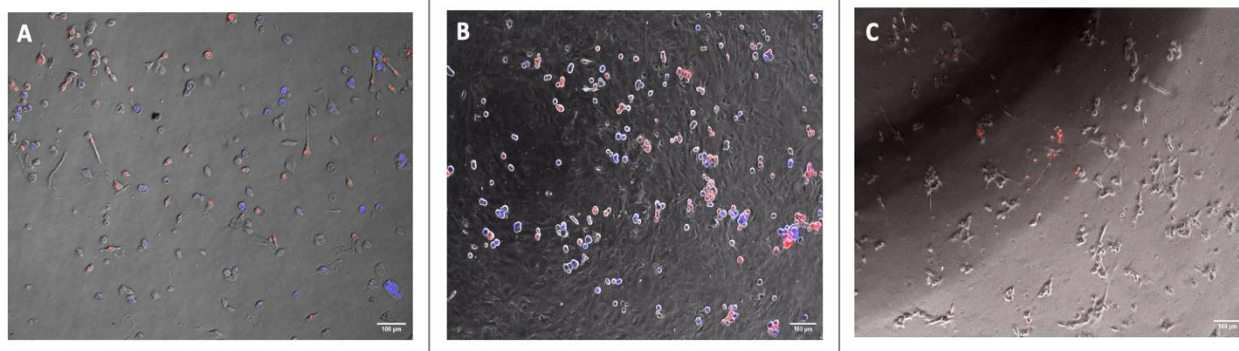


Figure 32. The Cells Distribution. The mixture of MDA-MB-231(Red)+MCF7 (Blue) on three substrates with 10x objective and 1x Zoom. **A)** In the Seeding area (Plate) **B)** In the Seeding area (MCF7 Pattern) **C)** Outside the Seeding area on the MDA-MB-231 side (MCF7-MDA-MB-231 Pattern).

The proportion of each cell type in each area was calculated as explained for MCF7=Red, 3T3=Blue (Tables 5-6, Fig. 34-35), and vice versa (Tables 7-8, Fig. 36-37).

Table 5. Cell Distribution on Single-Coating Substrates. MCF7 Cells=Red, 3T3 Cells=Blue.

Coating A	Red/Blue Ratio Inside the Seeding Area \pm SD	Red/Blue Ratio Outside the Seeding Area \pm SD
TCPS	1.49 \pm 0.59	3.60 \pm 0.84
Plain PDMS	1.47 \pm 0.46	4.41 \pm 1.25
MCF7 Pattern	3.40 \pm 2.30	4.56 \pm 1.41
3T3 Pattern	2.53 \pm 1.36	4.15 \pm 1.62

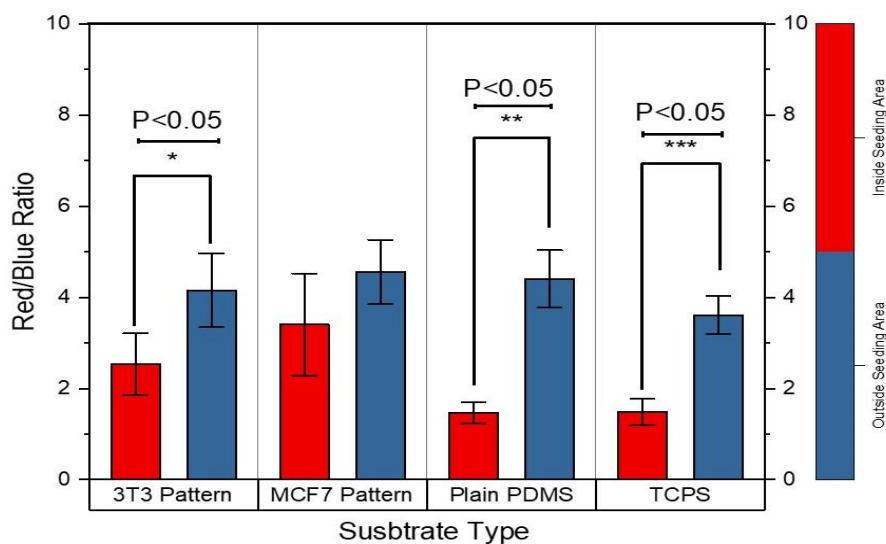


Figure 33. Diagram of Cell Distribution on Single-Coating Substrates. MCF7 Cells=Red, 3T3 Cells=Blue.

Table 6. Cell Distribution on Double-Coating Substrates. MCF7 Cells=Red, 3T3 Cells=Blue.

Coating A	Coating B	Red/Blue Ratio \pm SD	
		Outside Seeding area (Coating A)	Outside Seeding Area (Coating B)
TCPS	TCPS	3.57 \pm 1.14	4.02 \pm 1.54
Plain PDMS	Plain PDMS	4.84 \pm 2.21	5.71 \pm 2.30
MCF7 Pattern	MCF7 Pattern	4.39 \pm 1.39	5.25 \pm 1.60
3T3 Pattern	3T3 Pattern	3.75 \pm 1.36	4.27 \pm 2.15
Plain PDMS	MCF7 Pattern	3.59 \pm 1.59	4.92 \pm 0.79
Plain PDMS	3T3 Pattern	2.90 \pm 1.12	2.40 \pm 1.14
MCF7 Pattern	3T3 Pattern	12.24 \pm 6.8	6.12 \pm 4.20

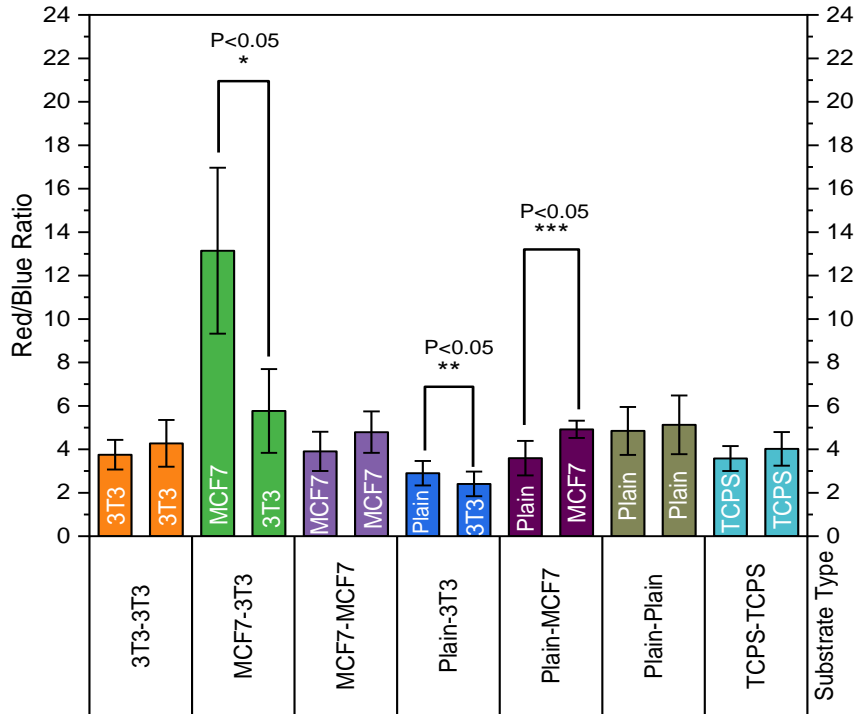


Figure 34. Diagram of Cell Distribution on Double-Coating Substrates. MCF7 Cells=Red, 3T3 Cells=Blue.

Table 5 and Figure 34 illustrate that the proportion of MCF7 to 3T3 cells inside and outside the seeding area of MCF7 patterned substrates is insignificant; however, these values for other Single-Coating substrates are significant. This demonstrates that MCF7 cells distribute almost equally inside and outside their primary seeding when cultured over their pattern. Conversely, the notable distinctions between the internal and external seeding regions for alternative substrates indicate that most cancerous cells prefer migrating beyond the seeding zone on the Single-Coating substrates when the topographical features diverge from their morphological characteristics. On the contrary, considering Table 6 and Figure 35, when the cellular mixture is cultured on Double-Coating substrates, the proportion of MCF7 to 3T3 cells concerning their MCF7 pattern beyond the seeding area is superior to that observed in the other substrate type. For instance, on the MCF7 pattern side of the MCF7 Pattern-3T3 Pattern substrates, this figure is two times higher than those on the 3T3 side. This observation is likewise evident on the Plain PDMS-MCF7 Pattern PDMS, wherein the MCF7 to 3T3 ratio is approximately 1.5 times greater on the MCF7 Pattern side than the Plain side. Subsequently, the assay was reiterated to investigate further the influence of the patterns on the migratory and separation behaviors of the cells; therefore, on this occasion, 3T3 cells were labeled with PMA-Coated Quantum Dots (Red) while MCF7 cells were stained with

Hoechst (Blue). The findings are outlined in Table 7 and Figure 36 regarding the Single-Coating substrates, with Table 8 and Figure 37 corresponding to the Double-Coating substrates.

Table 7. Cell Distribution on Single-Coating Substrates. 3T3 Cells=Red, MCF7 Cells=Blue.

Coating A	Red/Blue Ratio in Seeding Area \pm SD	Red/Blue Ratio outside Seeding Area \pm SD
TCPS	1.22 \pm 0.27	2.08 \pm 0.79
Plain PDMS	2.62 \pm 1.42	2.75 \pm 1.11
MCF7 Pattern	1.64 \pm 0.41	1.97 \pm 0.89
3T3 Pattern	1.53 \pm 0.85	3.06 \pm 1.13

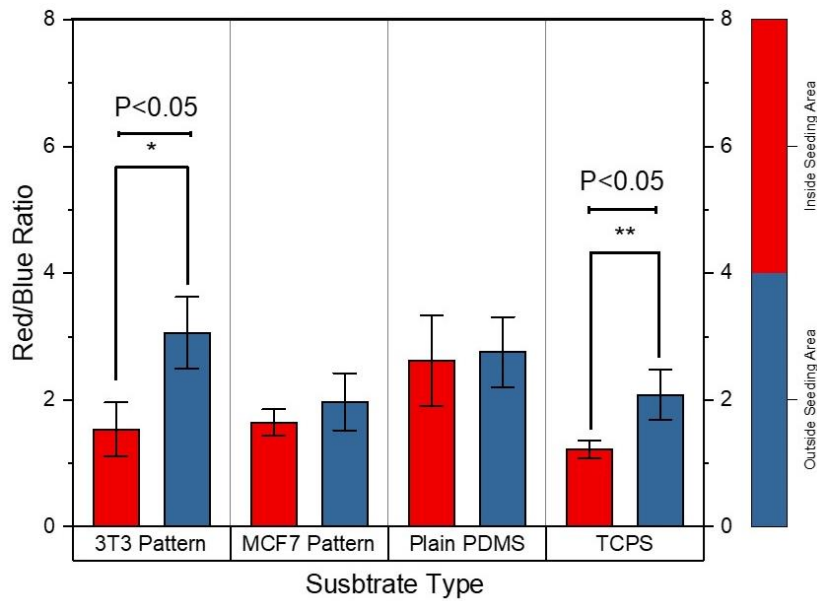


Figure 35. Diagram of Cell Distribution on Single-Coating Substrates. 3T3 Cells=Red, MCF7 Cells=Blue.

Table 8. Cell Distribution on Double-Coating Substrates. 3T3 Cells=Red, MCF7 Cells=Blue.

Coating A	Coating B	Red/Blue Ratio \pm SD	
		Outside Seeding Area (Coating A)	Outside Seeding Area (Coating B)
TCPS	TCPS	1.94 \pm 0.79	2.32 \pm 1.87
Plain PDMS	Plain PDMS	2.33 \pm 0.87	2.96 \pm 1.64
MCF7 Pattern	MCF7 Pattern	2.41 \pm 1.06	2.26 \pm 2.23
3T3 Pattern	3T3 Pattern	3.23 \pm 1.50	3.13 \pm 1.24
Plain PDMS	MCF7 Pattern	2.84 \pm 1.64	2.18 \pm 1.73
Plain PDMS	3T3 Pattern	3.47 \pm 2.21	4.44 \pm 2.21
MCF7 Pattern	3T3 Pattern	3.70 \pm 2.41	7.76 \pm 4.25

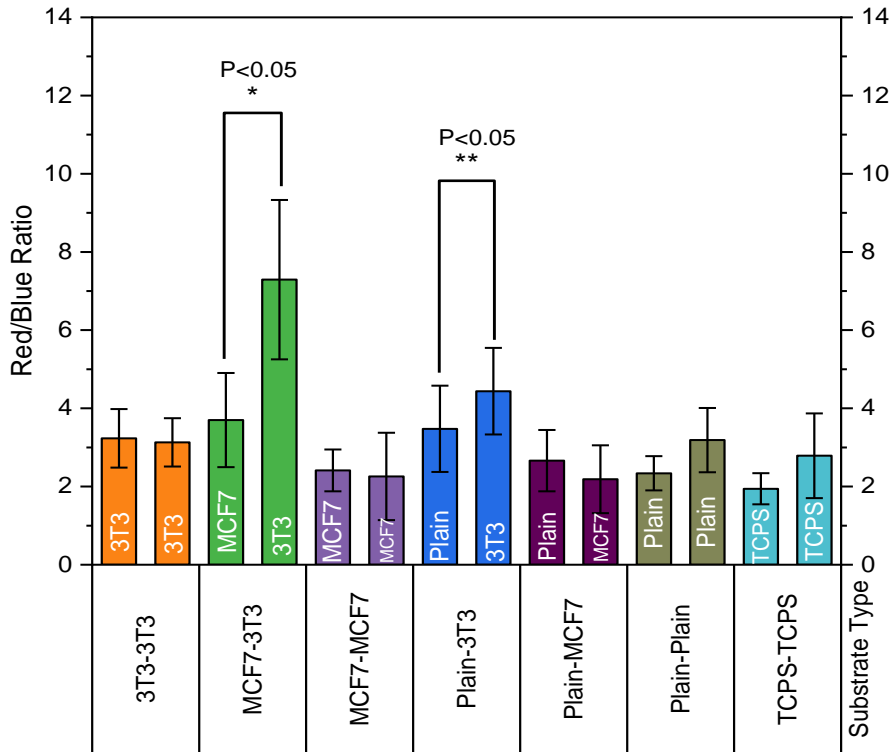


Figure 36. Diagram of Cell Distribution on Double-Coating Substrates. 3T3 Cells=Red, MCF7 Cells=Blue.

The results in Table 8 and Figure 37 highlight that the ratios of 3T3 cells to MCF7 cells are notably higher on the 3T3 pattern on Plain PDMS-3T3 Pattern and 3T3-MCF7 Pattern substrates, with 1.3 and 2.1 times, respectively. To further evaluate the influence of these imprinted in vitro models on the cell separation, two mixed breast cancer cell lines, the Red/Blue assay was conducted once more on the mixture of MCF7 (500 blue cells) and MDA-MB231 (500 red cells) cells to determine the efficacy of the pattern in facilitating cell separation, with the findings represented in Table 9, Figure 38 and Table 10, Figure 39 for Single and Double-Coating substrates, respectively.

Table 9. Cell Distribution on Single-Coating Substrates. MDA-MB-231Cells=Red, MCF7 Cells=Blue.

Coating A	Red/Blue Ratio in Seeding Area ± SD	Red/Blue Ratio outside Seeding Area ± SD
Petri Dish	1.14±0.36	3.26±1.99
Plain PDMS	1.80±0.86	1.63±1.12
MCF7 Pattern	1.93±1.64	1.91±1.26
MDA MB 231	2.06±1.41	4.72±2.93

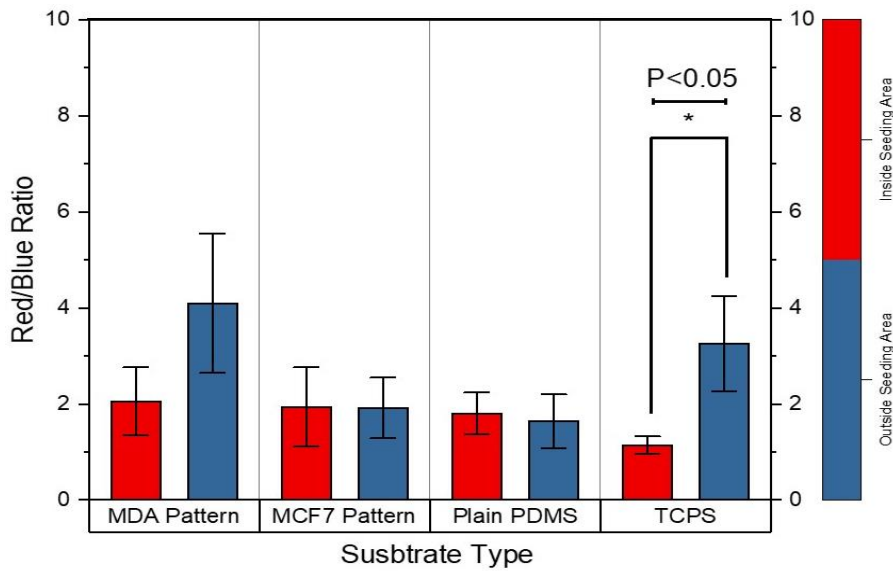


Figure 37. Diagram of Cell Distribution on Single-Coating Substrates. MDA-MB-231Cells=Red, MCF7 Cells=Blue.

The findings further elucidated that the spatial arrangements of the substrates can significantly affect cellular migratory behavior. When exposed to double-patterned substrates, the MCF7 and MDA-MB-231 cells exhibit enhanced motility, revealing a pronounced preference for their inherent patterns compared to other configurations. However, as seen in Table 9 and Figure 38, MDA-MB-231 cells have a higher proportion outside the seeding area on TCPS and MDA-MB-231 patterns. Notwithstanding, they exhibit a markedly selective behavior when interacting with Double-Coating substrates (Table 10, Figure 39). For instance, the ratio of MDA MB 231 to MCF7 cells on the MDA MB 231 patterned side is 2.4 times higher than the MCF7 side on the MDA MB 231-MCF7 Patterned samples. On the other hand, when the cell mixture is cultured on

the MCF7 Pattern-Plain PDMS substrates, this ratio is significantly higher on the plain side than on the MCF7 pattern side. In other words, like MCF7 cells, this shows that MDA-MB-231 cells exhibit a lack of affinity for migrating toward a substrate by a distinct cellular imprint, thereby underscoring the selective nature of the cells in pattern recognition.

Table 10. Cell Distribution on Double-Coating Substrates. MDA-MB-231 Cells=Red, MCF7 Cells=Blue.

Coating A	Coating B	Red/Blue Ratio	
		Outside Seeding Area (Coating A)	Outside Seeding Area (Coating B)
TCPS	TCPS	2.33±1.63	2.06±0.89
Plain PDMS	Plain PDMS	1.93±1.51	1.47±0.90
MCF7 Pattern	MCF7 Pattern	1.19±0.72	1.58±0.52
MDA MB 231	MDA MB 231	1.99±0.71	2.11±0.54
Plain PDMS	MCF7 Pattern	2.5±1.45	1.46±1.18
Plain PDMS	MDA MB 231	1.02±0.21	2.19±0.83
MCF7 Pattern	MDA MB 231	1.30±1.17	3.05±1.69

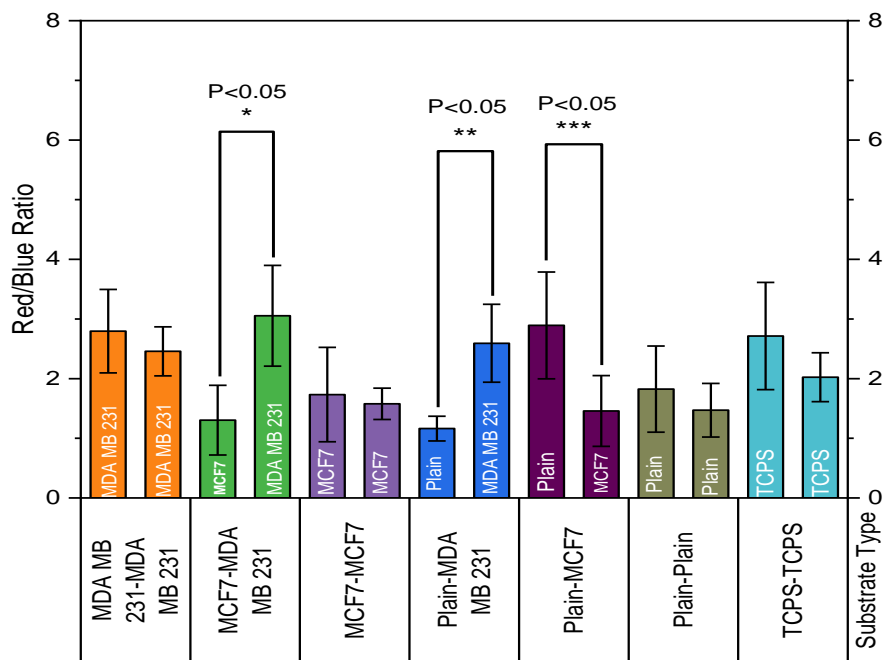


Figure 38. Diagram of Cell Distribution on Double-Coating Substrates. MDA-MB-231 Cells=Red, MCF7 Cells=Blue

Substrate topography positively influences cell migration by modulating cellular dynamics, mechanosensing, and directional locomotion. The interplay between cells and the microstructural attributes of their substrate can substantially affect cellular behavior, including migration patterns, which are integral to numerous physiological processes and biomaterial applications. Stochastic models, including those founded on the Ornstein-Uhlenbeck process, forecast cell migration patterns across various topographies. These models propose that cells can adopt migration trajectories that mirror the topographic features of the substrate, with linearity augmenting in correlation with ridge density[271]. Dynamic alterations in substrate topography, which emulate in vivo conditions, can significantly affect cellular functions such as migration, proliferation, and differentiation. The practical implications of this research are inspiring, as it provides valuable insights into how dynamic environments influence cell behavior, thus serving as essential tools for mechanobiological research. Understanding the interactions between substrate configuration and cellular migration is important. These interactions profoundly influence cellular migration by modulating various biological mechanisms, including contact guidance, topotaxis, and mechanosensing. Substrate stiffness, roughness, curvature, and confinement are key in orchestrating cell behavior and migration dynamics.

Stiffness and Contact Guidance

The stiffness of the substrate is paramount in influencing contact guidance, whereby cells align and migrate following topographical patterns. For example, fibroblasts exhibit a response in focal adhesions and actin alignment independent of stiffness; conversely, microtubules display a response contingent upon stiffness, impacting contact guidance. In contrast, breast carcinoma cells reveal a migration pattern that is dependent on stiffness, becoming increasingly directional as substrate stiffness rises[272]. The mechanical properties of substrates, such as stiffness, considerably influence governing cellular interactions and collective migratory behavior. An augmentation in substrate stiffness enhances cell-substrate adhesion, resulting in increased friction that subsequently affects migration dynamics[273].

Roughness and Topotaxis

Surface roughness constitutes another pivotal element that influences cellular migration. Cells, such as MG63, modulate their migratory velocity and trajectory in reaction to the roughness gradient present within the substrate. Cells migrate from areas exhibiting heightened roughness toward regions characterized by diminished roughness, concomitant with increased migratory speed. The intensity of the roughness gradient can act as an additional signaling cue, thereby influencing migratory behavior. This indicates that roughness's extent and gradient are critical determinants in guiding cell migration[274].

Curvature and Porosity

The microscale curvature of porous substrates exerts a significant influence on cellular dynamics. The geometry of pores and the distribution of their curvature can influence how cells change shape, migrate, and actin polymers assemble. These variations are interpreted by cells as an energetic landscape, thereby affecting their behavior[275]. Porous membranes and micropatterned substrates disrupt interactions between cells and substrates, fostering dynamic and migratory behaviors. The disruption of fibronectin fibrillogenesis coupled with increased migratory speeds on micropatterned substrates underscores the importance of surface discontinuities in regulating cell migration[276, 277].

Confinement and Collective Migration

The confinement of the substrate area has a consequential effect on collective cell migration by modulating cellular morphology and the forces at play. Confinement diminishes lamellipodial protrusive forces and focal adhesion maturation, resulting in less efficient migration. Conversely, alleviating confinement elevates contractile stress and protrusive forces, enhancing motility[278]. The mechanical microenvironment, including substrate deformation induced by traction stresses from cells, acts as a medium through which cells can perceive one another and synchronize their movements. This mechanical perception facilitates coordinated migration over extended distances[279].

While substrate topography significantly impacts cell migration, it is crucial to understand that other factors, such as biochemical signals and substrate stiffness, also play pivotal roles. The interplay among these elements can vary across cell types and environmental contexts, underscoring the intricate nature of cell migration mechanisms. This complexity is what makes our research field so fascinating and constantly evolving. Various physical and chemical conditions control the relation between surface characteristics and the uptake of pharmaceuticals or nanoparticle endocytosis. This includes the substrate's nanoscale details, the surface's chemical nature, and the nanoparticles' physicochemical distinctions. Nanoscale topographies, including pits, craters, and islands, profoundly influence cellular adhesion and functionality. For example, human osteoblasts exhibit lower adhesion on nano-pit and nano-pillar topographies than planar surfaces, which can modulate osteoblast adhesion and cellular activity[280]. Correspondingly, the micro and nanoscale topographical traits can notably shift the functions of embryonic stem cells, influencing their differentiation and self-renewal actions[281, 282]. The local topographic architecture of a surface can substantially affect the adsorption and functional dynamics of proteins. For instance, fibrinogen adsorbed onto nanostructured surfaces demonstrates a higher affinity for platelet binding than flat surfaces, indicating that topography can amplify biological interactions[283]. So, cell-imprinted models can also be used to study nanoparticle endocytosis and drug efficacy assessments. For example, Shahriari et al. have shown cell imprinted PDMS and GelMA contribute positively to the viability of breast cancer cells. In this study, MCF7 cells demonstrated an elevation of 11.9% in metabolic performance when cultivated on MCF7-imprinted PDMS substrates compared to Plain PDMS and a significant 44.2% elevation when grown on imprinted GelMA relative to the basic hydrogel. The higher viability is related to the

pseudo-3D environment facilitated by the imprinted substrates, which reproduce the natural cellular microenvironment more effectively than ordinary 2D cultures. However, breast cancer cells cultured on imprinted substrates exhibited more susceptibility to DOX²⁷ despite enhanced viability. Specifically, MCF7 cells on imprinted PDMS and GelMA²⁸ substrates manifested 37% and 50% greater cell mortality than cells on plain substrates. The heightened drug susceptibility is possibly attributable to the multiscale topography of the imprinted substrates, which can facilitate intracellular signaling and promote drug absorption[222].

EMT²⁹ is a complex biological phenomenon in which epithelial cells change into mesenchymal cells, resulting in greater migratory and invasive skills. This transition is important across physiological and pathological scenarios, encompassing embryonic development, tissue regeneration, fibrosis, and cancer metastasis[284, 285]. The physical parameters within the tumor microenvironment influence EMT considerably, thereby modulating cellular function and gene expression profiles. For instance, nano-patterned substrates can facilitate EMT by modifying cellular morphology and gene expression patterns. In a culture environment involving nanochips with tantalum oxide nanodots, breast cancer cells experienced significant changes in essential genes associated with EMT, characterized by lowered E-cadherin and raised N-cadherin and vimentin, suggesting EMT induction. These nanodots' spatial configuration significantly impacted the cells' transition, thereby underscoring the influence of micro-scale physical properties on cellular behavior[286]. This study has shown cells can migrate and settle in cell-imprinted patterns, so it is possible to study the effect of cell-imprinted models on EMT in future studies.

Cell imprinting represents an innovative methodology that can be employed across various cell types, providing a multifaceted strategy for cellular culture and differentiation. This technique finds application in regenerative medicine to cell differentiation, redifferentiation, and transdifferentiation. Substrates that have been imprinted with ADSCs, chondrocytes, tenocytes, and semi-fibroblasts demonstrate the capacity to elicit specific cellular phenotypes, indicating that this approach may supersede conventional tissue culture plates in fostering more effective regulation of cell phenotypes[113, 115, 126]. Furthermore, this technique is under investigation for its implications in personalized medicine and disease modeling, as it facilitates the creation of environments that replicate distinct cellular conditions. Such capabilities are instrumental in

²⁷ Doxorubicin (DOX)

²⁸ Gelatin Methacrylate (GelMA)

²⁹ Epithelial-Mesenchymal Transition (EMT)

elucidating disease mechanisms and advancing targeted therapeutic interventions[287].

The study of MCF7, MDA-MB-231, and 3T3 cellular models is crucial in oncological research, especially in elucidating the biological mechanisms underpinning breast cancer and the corresponding therapeutic responses. These cell lines function as experimental models to explore diverse dimensions of oncogenesis, encompassing cellular proliferation, therapeutic efficacy, and the intricacies of the tumor microenvironment. Each cell line provides valuable perspectives attributable to its unique properties and differential reactions to various experimental conditions. Hence, in this study, these three cell lines have been used as experimental models to study the interactions of cancerous and non-cancerous cells with surface topography. Furthermore, this study postulated that substrates with cell-imprinted designs could serve as innovative and smart cell culture substrates, facilitating the examination of migration patterns and separation of normal and cancerous cells. The findings indicate that cells exhibit a pronounced propensity to migrate towards patterns that exhibit morphological similarities to themselves. This evidence suggests that cell-imprinted substrates demonstrate considerable efficacy in separating cellular populations when a heterogeneous mixture of cells is cultured on Double-Coating imprinted PDMS, particularly when two distinct types of cell-imprinted morphologies are present on the surface.

Nevertheless, while cell imprinting presents groundbreaking avenues for engineering biomimetic tissues and cell-based therapeutic strategies, it is imperative to reflect upon the ramifications of its inherent limitations. For example, the necessity for comprehensive modification of materials and stringent safety protocols may augment the complexity and financial burden of implementing cellular imprinting methodologies. Furthermore, the technical hurdles linked to the attainment of meticulous cellular patterning could constrain the scalability and reproducibility of this innovative technology within clinical environments. Tackling these obstacles through ongoing research and development is vital for actualizing the complete potential of cell imprinting in biomedical applications.

Chapter 4:
**Conclusion and
Future Outlook**

4.1. Conclusion

As demonstrated in this study, cell imprinting represents an advanced methodology for fabricating surfaces that accurately emulate cellular morphology on a PDMS polymer substrate. The inherent hydrophobic characteristics of PDMS, primarily because of its chemical structure, result in diminished cell adhesion and are advantageous for examining migration patterns. This polymer is characterized by a low-energy siloxane backbone, complemented by non-polar methyl groups, which collectively reduce interactions with aqueous environments. The inherent flexibility of the polymer chains, in conjunction with potential surface roughness, further exacerbates this hydrophobicity. Although environmental parameters and surface modifications may temporarily alter its hydrophobic characteristics, PDMS remains a highly adaptable material with diverse applications spanning microfluidics, biotechnology, and medical devices, owing to its fundamental water-repellent properties. Various surface modification strategies have been devised to augment its cell-adhesive capabilities. The approaches include using ECM protein coverings, chemical bonding with bioactive compounds, and integrating Polydopamine as a separating agent. Each approach presents distinct advantages and can be customized for applications. However, persistent challenges exist in achieving long-term stability, specifically regarding the capacity of a surface to sustain its cell-adhesive properties over prolonged durations and to maintain uniformity. The results of this investigation not only enhance our comprehension of cellular behaviors on cell-imprinted substrates but also offer valuable perspectives for subsequent research and applications within the realms of tissue engineering and biomaterials.

4.2. Future Outlook

Furthermore, *in vitro* models investigating cancer cell migration have evolved considerably, progressing from essential two-dimensional assays to sophisticated three-dimensional systems. These innovative systems more faithfully reproduce the TME, hence supplying researchers with a more reliable framework for inquiry, which is crucial for understanding metastasis mechanisms and appraising potential therapeutic measures. It's important to note that constant upgrades are crucial to refining their usability and exactness, thus accentuating the demand for perpetual study and progress in this sector. Although substrate patterning holds substantial sway over cellular migration, considering the effects of various other factors, including genetic regulation and

biochemical signaling, is equally essential for understanding cell conduct. Moreover, the interplay of various substrate characteristics, including stiffness and roughness, may yield complex migration patterns that warrant further examination. A comprehensive understanding of these interactions could potentially advance biomaterial design and applications in biomedicine, necessitating that future research optimizes this technique to ensure robust and durable cell adhesion for various biomedical applications.

Moreover, despite the numerous advancements achieved, challenges and limitations impede progress in cell imprinting. A primary obstacle resides in reproducibility and scalability, which can adversely affect the uniformity of experimental outcomes. This encompasses difficulties sustaining consistent rates of cell adhesion and growth and challenges in duplicating the precise conditions characteristic of the cellular microenvironment. In addition, irrespective of the numerous investigations that underscore the advantages of cell imprinting in experimental conditions, the shift of these results to practical applications in living beings is fraught with difficulties, primarily stemming from the dynamic and multifaceted qualities of living tissues. Additionally, the surface properties of materials utilized in cell imprinting are critical determinants influencing cellular behavior. Substrates that closely mimic natural tissues' properties could be engineered by deliberately modifying surface chemistry, topographical attributes, and mechanical properties. Enhancing the efficacy of cell imprinting is imperative, and sustained research efforts are crucial to address the challenges associated with reproducibility. Effectively applying these insights in clinical settings is fundamental to ensure that such progress can be fully harnessed in regenerative medicine.

Chapter 5:
Bibliography

1. Aifiah, N., et al *Overview of Cancers*. Journal of Clinical and Medical Images Case Reports (JCMICR), 2022. **2**(6).
2. Betorz, J., et al., *A full computational model of cell motility: Early spreading, cell migration and competing taxis*. bioRxiv, 2022: p. 2022.09. 28.509519.
3. Blagoev, K.B. and H. Levine, *Physics of Molecular and Cellular Processes*. 2022: Springer.
4. Ogorodnik, E., et al., *Mechanical Cues for Triggering and Regulating Cellular Movement Selectively at the Single-Cell Level*. The Journal of Physical Chemistry B, 2023. **127**(4): p. 866-873.
5. Chelly, H. and P. Recho, *Cell motility as an energy minimization process*. Physical Review E, 2022. **105**(6): p. 064401.
6. López, J.I. and I.M. De la Fuente, *An Approach to Cell Motility as a Key Mechanism in Oncology*. 2021, MDPI. p. 3576.
7. Bouchalova, P. and P. Bouchal, *Current methods for studying metastatic potential of tumor cells*. Cancer cell international, 2022. **22**(1): p. 394.
8. Migliaccio, G., et al., *Exploring cell migration mechanisms in cancer: from wound healing assays to cellular automata models*. Cancers, 2023. **15**(21): p. 5284.
9. Gonzalez-Orozco, J.C., S. Gaona-Domínguez, and I. Camacho-Arroyo, *In Vitro Models for Studying Tumor Progression*. Cancer Cell Signaling: Methods and Protocols, 2021: p. 193-206.
10. Mehta, P., et al., *Microfluidics meets 3D cancer cell migration*. Trends in Cancer, 2022. **8**(8): p. 683-697.
11. Lee, M., et al., *Hydrophobic surface induced pro-metastatic cancer cells for in vitro extravasation models*. Bioactive Materials, 2024. **34**: p. 401-413.
12. Shinsato, Y., et al., *Direct comparison of five different 3D extracellular matrix model systems for characterization of cancer cell migration*. Cancer Reports, 2020. **3**(5): p. e1257.
13. Choi, J.R., et al., *In vitro human cancer models for biomedical applications*. Cancers, 2022. **14**(9): p. 2284.
14. Kasper, C., V. Charwat, and A. Lavrentieva, *Cell culture technology*. 2018: Springer.
15. Rychly, J. and B.J. Nebe, *Cell-material interaction*. BioNanoMaterials, 2013. **14**(3-4): p. 153-160.
16. Hosseinzadeh, S., et al., *Cell interactions under controlled of surface substrate*. The Journal of Applied Tissue Engineering, 2016. **3**(1): p. 6-24.
17. Kasper, C., F. Witte, and R. Pörtner, *Tissue engineering III: cell-surface interactions for tissue culture*. Vol. 126. 2012: Springer.
18. Martini, D., et al., *Interaction of Epithelial Cells with Surfaces and Surfaces Decorated by Molecules*. arXiv preprint arXiv:1303.0392, 2013.
19. Wegener, J., *Cell surface interactions*. Wiley Encyclopedia of Biomedical Engineering, 2006.
20. Misra, R. and A.M. Boriek, *Mechanistic understanding of the interaction of cells with nanostructured surfaces within the framework of biological functions*. Materials Technology, 2023. **38**(1): p. 2216529.
21. Keaveney, J., *Collective atom–light interactions in dense atomic vapours*. 2014: Springer.
22. Vitte, J., et al., *Is there a predictable relationship between surface physical-chemical properties and cell behaviour at the interface?* eCells and Materials Journal, 2004. **30**(7): p. 52-63.
23. Wilde, C., et al., *Translating the force—mechano-sensing GPCRs*. American Journal of Physiology-Cell Physiology, 2022. **322**(6): p. C1047-C1060.
24. Jensen, L.F., J.F. Bentzon, and J. Albarrán-Juárez, *The phenotypic responses of vascular smooth muscle cells exposed to mechanical cues*. Cells, 2021. **10**(9): p. 2209.
25. Mosaddad, S.A., et al., *Response to mechanical cues by interplay of YAP/TAZ transcription factors and key mechanical checkpoints of the cell: a comprehensive review*. Cell Physiol Biochem, 2021. **55**(1): p. 33-60.

Bibliography

26. Weissenbruch, K., M. Hippler, and M. Bastmeyer, *Zelluläres Tauziehen: Wie Zellen auf mechanischen Stress antworten*. BIOSpektrum, 2021. **27**(4): p. 385-389.
27. Anselme, K., et al., *Role of the nucleus as a sensor of cell environment topography*. *Advanced healthcare materials*, 2018. **7**(8): p. 1701154.
28. Adhikari, J., et al., *Effects of surface patterning and topography on the cellular functions of tissue engineered scaffolds with special reference to 3D bioprinting*. *Biomaterials Science*, 2023. **11**(4): p. 1236-1269.
29. Li, X., et al., *Nanoscale surface topography reduces focal adhesions and cell stiffness by enhancing integrin endocytosis*. *Nano letters*, 2021. **21**(19): p. 8518-8526.
30. Ge, L., et al., *Topography-Mediated Enhancement of Nonviral Gene Delivery in Stem Cells*. *Pharmaceutics*, 2022. **14**(5): p. 1096.
31. Tudoreanu, R., et al., *Insight and recent advances into the role of topography on the cell differentiation and proliferation on biopolymeric surfaces*. *International Journal of Molecular Sciences*, 2022. **23**(14): p. 7731.
32. Sorzabal-Bellido, I., et al., *Effect of Local Topography on Cell Division of Staphylococcus spp*. *Nanomaterials*, 2022. **12**(4): p. 683.
33. Lopez Marquez, A., et al., *How fiber surface topography affects interactions between cells and electrospun scaffolds: A systematic review*. *Polymers*, 2022. **14**(1): p. 209.
34. Liu, Y., et al., *Biointerface topography mediates the interplay between endothelial cells and monocytes*. *RSC advances*, 2020. **10**(23): p. 13848-13854.
35. Vermeulen, S., et al., *Surface topography is a context-dependent activator of TGF- β signaling in mesenchymal stem cells*. *bioRxiv*, 2020: p. 2020.01. 13.903195.
36. Kimura, T., et al., *Surface topography of PDMS replica transferred from various decellularized aortic lumens affects cellular orientation*. *ACS Biomaterials Science & Engineering*, 2019. **5**(11): p. 5721-5726.
37. Venturini, V., et al., *The nucleus measures shape deformation for cellular proprioception and regulates adaptive morphodynamics*. *BioRxiv*, 2019: p. 865949.
38. Hancock, R., *The nucleus*. 2015: Springer.
39. Khavari, A. and A.J. Ehrlicher, *Nuclei deformation reveals pressure distributions in 3D cell clusters*. *PloS one*, 2019. **14**(9): p. e0221753.
40. Damato, M. and M. Maffia, *The mechanobiology of the nucleus*. *JDREAM. Journal of interDisciplinary REsearch Applied to Medicine*, 2020. **4**(2): p. 7-14.
41. Navarro, A.P., M.A. Collins, and E.S. Folker, *The nucleus is a conserved mechanosensation and mechanoresponse organelle*. *Cytoskeleton*, 2016. **73**(2): p. 59-67.
42. Venturini, V., et al., *The nucleus measures shape changes for cellular proprioception to control dynamic cell behavior*. *Science*, 2020. **370**(6514): p. eaba2644.
43. González-Novo, R., et al., *3D environment promotes persistent changes in lamin B1 distribution, the biomechanical signature of the nucleus, and adaptative survival and migratory functions*. *bioRxiv*, 2023: p. 2023.04. 10.536202.
44. Haage, A. and A. Dhasarathy, *Working a second job: Cell adhesion proteins that moonlight in the nucleus*. *Frontiers in Cell and Developmental Biology*, 2023. **11**: p. 1163553.
45. Howard, T.R. and I.M. Cristea, *Interrogating host antiviral environments driven by nuclear DNA sensing: a multiomic perspective*. *Biomolecules*, 2020. **10**(12): p. 1591.
46. Ding, X., et al., *Cell separation using tilted-angle standing surface acoustic waves*. *Proceedings of the National Academy of Sciences*, 2014. **111**(36): p. 12992-12997.
47. Roberts, J.A., K.A. Elliott, and Z.H. Gonzalez-Carranza, *Abscission, dehiscence, and other cell separation processes*. *Annual review of plant biology*, 2002. **53**(1): p. 131-158.

Bibliography

48. Tomlinson, M.J., et al., *Cell separation: Terminology and practical considerations*. Journal of tissue engineering, 2013. **4**: p. 2041731412472690.
49. Vaghef-Koodehi, A., O.D. Ernst, and B.H. Lapizco-Encinas, *Separation of cells and microparticles in insulator-based electrokinetic systems*. Analytical Chemistry, 2023. **95**(2): p. 1409-1418.
50. Witek, M.A., I.M. Freed, and S.A. Soper, *Cell separations and sorting*. Analytical chemistry, 2019. **92**(1): p. 105-131.
51. Vahey, M.D. and J. Voldman, *An equilibrium method for continuous-flow cell sorting using dielectrophoresis*. Analytical chemistry, 2008. **80**(9): p. 3135-3143.
52. Gerling, T., et al., *High-precision, low-complexity, high-resolution microscopy-based cell sorting*. Lab on a Chip, 2023. **23**(14): p. 3172-3185.
53. Sun, D., *Robotic Cell Manipulation*. 2022: Academic Press.
54. Box, A., et al., *Evaluating the effects of cell sorting on gene expression*. Journal of biomolecular techniques: JBT, 2020. **31**(3): p. 100.
55. Lin, Y.-N. and A. Wellstein, *Cell migration*, in *Cell Movement in Health and Disease*. 2022, Elsevier. p. 67-82.
56. Wu, D. and F. Lin, *Cell Migration*. 2011.
57. Davies, J.A., *Mechanisms of morphogenesis*. 2023: Elsevier.
58. Ridley, A.J., et al., *Cell migration: integrating signals from front to back*. Science, 2003. **302**(5651): p. 1704-1709.
59. Horwitz, A.R. and J.T. Parsons, *Cell migration--movin'on*. Science, 1999. **286**(5442): p. 1102-1103.
60. Skamrahl, M., *Mechanics and motility of epithelial cells: From single cell behavior to collective migration*. 2023.
61. Stower, M., et al., *Single-cell phenomics reveals behavioural and mechanical heterogeneities underpinning collective migration during mouse anterior patterning*. bioRxiv, 2023: p. 2023.03.31.534937.
62. Xin, Z., et al., *Quantitative analysis of collective migration by single-cell tracking aimed at understanding cancer metastasis*. International Journal of Molecular Sciences, 2022. **23**(20): p. 12372.
63. Xin, Z., et al., *Time-series clustering of single-cell trajectories in collective cell migration*. Cancers, 2022. **14**(19): p. 4587.
64. González, L. and A. Mugler, *Collective effects in flow-driven cell migration*. Physical Review E, 2023. **108**(5): p. 054406.
65. Wen, Y., et al., *Single Living Cell Analysis Decodes Dynamical Signaling Patterns Triggering Different Phenotypes of Cell Migration*. Analytical Chemistry, 2023. **95**(14): p. 6080-6089.
66. Zhou, J., et al., *Single Cell Analysis of Inertial Migration by Circulating Tumor Cells and Clusters*. Micromachines, 2023. **14**(4): p. 787.
67. Shao, N., et al., *A Bidirectional Single-Cell Migration and Retrieval Chip for Quantitative Study of Dendritic Cell Migration*. Advanced Science, 2023. **10**(8): p. 2204544.
68. Zhou, M., et al., *High-Throughput Cellular Heterogeneity Analysis in Cell Migration at the Single-Cell Level (Small 6/2023)*. Small, 2023. **19**(6): p. 2370037.
69. Mishra, A.K., et al., *Cell interactions in collective cell migration*. Development, 2019. **146**(23): p. dev172056.
70. Muñoz-Soriano, V. and N. Paricio, *Collective Cell Migration in Tissue Building*. eLS: p. 1-9.
71. Rørth, P., *Collective cell migration*. Annual review of cell and developmental, 2009. **25**: p. 407-429.
72. Weijer, C.J., *Collective cell migration in development*. Journal of cell science, 2009. **122**(18): p. 3215-3223.
73. Gupta, T. and A. Giangrande, *Collective cell migration: "all for one and one for all"*. Journal of Neurogenetics, 2014. **28**(3-4): p. 190-198.

Bibliography

74. Schumacher, L., *Collective cell migration in development*. Cell migrations: causes and functions, 2019: p. 105-116.
75. Saw, T.B., et al., *Mechanobiology of collective cell migration*. Cellular and Molecular Bioengineering, 2015. **8**: p. 3-13.
76. Dimitriou, N.M., et al., *Cancer cell sedimentation in 3D cultures reveals active migration regulated by self-generated gradients and adhesion sites*. bioRxiv, 2023: p. 2023.02. 15.528731.
77. Kinahan, M.W., M. Thali, and M. Symeonides, *Migrate3D: Software for simplified post-tracking analysis of 3D and 2D cell migration data*. Research Square, 2023.
78. Zhou, J.Z., et al., *Quantification of T-cell Migration in Confined and 3D Conditions*. Jornada de Jóvenes Investigadores del I3A, 2023. **11**.
79. Pawluchin, A. and M. Galic, *Moving through a changing world: single cell migration in 2D vs. 3D*. Frontiers in Cell and Developmental Biology, 2022. **10**: p. 1080995.
80. Cowan, J.M., et al., *Non-muscle myosin II and the plasticity of 3D cell migration*. Frontiers in cell and developmental biology, 2022. **10**: p. 1047256.
81. Cheng, Y. and S.W. Pang, *Effects of nanopillars and surface coating on dynamic traction force*. Microsystems & Nanoengineering, 2023. **9**(1): p. 6.
82. Werner, M., et al., *Surface curvature differentially regulates stem cell migration and differentiation via altered attachment morphology and nuclear deformation*. Advanced science, 2017. **4**(2): p. 1600347.
83. Angelini, T.E., et al., *Cell migration driven by cooperative substrate deformation patterns*. Physical review letters, 2010. **104**(16): p. 168104.
84. Merino-Casallo, F., et al., *Unravelling cell migration: defining movement from the cell surface*. Cell adhesion & migration, 2022. **16**(1): p. 25-64.
85. Chen, W.-C., et al. *The migration of cancer and normal cells in response to the surface topography and rigidity*. in *2011 6th IEEE International Conference on Nano/Micro Engineered and Molecular Systems*. 2011. IEEE.
86. Dabare, P.R.L., et al., *Mechanistic Insight in Surface Nanotopography Driven Cellular Migration*. ACS Biomaterials Science & Engineering, 2021. **7**(10): p. 4921-4932.
87. Pulsipher, A. and M.N. Yousaf, *Surface chemistry and cell biological tools for the analysis of cell adhesion and migration*. ChemBioChem, 2010. **11**(6): p. 745-753.
88. Liu, L., et al., *Endothelial cell migration on surface-density gradients of fibronectin, VEGF, or both proteins*. Langmuir, 2007. **23**(22): p. 11168-11173.
89. Mirabelli, P., L. Coppola, and M. Salvatore, *Cancer cell lines are useful model systems for medical research*. Cancers, 2019. **11**(8): p. 1098.
90. De, S.K., *Fundamentals of cancer detection, treatment, and prevention*. 2022: John Wiley & Sons.
91. Pham, P.V. and P. Van Pham, *Introduction to Breast Cancer*. Breast Cancer Stem Cells & Therapy Resistance, 2015: p. 1-4.
92. Etikan, I., R. Alkassim, and S. Abubakar, *Statistical analysis on the reported cases of breast cancer*. Biometrics & Biostatistics International Journal, 2016. **4**(1).
93. Kurle, P., *On breast cancer*. Khirurgiia, 1968. **44**(11): p. 52-57.
94. Dolgushin, M., V. Kornienko, and I. Pronin, *Breast Cancer (BC)*, in *Brain Metastases: Advanced Neuroimaging*. 2018, Springer International Publishing: Cham. p. 143-178.
95. Rai, S., et al., *Breast Cancer-An Overview of the Disease*. 2022.
96. Parker, R.G., et al., *Cancer of the breast*. Radiation oncology for cure and palliation, 2003: p. 97-107.
97. Garroni, G., et al., *Adipose-Derived Stem Cell Features and MCF-7*. Cells, 2021. **10**(7): p. 1754.
98. Jiao, Y., et al., *Pyroptosis of MCF7 cells induced by the secreted factors of hUCMSCs*. Stem cells international, 2018. **2018**.

Bibliography

99. Lee, A.V., S. Oesterreich, and N.E. Davidson, *MCF-7 cells—changing the course of breast cancer research and care for 45 years*. Journal of the National Cancer Institute, 2015. **107**(7): p. djv073.
100. Comşa, Ş., A.M. Cimpean, and M. Raica, *The story of MCF-7 breast cancer cell line: 40 years of experience in research*. Anticancer research, 2015. **35**(6): p. 3147-3154.
101. Hermansyah, D., et al., *Combination curcuma longa and Phyllanthus niruri extract potentiate antiproliferative in triple negative breast cancer MDAMB-231 cells*. Asian Pacific Journal of Cancer Prevention: APJCP, 2023. **24**(5): p. 1495.
102. Huang, Z., P. Yu, and J. Tang, *Characterization of triple-negative breast cancer MDA-MB-231 cell spheroid model*. OncoTargets and therapy, 2020: p. 5395-5405.
103. Rafighdoust, Z., et al., *Isolation and characterization of exosomes derived from breast cancer MDA-MB-231 cell line*. Gene, Cell and Tissue, 2021. **8**(1).
104. Lucero, M., et al., *Stem-like cells from invasive breast carcinoma cell line MDA-MB-231 express a distinct set of Eph receptors and ephrin ligands*. Cancer Genomics & Proteomics, 2020. **17**(6): p. 729-738.
105. Bare, D.J., et al., *Expression and function of voltage gated proton channels (Hv1) in MDA-MB-231 cells*. PLoS One, 2020. **15**(5): p. e0227522.
106. Feliksiak, K., et al., *Vimentin association with nuclear grooves in normal MEF 3T3 cells*. International Journal of Molecular Sciences, 2020. **21**(20): p. 7478.
107. Fu, J., T. Murray, and R.M. Wynne. *Imaging 3T3 cells in photonic crystal fibers*. in *Sensors and Smart Structures Technologies for Civil, Mechanical, and Aerospace Systems 2020*. 2020. SPIE.
108. Martí, A., et al., *Operation of the three terminal heterojunction bipolar transistor solar cell*. physica status solidi c, 2017. **14**(10): p. 1700191.
109. Matsuki-Fukushima, M., et al., *Store operated calcium entry in NIH-3T3 cells*. The Journal of Medical Investigation, 2009. **56**(Supplement): p. 381-382.
110. Taheri, S., et al., *Engineered substrates incapable of induction of chondrogenic differentiation compared to the chondrocyte imprinted substrates*. Biomedical Materials, 2023. **18**(2): p. 025006.
111. Kamguyan, K., et al., *Cell-imprinted substrates: In search of nanotopographical fingerprints that guide stem cell differentiation*. Nanoscale Advances, 2021. **3**(2): p. 333-338.
112. Babaei, M., S. Bonakdar, and B. Nasernejad, *Selective biofunctionalization of 3D cell-imprinted PDMS with collagen immobilization for targeted cell attachment*. Scientific Reports, 2022. **12**(1): p. 12837.
113. Nazbar, A., et al., *Molecular imprinting as a simple way for the long-term maintenance of the stemness and proliferation potential of adipose-derived stem cells: an in vitro study*. Journal of Materials Chemistry B, 2022. **10**(35): p. 6816-6830.
114. Ghazali, Z.S., et al., *Neural priming of adipose-derived stem cells by cell-imprinted substrates*. Biofabrication, 2021. **13**(3): p. 035009.
115. Yazdian Kashani, S., M. Keshavarz Moraveji, and S. Bonakdar, *Computational and experimental studies of a cell-imprinted-based integrated microfluidic device for biomedical applications*. Scientific Reports, 2021. **11**(1): p. 12130.
116. Leclech, C. and C. Villard, *Cellular and subcellular contact guidance on microfabricated substrates*. Frontiers in Bioengineering and Biotechnology, 2020. **8**: p. 551505.
117. Keyhanvar, N., et al., *The Combined Thermo-responsive Cell-Imprinted Substrate, Induced Differentiation, and "KLC Sheet" Formation*. Advanced Pharmaceutical Bulletin, 2022. **12**(2): p. 356.
118. Hasannejad, F., et al., *Regulation of cell fate by cell imprinting approach in vitro*. BiolImpacts, 2023. **14**(3): p. 29945-29945.
119. Mahmoudi, M., et al., *Cell-imprinted substrates direct the fate of stem cells*. ACS nano, 2013. **7**(10): p. 8379-8384.

Bibliography

120. Narayanamurthy, V., et al., *Direct cell imprint lithography in superconductive carbon black polymer composites: process optimization, characterization and in vitro toxicity analysis*. Bioinspiration & biomimetics, 2019. **15**(1): p. 016002.
121. Kavand, H., et al., *Cell-imprint surface modification by contact photolithography-based approaches: direct-cell photolithography and optical soft lithography using PDMS cell imprints*. ACS applied materials & interfaces, 2019. **11**(11): p. 10559-10566.
122. Chang, S., et al., *Derivation and investigation of the first human cell-based model of Beckwith-Wiedemann syndrome*. Epigenetics, 2021. **16**(12): p. 1295-1305.
123. Yao, M., et al., *Natural tissue-imprinted biointerface for the topographical education of a biomimetic cell sheet*. Langmuir, 2022. **38**(26): p. 7921-7928.
124. Lieberzeit, P.A., et al., *Softlithography in chemical sensing—analytes from molecules to cells*. Sensors, 2005. **5**(12): p. 509-518.
125. Gao, S., S. Chen, and Q. Lu, *Cell-imprinted biomimetic interface for intelligent recognition and efficient capture of CTCs*. Biomaterials science, 2019. **7**(10): p. 4027-4035.
126. Bonakdar, S., et al., *Cell-imprinted substrates modulate differentiation, redifferentiation, and transdifferentiation*. ACS applied materials & interfaces, 2016. **8**(22): p. 13777-13784.
127. McCole, R.B. and R.J. Oakey, *Unwitting hosts fall victim to imprinting*. Epigenetics, 2008. **3**(5): p. 258-260.
128. Zhou, X., et al., *Patterning of two-level topographic cues for observation of competitive guidance of cell alignment*. ACS applied materials & interfaces, 2012. **4**(8): p. 3888-3892.
129. Rojas-Rodríguez, M., et al., *Cellular Contact Guidance on Liquid Crystalline Networks with Anisotropic Roughness*. ACS Applied Materials & Interfaces, 2023. **15**(11): p. 14122-14130.
130. Saravanan, V. and V.K. Tippavajhala, *Quantum Dots: Targeted and Traceable Drug Delivery System*. Research Journal of Pharmacy and Technology, 2022. **15**(12): p. 5895-5902.
131. Thakur, S. and S. Sharma, *Biomedical applications of single-particle based material: quantum dots*. Int. J. Radiol. Radiat. Ther, 2022. **9**: p. 121-127.
132. Al-Douri, Y., *Graphene, Nanotubes and Quantum Dots-Based Nanotechnology: Fundamentals and Applications*. 2022: Woodhead Publishing.
133. Kargozar, S., et al., *Quantum dots: a review from concept to clinic*. Biotechnology Journal, 2020. **15**(12): p. 2000117.
134. Abrar, M.A. and A.K.P. Chavan. *Design of Area Efficient Multiply Accumulator Unit in Quantum Dot Cellular Automata (QCA)*. in *Proceeding of Fifth International Conference on Microelectronics, Computing and Communication Systems: MCCS 2020*. 2021. Springer.
135. Parameswaranpillai, J., P. Das, and S. Ganguly, *Quantum Dots and Polymer Nanocomposites: Synthesis, Chemistry, and Applications*. 2022: CRC Press.
136. Singh, M.P., *A review on synthesis of quantum dots and their biomedical applications*. 2022.
137. 윤규식, *Carbon and Graphene Quantum Dots for Biomedical Applications*. 2023: elsevier.
138. Nguyen, H.A., et al., *Colossal Core/Shell CdSe/CdS Quantum Dot Emitters*. ACS nano, 2024.
139. Ashokan, A., J.A. Hutchison, and P. Mulvaney, *Spectroelectrochemistry of CdSe/CdS Core–Shell Quantum Dots*. Chemistry of Materials, 2024. **36**(4): p. 1810-1817.
140. Zavodinsky, V., O. Gorkusha, and A. Kuz'menko, *Electronic Structure of CdS Nanoparticles and CdSe/CdS Nanosystems*. Semiconductor Science and Information Devices, 2022. **4**(2): p. 29-34.
141. Jia, Q.-Y., et al., *Characterization of CdSe QDs biosynthesized by a recombinant Rhodospseudomonas palustris*. Biochemical Engineering Journal, 2023. **191**: p. 108771.
142. Samal, S.K., et al., *Bio-nanohybrid gelatin/quantum dots for cellular imaging and biosensing applications*. International journal of molecular sciences, 2022. **23**(19): p. 11867.
143. Kim, H., *Biological imaging applications using colloidal quantum dots with enhanced photoluminescence intensity*. Molecular Crystals and Liquid Crystals, 2022. **744**(1): p. 92-99.

Bibliography

144. Rathee, N. and N. Jaggi, *Cytotoxicity Measurements of CdSe and Ag Hybrid Nano Composites for In-vitro Bioimaging Applications*. 2022.
145. Batabyal, S.K., et al., *Carbon Quantum Dots for Sustainable Energy and Optoelectronics*. 2023: Elsevier.
146. Hirotsaki, N., et al., *Fluorophore, method for producing same, light-emitting device using fluorophore, image display device, pigment, and ultraviolet absorbent*. 2017, Google Patents.
147. Sauer, M., J. Hofkens, and J. Enderlein, *Handbook of fluorescence spectroscopy and imaging: from ensemble to single molecules*. 2010: John Wiley & Sons.
148. Kasper, R., et al., *Fluorophores: Single-Molecule STED Microscopy with Photostable Organic Fluorophores (Small 13/2010)*. *small*, 2010. **6**(13).
149. Zhang, Y., et al., *Photoactivatable fluorophores for bioimaging applications*. *ACS applied optical materials*, 2023. **1**(3): p. 640-651.
150. Rodig, S.J., *Detecting fluorochrome-labeled cells*. *Cold Spring Harbor Protocols*, 2021. **2021**(6): p. pdb. prot099747.
151. Kumar, P., et al., *Multifunctional fluorophores for live-cell imaging and affinity capture of proteins*. *bioRxiv*, 2022: p. 2022.07. 02.498544.
152. Kurutos, A., et al., *RNA-targeting low-molecular-weight fluorophores for nucleoli staining: Synthesis, in silico modelling and cellular imaging*. *New Journal of Chemistry*, 2021. **45**(29): p. 12818-12829.
153. de Castro, M.A.G., C. Höbartner, and F. Opazo, *Staining of Membrane Receptors with Fluorescently-labeled DNA Aptamers for Super-resolution Imaging*. *Bio-protocol*, 2017. **7**(17): p. e2541-e2541.
154. Lee, M.-Y., *Microarray bioprinting technology*. *Microarray Bioprinting Technology*, 2016. **10**: p. 978-3.
155. Kirk, M.J., et al., *Cell-surface targeting of fluorophores in Drosophila for rapid neuroanatomy visualization*. *ACS Chemical Neuroscience*, 2023. **14**(5): p. 909-916.
156. Hawa, G., *Application of Fluorescence in Life Sciences for Basic Research and Medical Diagnostics*. *Fluorescence in Industry*, 2019: p. 341-363.
157. Zaitsev, S.Y., et al., *Cell staining by photo-activated dye and its conjugate with chitosan*. *Cell Biochemistry and Biophysics*, 2015. **71**: p. 1475-1481.
158. Li, M.-J., M.J. Bertocchi, and R.G. Weiss, *Photophysics of Pyrenyl-Functionalized Poly (isobutylene-alt-maleic anhydride) and Poly (isobutylene-alt-maleic N-alkylimide). Influence of Solvent, Degree of Substitution, and Temperature*. *Macromolecules*, 2017. **50**(5): p. 1919-1929.
159. Hühn, J., et al., *Selected standard protocols for the synthesis, phase transfer, and characterization of inorganic colloidal nanoparticles*. *Chemistry of Materials*, 2017. **29**(1): p. 399-461.
160. Liu, Y. and J. Xu, *High-resolution microscopy for imaging cancer pathobiology*. *Current pathobiology reports*, 2019. **7**: p. 85-96.
161. Reffner, J.A. and B.W. Kammrath, *Solving Problems with Microscopy: Real-life Examples in Forensic, Life and Chemical Sciences*. 2023: John Wiley & Sons.
162. Alexander, M.R. and P. Williams, *Water contact angle is not a good predictor of biological responses to materials*. *Biointerphases*, 2017. **12**(2).
163. Menzies, K.L. and L. Jones, *The impact of contact angle on the biocompatibility of biomaterials*. *Optometry and Vision Science*, 2010. **87**(6): p. 387-399.
164. Paxton, N.C. and M.A. Woodruff, *Measuring contact angles on hydrophilic porous scaffolds by implementing a novel raised platform approach: A technical note*. *Polymers for Advanced Technologies*, 2022. **33**(10): p. 3759-3765.
165. Malashchenko, V., et al. *Bone-like multilevel calcium phosphate coating modulates an interaction of mesenchymal stem cells and tumor cells*. in *AIP Conference Proceedings*. 2019. AIP Publishing.

Bibliography

166. Boyce, J.F. and D.E. Brooks, *Contact angles as an analytical tool for investigating two-phase interactions with biological surfaces: a review*. Separations Using Aqueous Phase Systems: Applications in Cell Biology and Biotechnology, 1989: p. 239-247.
167. Yustisia, Y., *The role of cell adhesion to biomaterial*. STOMATOGNATIC-Jurnal Kedokteran Gigi, 2015. **8**(2): p. 86-89.
168. Oshida, Y., R. Sachdeva, and S. Miyazaki, *Changes in contact angles as a function of time on some pre-oxidized biomaterials*. Journal of Materials Science: Materials in Medicine, 1992. **3**: p. 306-312.
169. Andrade, J., *Contact angle analysis of biomedical polymers: From air to water to electrolytes*, in *Polymers in Medicine II: Biomedical and Pharmaceutical Applications*. 1986, Springer. p. 29-40.
170. Paap, U., et al., *Probing Surface and Interfacial Tension of Ionic Liquids in Vacuum with the Pendant Drop and Sessile Drop Method*. International Journal of Molecular Sciences, 2022. **23**(21): p. 13158.
171. Ponomar, M., et al., *Sessile drop method: Critical analysis and optimization for measuring the contact angle of an ion-exchange membrane surface*. Membranes, 2022. **12**(8): p. 765.
172. Singh, M.K. and A. Singh, *Characterization of Polymers and Fibers*. 2021: Woodhead Publishing.
173. Errico, S., et al., *Different experimental approaches for Fourier-transform infrared spectroscopy applications in biology and biotechnology: A selected choice of representative results*. Biotechnology and Applied Biochemistry, 2023. **70**(3): p. 937-961.
174. Nandiyanto, A.B.D., R. Ragadhita, and M. Fiandini, *Interpretation of Fourier Transform Infrared Spectra (FTIR): A practical approach in the polymer/plastic thermal decomposition*. Indonesian Journal of Science and Technology, 2023. **8**(1): p. 113-126.
175. Pathare, P.B. and M.S. Rahman, *Nondestructive quality assessment techniques for fresh fruits and vegetables*. 2022: Springer Nature.
176. VILLEGAS-ALCARAZ, J.F., et al., *SiO₂/PDMS functionalized hybrid ceramics: effect of functional group on hydrophobic behavior*. Journal Simulation and Laboratory, 2023: p. 10-27.
177. El-Agramy, A. and A. Shabaka, *Infrared absorption spectra of polystyrene doped with some charge-transfer complexes*. Polymer degradation and stability, 1992. **37**(2): p. 159-162.
178. Zolotarev, V., *Comparison of polystyrene IR spectra obtained by the T, R, ATR, and DR methods*. Optics and Spectroscopy, 2017. **122**: p. 749-756.
179. Alburnia, A.R., P. Musto, and G. Guerra, *FTIR spectra of pure helical crystalline phases of syndiotactic polystyrene*. Polymer, 2006. **47**(1): p. 234-242.
180. Şerban, S.G., L.M. Strugariu, and S. Jitian, *The influence of solvents on the appearance of the absorption bands of the polystyrene films deposited from solutions on metal mirrors*. Optica Applicata, 2023. **53**(1).
181. Magonov, S.N., D. Shen, and R. Qian, *Fourier transform infra-red spectroscopy of atactic polystyrene in the glass transition region*. Die Makromolekulare Chemie: Macromolecular Chemistry and Physics, 1989. **190**(10): p. 2563-2570.
182. Knysh, A., P. Sokolov, and I. Nabiev, *Dynamic Light Scattering Analysis in Biomedical Research and Applications of Nanoparticles and Polymers*. Journal of Biomedical Photonics & Engineering, 2023. **9**(2): p. 020203.
183. Salazar, M., et al., *A user-friendly graphical user interface for dynamic light scattering data analysis*. Soft Matter, 2023. **19**(34): p. 6535-6544.
184. Jia, Z., et al., *Dynamic light scattering: a powerful tool for in situ nanoparticle sizing*. Colloids and Interfaces, 2023. **7**(1): p. 15.
185. Grigoryeva, N., *Fluorescence Methods for Investigation of Living Cells and Microorganisms*. 2020: BoD—Books on Demand.
186. Santonocito, R., et al., *Fluorescence sensing by carbon nanoparticles*. Nanoscale Advances, 2022. **4**(8): p. 1926-1948.

Bibliography

187. Zhang, Y., et al., *Nanomaterials used in fluorescence polarization based biosensors*. International Journal of Molecular Sciences, 2022. **23**(15): p. 8625.
188. Lall, N., et al., *Viability reagent, PrestoBlue, in comparison with other available reagents, utilized in cytotoxicity and antimicrobial assays*. International journal of microbiology, 2013. **2013**(1): p. 420601.
189. Sonnaert, M., et al., *Quantitative validation of the presto blue™ metabolic assay for online monitoring of cell proliferation in a 3D perfusion bioreactor system*. Tissue Engineering Part C: Methods, 2015. **21**(6): p. 519-529.
190. Rathee, N. and N. Jaggi, *Time controlled growth of CdSe QDs for applications in white light emitting diodes*. Vacuum, 2019. **169**: p. 108910.
191. Rice, Q., et al., *Time-Resolved and Temperature-Dependent Fractional Amplitude Contributions to the Broadband Emission of CdSe Quantum Dots*. Crystals, 2021. **11**(11): p. 1284.
192. Samuel, B., et al., *Surface defect assisted broad spectra emission from CdSe quantum dots for white LED application*. Materials Research Express, 2018. **5**(2): p. 025009.
193. Heydaripour, F., et al., *Conversion of the yellow to blue emission of CdSe quantum dots (QDs) via ZnSe shell growth*. Journal of Materials Science: Materials in Electronics, 2019. **30**: p. 11378-11382.
194. Boncler, M., et al., *Comparison of PrestoBlue and MTT assays of cellular viability in the assessment of anti-proliferative effects of plant extracts on human endothelial cells*. Journal of pharmacological and toxicological methods, 2014. **69**(1): p. 9-16.
195. Luzak, B., P. Siarkiewicz, and M. Boncler, *An evaluation of a new high-sensitivity PrestoBlue assay for measuring cell viability and drug cytotoxicity using EA. hy926 endothelial cells*. Toxicology in Vitro, 2022. **83**: p. 105407.
196. Singh, P., M. Harbola, and A. Mookerjee, *Modeling, Characterization, and Production of Nanomaterials*. Woodhead, Waltham, MA, 2015. **1**: p. 407-418.
197. McBean, P., et al., *The user adjustable pole-piece: expanding TEM functionality without compromise*. Microscopy and Microanalysis, 2022. **28**(S1): p. 2636-2638.
198. McBean, P., et al., *Multiphysics Simulation for TEM Objective Lens Evaluation & Design*. Microscopy and Microanalysis, 2022. **28**(S1): p. 2494-2495.
199. Hilal, N., et al., *Membrane characterization*. 2017: Elsevier.
200. Nilles, J., J. Weiss, and D. Theile, *Crystal violet staining is a reliable alternative to bicinchoninic acid assay-based normalization*. Biotechniques, 2022. **73**(3): p. 131-135.
201. Castro, J., et al., *Crystal violet staining alone is not adequate to assess synergism or antagonism in multi-species biofilms of bacteria associated with bacterial vaginosis*. Frontiers in Cellular and Infection Microbiology, 2022. **11**: p. 795797.
202. Sajjad, A., et al., *Effectiveness of crystal violet stain for localization of mitotic activity in oral squamous cell carcinoma*. Journal of Fatima Jinnah Medical University, 2019. **13**(4): p. 166-169.
203. Cordeiro, M.M., et al., *Interaction of Hoechst 33342 with Lipid Membranes at Different pH Values*. 2023.
204. Fuchs, H., et al., *Breaking a Dogma: High-Throughput Live-Cell Imaging in Real-Time with Hoechst 33342*. Advanced Healthcare Materials, 2023. **12**(20): p. 2300230.
205. Merolli, A. and C. Bektas, *Hoechst 33342 as a marker for imaging neurites of Dorsal Root Ganglion in vitro*. Journal of Anatomy, 2022. **240**(5): p. 998-1001.
206. Swain, B.M., et al., *Complexities of a protonatable substrate in measurements of Hoechst 33342 transport by multidrug transporter LmrP*. Scientific Reports, 2020. **10**(1): p. 20026.
207. Filipe, H., et al., *Effect of protonation state on the interaction of Hoechst 33342 with lipid membranes—An experimental and computational study*. 2017.
208. Neuberger, A. and H.W. van Veen, *Hoechst 33342 is a hidden “Janus” amongst substrates for the multidrug efflux pump LmrP*. Plos one, 2015. **10**(11): p. e0141991.

Bibliography

209. Lalande, M.E., V. Ling, and R.G. Miller, *Hoechst 33342 dye uptake as a probe of membrane permeability changes in mammalian cells*. Proceedings of the National Academy of Sciences, 1981. **78**(1): p. 363-367.
210. Schendzielorz, P., et al., *Labeling adipose-derived stem cells with Hoechst 33342: usability and effects on differentiation potential and DNA damage*. Stem Cells International, 2016. **2016**.
211. Crowley, L.C., B.J. Marfell, and N.J. Waterhouse, *Analyzing cell death by nuclear staining with Hoechst 33342*. Cold Spring Harbor Protocols, 2016. **2016**(9): p. pdb. prot087205.
212. Zheng, J., et al., *Toxicity of Hoechst 33342: implication in side population analysis*. Cellular and Molecular Biology, 2016. **62**(7): p. 27-30.
213. Chen, J., et al., *A multidrug-resistant P-glycoprotein assembly revealed by tariquidar-probe's super-resolution imaging*. Nanoscale, 2021. **13**(40): p. 16995-17002.
214. Hitchcock, S.A., *Structural modifications that alter the P-glycoprotein efflux properties of compounds*. Journal of medicinal chemistry, 2012. **55**(11): p. 4877-4895.
215. Law, K.-Y., *Definitions for hydrophilicity, hydrophobicity, and superhydrophobicity: getting the basics right*. 2014, ACS Publications. p. 686-688.
216. Sun, Y., et al., *Improving performance of cell imprinted PDMS by integrating boronate affinity and local post-imprinting modification for selective capture of circulating tumor cells from cancer patients*. Biosensors and Bioelectronics, 2023. **223**: p. 115023.
217. Mihara, S. and S. Takeoka, *Preparation and characterization of highly elongated polydimethylsiloxane nanosheets*. Polymers for Advanced Technologies, 2022. **33**(4): p. 1180-1189.
218. Huang, J., et al., *Highly stretchable, soft and sticky PDMS elastomer by solvothermal polymerization process*. Nano Research, 2021. **14**: p. 3636-3642.
219. Sales, F.C., et al., *Mechanical characterization of PDMS with different mixing ratios*. Procedia Structural Integrity, 2022. **37**: p. 383-388.
220. Kemkemer, R., et al., *Surface modification of Polydimethylsiloxane by hydrogels for microfluidic applications*. Current directions in biomedical engineering, 2019. **5**(1): p. 93-96.
221. Paul, A., et al., *Micro- and nano-patterned elastin-like polypeptide hydrogels for stem cell culture*. Soft Matter, 2017. **13**(34): p. 5665-5675.
222. Shahriyari, F., et al., *Effect of cell imprinting on viability and drug susceptibility of breast cancer cells to doxorubicin*. Acta Biomaterialia, 2020. **113**: p. 119-129.
223. Kavand, H., et al., *A conductive cell-imprinted substrate based on CNT-PDMS composite*. Biotechnology and Applied Biochemistry, 2019. **66**(3): p. 445-453.
224. Heath, D.E., et al., *Regenerating the cell resistance of micromolded PEG hydrogels*. Lab on a Chip, 2015. **15**(9): p. 2073-2089.
225. Lusina, A. and M. Cegłowski, *Molecularly imprinted polymers as state-of-the-art drug carriers in hydrogel transdermal drug delivery applications*. Polymers, 2022. **14**(3): p. 640.
226. Guruvankar, S., et al., *Wettability enhancement of polystyrene with electron cyclotron resonance plasma with argon*. Journal of applied polymer science, 2003. **90**(6): p. 1618-1623.
227. Choi, S.C., et al., *Relation between hydrophilicity and cell culturing on polystyrene Petri dish modified by ion-assisted reaction*. Journal of applied polymer science, 1999. **73**(1): p. 41-46.
228. Barsbay, M. and O. Güven, *Modification of polystyrene cell-culture-dish surfaces by consecutive grafting of poly (acrylamide)/poly (N-isopropylacrylamide) via reversible addition-fragmentation chain transfer-mediated polymerization*. European Polymer Journal, 2021. **147**: p. 110330.
229. Hickman, G.J., et al., *Fabrication, characterisation and performance of hydrophilic and superhydrophilic silica as cell culture surfaces*. Journal of Materials Chemistry, 2012. **22**(24): p. 12141-12148.
230. Mitchell, S., et al., *Isopropyl alcohol plasma modification of polystyrene surfaces to influence cell attachment behaviour*. Surface science, 2004. **561**(1): p. 110-120.

Bibliography

231. Parhi, P., A. Golas, and E.A. Vogler, *Role of proteins and water in the initial attachment of mammalian cells to biomedical surfaces: a review*. Journal of Adhesion Science and Technology, 2010. **24**(5): p. 853-888.
232. Hickman, G.J., et al., *The importance and clinical relevance of surfaces in tissue culture*. ACS Biomaterials Science & Engineering, 2016. **2**(2): p. 152-164.
233. Bain, J.R. and A.S. Hoffman, *Tissue-culture surfaces with mixtures of aminated and fluorinated functional groups. Part 1. Synthesis and characterization*. Journal of Biomaterials Science, Polymer Edition, 2003. **14**(4): p. 325-339.
234. Brecher, C., et al. *Development and characterization of high volume producible micro structured surfaces for tissue engineering applications*. in *World Congress on Medical Physics and Biomedical Engineering, September 7-12, 2009, Munich, Germany: Vol. 25/10 Biomaterials, Cellular and Tussue Engineering, Artificial Organs*. 2010. Springer.
235. Sivanesan, I., et al., *A fumigation-based surface sterilization approach for plant tissue culture*. International journal of environmental research and public health, 2021. **18**(5): p. 2282.
236. Hsieh, C.-J., *Studies on Surface Modifications of Materials for Tissue Engineering Applications*. 2006, University of Pittsburgh.
237. Boronat, C., et al., *Effects of UVC irradiation on polystyrene for healthcare packaging: Study by FTIR and Raman spectroscopy with thermoluminescence*. Polymer Degradation and Stability, 2024. **222**: p. 110700.
238. Hamzah, M.Q., et al. *Preparation and characterization of polystyrene nanosphere*. in *AIP Conference Proceedings*. 2023. AIP Publishing.
239. Cordoba, A., et al., *A Novel In Situ Sol-Gel Synthesis Method for PDMS Composites Reinforced with Silica Nanoparticles*. Polymers, 2024. **16**(8): p. 1125.
240. La Manna, P., et al., *In Situ FT-IR Spectroscopy Investigation of the Water Sorption of Amphiphilic PDMS Crosslinked Networks*. Macromolecular Chemistry and Physics, 2017. **218**(18): p. 1600585.
241. Atazadeh, A. and E. Ameri, *Synthesis of PMHS–PDMS composite membranes embedded with silica nanoparticles and their application to separate of DMSO from aqueous solutions*. Polymer Bulletin, 2021. **78**(9): p. 5003-5028.
242. Suea-Ngam, A., M. Srisa-Art, and Y. Furutani, *PDMS-based microfluidic device for infrared-transmission spectro-electrochemistry*. Bulletin of the Chemical Society of Japan, 2018. **91**(5): p. 728-734.
243. Koleżyński, A. and M. Król, *Molecular Spectroscopy—Experiment and Theory*. 2019.
244. Srinivasan, A., et al., *Infrared dielectric function of polydimethylsiloxane and selective emission behavior*. Applied Physics Letters, 2016. **109**(6).
245. Ghasemi, H. and M.H. Mozaffari, *Synthesis and optoelectronic properties of CdSe quantum dots*. arXiv preprint arXiv:2105.08575, 2021.
246. Najeeb, M.A., et al., *Structural, morphological and optical properties of PEDOT: PSS/QDs nano-composite films prepared by spin-casting*. Physica E: Low-dimensional Systems and Nanostructures, 2016. **83**: p. 64-68.
247. Singh, R., A.K. Bajpai, and A.K. Shrivastava, *CdSe QDs reinforced poly (1, 8 diaminonaphthalene)(PDAN) offers improved thermal and AC conductivity properties*. SN Applied Sciences, 2019. **1**: p. 1-9.
248. Lee, K.-H., et al., *Over 40 cd/A efficient green quantum dot electroluminescent device comprising uniquely large-sized quantum dots*. ACS nano, 2014. **8**(5): p. 4893-4901.
249. Kwon, Y.-T., et al., *Synthesis of CdSe/ZnSe quantum dots passivated with a polymer for oxidation prevention*. Surface and Coatings Technology, 2014. **259**: p. 83-86.
250. Güleröglü, G. and C. Ünlü, *Spectroscopic investigation of defect-state emission in CdSe quantum dots*. Turkish Journal of Chemistry, 2021. **45**(3): p. 520-527.

Bibliography

251. Yang, K., et al., *An aqueous gold nanorod and CdSe quantum dots hybrid nanomaterial: A potential plasmon enhanced fluorescence structure for bio-probe fabrication*. Chemical Engineering Journal, 2021. **426**: p. 131571.
252. Guan, K., et al., *Nanoparticles Internalization through HIP-55-Dependent Clathrin Endocytosis Pathway*. Nano Letters, 2023. **23**(24): p. 11477-11484.
253. Okafor, O. and K. Kim, *Cytotoxicity of Quantum Dots in Receptor-Mediated Endocytic and Pinocytic Pathways in Yeast*. International Journal of Molecular Sciences, 2024. **25**(9): p. 4714.
254. Le, N., et al., *Red CdSe/ZnS QDs' Intracellular Trafficking and Its Impact on Yeast Polarization and Actin Filament*. Cells, 2023. **12**(3): p. 484.
255. Karabanovas, V., et al., *Surface properties of quantum dots define their cellular endocytic routes, mitogenic stimulation and suppression of cell migration*. Journal of biomedical nanotechnology, 2014. **10**(5): p. 775-786.
256. Manshian, B.B., et al., *The role of intracellular trafficking of CdSe/ZnS QDs on their consequent toxicity profile*. Journal of Nanobiotechnology, 2017. **15**: p. 1-14.
257. Hens, B., et al., *The future of anticancer drugs: A cytotoxicity assessment study of CdSe/ZnS quantum dots*. Journal of Nanotheranostics, 2020. **1**(1): p. 3.
258. Kumar, A. and P. Kumar, *Cytotoxicity of quantum dots: Use of quasiSMILES in development of reliable models with index of ideality of correlation and the consensus modelling*. Journal of Hazardous Materials, 2021. **402**: p. 123777.
259. Kumari, A., et al., *Proficient surface modification of CdSe quantum dots for highly luminescent and biocompatible probes for bioimaging: a comparative experimental investigation*. Journal of Luminescence, 2018. **199**: p. 174-182.
260. Mirnajafizadeh, F., et al., *Nanoparticles for bioapplications: study of the cytotoxicity of water dispersible quantum dots*. 2018.
261. Mirnajafizadeh, F., et al., *Nanoparticles for bioapplications: study of the cytotoxicity of water dispersible CdSe (S) and CdSe (S)/ZnO quantum dots*. Nanomaterials, 2019. **9**(3): p. 465.
262. Rathee, N., K. Khurana, and N. Jaggi. *Toxicology studies of CdSe QDs and Ag composites with CdSe for in-vitro bio imaging applications*. in *AIP Conference Proceedings*. 2020. AIP Publishing.
263. Soto, L., *New trends and future perspectives on plasma focus research*. Plasma Physics and Controlled Fusion, 2005. **47**(5A): p. A361.
264. Wang, H., et al., *TEM sample preparation of patterned quantum dots*. Microscopy and Microanalysis, 2019. **25**(S2): p. 790-791.
265. Rivera, C., *Gentian Violet Used as an Epithelial Cell Monolayer Stain in the Scratch Wound Healing Assay*. Analytical and Quantitative Cytopathology and Histopathology, 2016. **38**(2): p. 137-138.
266. Saito, K.-i., et al., *A modified and convenient method for assessing tumor cell invasion and migration and its application to screening for inhibitors*. Biological and Pharmaceutical Bulletin, 1997. **20**(4): p. 345-348.
267. Chadha, V., et al., *Evaluating scanning electron microscopy for the measurement of small-scale topography*. Surface Topography: Metrology and Properties, 2024.
268. Abdallah, Z., A. Fay, and S. Bonnet. *3D SEM metrology of microstructures for high volume manufacturing*. in *38th European Mask and Lithography Conference (EMLC 2023)*. 2023. SPIE.
269. Pennisi, C.P., et al. *The influence of surface properties of plasma-etched polydimethylsiloxane (PDMS) on cell growth and morphology*. in *2010 Annual International Conference of the IEEE Engineering in Medicine and Biology*. 2010. IEEE.
270. Wala, J., D. Maji, and S. Das, *Influence of physico-mechanical properties of elastomeric material for different cell growth*. Biomedical Materials, 2017. **12**(6): p. 065002.
271. Mitchinson, A., et al., *A stochastic model for topographically influenced cell migration*. Journal of Theoretical Biology, 2024. **581**: p. 111745.

Bibliography

272. Comelles, J., et al., *Soft topographical patterns trigger a stiffness-dependent cellular response to contact guidance*. *Materials Today Bio*, 2023. **19**: p. 100593.
273. Vazquez, K., A. Saraswathibhatla, and J. Notbohm, *Effect of substrate stiffness on friction in collective cell migration*. *Scientific Reports*, 2022. **12**(1): p. 2474.
274. Shivani, S., et al., *Programmed topographic substrates for studying roughness gradient-dependent cell migration using two-photon polymerization*. *Frontiers in Cell and Developmental Biology*, 2022. **10**: p. 825791.
275. Gonthier, A.R., et al., *Effect of Porous Substrate Topographies on Cell Dynamics: A Computational Study*. *ACS Biomaterials Science & Engineering*, 2023. **9**(10): p. 5666-5678.
276. Allahyari, Z., et al., *Altered Cell-Substrate Behavior on Microporous Membranes is a Result of Disruption and Grip*. *bioRxiv*, 2019: p. 563361.
277. Allahyari, Z., et al., *Micropatterned poly (ethylene glycol) islands disrupt endothelial cell–substrate interactions differently from microporous membranes*. *ACS biomaterials science & engineering*, 2019. **6**(2): p. 959-968.
278. Mohammed, D., et al., *Substrate area confinement is a key determinant of cell velocity in collective migration*. *Nature Physics*, 2019. **15**(8): p. 858-866.
279. Bose, S., K. Dasbiswas, and A. Gopinath, *Substrate mediated elastic coupling between motile cells modulates inter–cell interactions and enhances cell–cell contact*. *bioRxiv*, 2021: p. 2021.03.06.434234.
280. Biggs, M.J., et al., *Interactions with nanoscale topography: adhesion quantification and signal transduction in cells of osteogenic and multipotent lineage*. *Journal of Biomedical Materials Research Part a: An Official Journal of the Society for Biomaterials, the Japanese Society for Biomaterials, and the Australian Society for Biomaterials and the Korean Society for Biomaterials*, 2009. **91**(1): p. 195-208.
281. LaPointe, V.L., et al., *Nanoscale topography and chemistry affect embryonic stem cell self-renewal and early differentiation*. *Advanced healthcare materials*, 2013. **2**(12): p. 1644-1650.
282. Macgregor, M., et al., *The role of controlled surface topography and chemistry on mouse embryonic stem cell attachment, growth and self-renewal*. *Materials*, 2017. **10**(9): p. 1081.
283. Sutherland, D.S., et al., *Influence of nanoscale surface topography and chemistry on the functional behaviour of an adsorbed model macromolecule*. *Macromolecular Bioscience*, 2001. **1**(6): p. 270-273.
284. Acloque, H., J. Yang, and E. Theveneau, *Epithelial-to-Mesenchymal Plasticity from development to disease: an introduction to the special issue*. 2023.
285. Cao, Y., *Epithelial-Mesenchymal Transition: A Groundless Skyscraper*. 2024.
286. Dhawan, U., et al., *Nanochip-induced epithelial-to-mesenchymal transition: impact of physical microenvironment on cancer metastasis*. *ACS applied materials & interfaces*, 2018. **10**(14): p. 11474-11485.
287. Hasannejad, F., et al., *Regulation of cell fate by cell imprinting approach in vitro*. *BiolImpacts: BI*, 2024. **14**(3).

Acknowledgment

This dissertation signifies the apex of a profound academic odyssey, and I deeply appreciate all individuals who have provided their support and guidance throughout this endeavor.

Above all else, I wish to convey my deepest appreciation to my supervisors, Prof. Wolfgang J. Parak and Dr. Shahin Bonakdar, for their exceptional mentorship, enduring support, and thoughtful evaluations during this research process. Their expertise and encouragement were pivotal in the development of this dissertation.

My sincere appreciation is directed towards my colleagues and friends who offered encouragement, engaged in enlightening discussions, and fostered a sense of community throughout this academic venture. Your unwavering support has served as a continual source of inspiration.

I am incredibly thankful for the steadfast affection, patience, and trust my family shows in me. To my parents and my beloved wife, Farzaneh Aavani, your sacrifices, and unwavering support have constituted the foundation of my academic endeavors. This achievement would not have been feasible without your contributions.

Lastly, I would like to express my gratitude for the financial and organizational support afforded by DAAD and The University of Hamburg, which enabled the successful execution of this research.

I want to express my sincere appreciation to everyone involved in this journey.

Appendix

A1. Declaration Upon Oath

Hiermit versichere ich an Eides statt, dass ich die vorliegende Dissertation selbst verfasst und keine anderen als die angegebenen Quellen und Hilfsmittel benutzt habe.

I hereby declare upon oath that I have written the present dissertation independently and have not used further resources and aids than those stated in the dissertation.





Ort, den | City, date

Hamburg, Germany, 09.10.2024







Unterschrift|Signature






Hosseinkazemi




A2. List of the Hazardous Substances




CAS No. ³⁰	Material Name	H-Statement ³¹	P-Statement ³²	GHS ³³ Sign
9006-65-9	Polydimethylsiloxane	<ul style="list-style-type: none"> • H315: Causes skin irritation (if additives irritate). • H319: Causes serious eye irritation (if applicable, based on the formulation). • H335: May cause respiratory irritation (for forms like aerosols or fine mists). • H400: Very toxic to aquatic life (if additives have environmental hazards). 	<ul style="list-style-type: none"> • P264: Wash hands thoroughly after handling. • P280: Wear protective gloves/protective clothing/eye protection/face protection. • P302 + P352: IF ON SKIN: Wash with plenty of water. • P305 + P351 + P338: IF IN EYES: Rinse cautiously with water for several minutes. Remove contact lenses, if present, and easy to do. • P273: Avoid release to the environment. • P501: Dispose of contents/container to an approved waste disposal facility. 	 
1310-73-2	Sodium Hydroxide	<ul style="list-style-type: none"> • H314: Causes severe skin burns and eye damage. • H290: It may be corrosive to metals (depending on concentration and form). 	<ul style="list-style-type: none"> • P260: Do not breathe dust or mist. • P264: Wash hands thoroughly after handling. • P280: Wear protective gloves/protective clothing/eye protection/face protection. • P301 + P330 + P331: IF SWALLOWED: Rinse mouth. Do NOT induce vomiting. • P303 + P361 + P353: IF ON SKIN (or hair): Immediately remove all contaminated clothing. Rinse skin with water or shower. • P304 + P340: IF INHALED: Remove person to fresh air and keep comfortable for breathing. • P305 + P351 + P338: IF IN EYES: Rinse cautiously with water for several minutes. Remove contact lenses, if present, and easy to do. Continue rinsing. • P310: Immediately call a POISON CENTER or doctor. • P321: Specific treatment may be needed (refer to SDS or medical 	 

³⁰ Chemical Abstracts Service Number (CAS No.)³¹ Hazard Statements (H-Statements)³² Precautionary Statements (P-Statements)³³ Globally Harmonized System of Classification and Labelling of Chemicals (GHS)

			advice). <ul style="list-style-type: none"> • P363: Wash contaminated clothing before reuse. • P501: Dispose of contents/container according to local regulations. 	
111-30-8	Glutaraldehyde	<ul style="list-style-type: none"> • H301: Toxic if swallowed. • H311: Toxic in contact with skin. • H314: Causes severe skin burns and eye damage. • H317: May cause an allergic skin reaction. • H331: Toxic if inhaled. • H334: May cause allergy or asthma symptoms or breathing difficulties if inhaled. • H335: May cause respiratory irritation. • H400: Very toxic to aquatic life. • H410: Very toxic to aquatic life with long-lasting effects. 	<ul style="list-style-type: none"> • P260: Do not breathe dust/fume/gas/mist/vapors/spray. • P264: Wash hands thoroughly after handling. • P270: Do not eat, drink, or smoke when using this product. • P280: Wear protective gloves/protective clothing/eye protection/face protection. • P301 + P310: IF SWALLOWED: Immediately call a POISON CENTER or doctor. • P302 + P352: IF ON SKIN: Wash with plenty of water. • P303 + P361 + P353: IF ON SKIN (or hair): Immediately remove all contaminated clothing. Rinse skin with water/shower. • P304 + P340: IF INHALED: Remove person to fresh air and keep comfortable for breathing. • P305 + P351 + P338: IF IN EYES: Rinse cautiously with water for several minutes. Remove contact lenses, if present and easy to do. Continue rinsing. • P308 + P313: IF exposed or concerned: Get medical advice/attention. • P333 + P313: If skin irritation or rash occurs, Get medical advice/attention. • P363: Wash contaminated clothing before reuse. • P501: Dispose of contents/container under local/regional/national/international regulations. 	   
30525-89-4	Paraformaldehyde	<ul style="list-style-type: none"> • H228: Flammable solid. • H301: Toxic if swallowed. • H311: Toxic in contact with skin. • H314: Causes severe skin burns and eye damage. 	<ul style="list-style-type: none"> • P201: Obtain special instructions before use. • P202: Do not handle until all safety precautions have been read and understood. • P210: Avoid heat, hot surfaces, sparks, open flames, and other ignition sources. No smoking. • P260: Do not breathe 	 

	<ul style="list-style-type: none"> • H317: May cause an allergic skin reaction. • H331: Toxic if inhaled. • H335: May cause respiratory irritation. • H341: Suspected of causing genetic defects. • H350: May cause cancer. • H373: May cause damage to organs through prolonged or repeated exposure. • H410: Very toxic to aquatic life with long-lasting effects. 	<p>dust/fume/gas/mist/vapors/spray.</p> <ul style="list-style-type: none"> • P264: Wash hands thoroughly after handling. • P270: Do not eat, drink, or smoke when using this product. • P271: Use only outdoors or in a well-ventilated area. • P280: Wear protective gloves/protective clothing/eye protection/face protection. • P301 + P310: IF SWALLOWED: Immediately call a POISON CENTER or doctor. • P302 + P352: IF ON SKIN: Wash with plenty of water. • P304 + P340: IF INHALED: Remove person to fresh air and keep comfortable for breathing. • P305 + P351 + P338: IF IN EYES: Rinse cautiously with water for several minutes. Remove contact lenses, if present, and easy to do. Continue rinsing. • P308 + P313: IF exposed or concerned: Get medical advice/attention. • P333 + P313: If skin irritation or rash occurs, Get medical advice/attention. • P403 + P233: Store in a well-ventilated place. Keep the container tightly closed. • P501: Dispose of contents/container under local/regional/national/international regulations. 	 
<p>67-66-3 Trichloromethane</p>	<ul style="list-style-type: none"> • H302: Harmful if swallowed. • H315: Causes skin irritation. • H319: Causes serious eye irritation. • H332: Harmful if inhaled. • H336: May cause drowsiness or dizziness. • H351: Suspected of causing cancer. • H361d: Suspected of damaging the unborn child. • H373: May cause damage to organs (liver, kidneys, central nervous system) through 	<ul style="list-style-type: none"> • P201: Obtain special instructions before use. • P202: Do not handle until all safety precautions have been read and understood. • P260: Do not breathe dust/fume/gas/mist/vapors/spray. • P264: Wash hands thoroughly after handling. • P270: Do not eat, drink, or smoke when using this product. • P271: Use only outdoors or in a well-ventilated area. • P280: Wear protective gloves/protective clothing/eye protection/face protection. • P301 + P310: IF SWALLOWED: Immediately call a POISON CENTER or doctor. 	  

	<p>prolonged or repeated exposure.</p> <ul style="list-style-type: none"> • H412: Harmful to aquatic life with long-lasting effects. 	<ul style="list-style-type: none"> • P304 + P340: IF INHALED: Remove person to fresh air and keep comfortable for breathing. • P305 + P351 + P338: IF IN EYES: Rinse cautiously with water for several minutes. Remove contact lenses, if present and easy to do. Continue rinsing. • P308 + P313: IF exposed or concerned: Get medical advice/attention. • P403 + P233: Store in a well-ventilated place. Keep the container tightly closed. • P405: Store locked up. • P501: Dispose of contents/container in accordance with local/regional/national/international regulation
<p>7647-01-0</p> <p>Hydrochloric Acid</p>	<ul style="list-style-type: none"> • H314: Causes severe skin burns and eye damage. • H335: May cause respiratory irritation. • H290: May be corrosive to metals (depending on concentration). 	<ul style="list-style-type: none"> • P260: Do not breathe dust/fume/gas/mist/vapors/spray. • P264: Wash hands thoroughly after handling. • P280: Wear protective gloves/protective clothing/eye protection/face protection. • P301 + P330 + P331: IF SWALLOWED: Rinse mouth. Do NOT induce vomiting. • P303 + P361 + P353: IF ON SKIN (or hair): Immediately remove all contaminated clothing. Rinse skin with water or shower. • P304 + P340: IF INHALED: Remove person to fresh air and keep comfortable for breathing. • P305 + P351 + P338: IF IN EYES: Rinse cautiously with water for several minutes. Remove contact lenses, if present, and easy to do. Continue rinsing. • P310: Immediately call a POISON CENTER or doctor. • P363: Wash contaminated clothing before reuse. • P501: Dispose of contents/container under local/regional/national/international regulations. <div style="display: flex; align-items: center; justify-content: center;">   </div>
<p>875756-97-1</p> <p>Bisbenzimidide</p>	<ul style="list-style-type: none"> • H315: Causes skin irritation (possible in high concentrations). • H319: Causes serious eye irritation. 	<ul style="list-style-type: none"> • P261: Avoid breathing dust/fume/gas/mist/vapors/spray. • P264: Wash hands thoroughly after handling. • P280: Wear protective <div style="display: flex; align-items: center; justify-content: center;">  </div>

	<ul style="list-style-type: none"> • H335: May cause respiratory irritation. • H341: Suspected of causing genetic defects (due to its DNA-binding properties) 	<p>gloves/eye protection/face protection.</p> <ul style="list-style-type: none"> • P302 + P352: IF ON SKIN: Wash with plenty of water. • P305 + P351 + P338: IF IN EYES: Rinse cautiously with water for several minutes. Remove contact lenses, if present, and easy to do. Continue rinsing. • P308 + P313: IF exposed or concerned: Get medical advice/attention.
<p style="text-align: center;">Tris(4- 548-62-9 (dimethylamino)phenyl)methylum chloride</p>	<ul style="list-style-type: none"> • H302: Harmful if swallowed. • H315: Causes skin irritation. • H319: Causes serious eye irritation. • H341: Suspected of causing genetic defects (mutagenic properties). • H350: May cause cancer (classified as a possible carcinogen). • H411: Toxic to aquatic life with long-lasting effects. 	<ul style="list-style-type: none"> • P201: Obtain special instructions before use. • P202: Do not handle until all safety precautions have been read and understood. • P260: Do not breathe dust/fume/gas/mist/vapors/spray. • P264: Wash hands thoroughly after handling. • P270: Do not eat, drink, or smoke when using this product. • P273: Avoid release to the environment. • P280: Wear protective gloves/protective clothing/eye protection/face protection. • P301 + P312: IF SWALLOWED: Call a POISON CENTER or doctor if you feel unwell. • P302 + P352: IF ON SKIN: Wash with plenty of water. • P305 + P351 + P338: IF IN EYES: Rinse cautiously with water for several minutes. Remove contact lenses, if present and easy to do. Continue rinsing. • P308 + P313: IF exposed or concerned: Get medical advice/attention. • P391: Collect spillage (to minimize environmental damage). • P501: Dispose of contents/container in accordance with local/regional/national/international regulations. <div style="text-align: right;">   </div>
<p>26426-80-2 Poly(isobutylene-alt-maleic anhydride)</p>	<ul style="list-style-type: none"> • H319: Causes serious eye irritation. • H315: Causes skin irritation. • H335: May cause respiratory irritation (if 	<ul style="list-style-type: none"> • P261: Avoid breathing dust/fume/gas/mist/vapors/spray. • P264: Wash hands thoroughly after handling. • P270: Do not eat, drink, or smoke when using this product. <div style="text-align: right;">  </div>

inhaled as dust or aerosol).

- **H413:** May cause long-lasting harmful effects to aquatic life.

- **P280:** Wear protective gloves/protective clothing/eye protection/face protection.
- **P302 + P352:** IF ON SKIN: Wash with plenty of water.
- **P305 + P351 + P338:** IF IN EYES: Rinse cautiously with water for several minutes. Remove contact lenses, if present and easy to do. Continue rinsing.
- **P308 + P313:** IF exposed or concerned: Get medical advice/attention.
- **P391:** Collect spillage to minimize environmental impact.
- **P501:** Dispose of contents/container in accordance with local/regional/national/international regulations.

